HAIR GROWTH IS INDUCED BY BLOCKADE OF MACROPHAGE-DERIVED ONCOSTATIN M AND DOWNSTREAM JAK-STAT5 SIGNALING IN HAIR FOLLICLE STEM CELLS

ETIENNE C.E. WANG

Submitted in Partial Fulfillment of the
Requirement for the Degree of
Doctor of Philosophy
under the Executive Committee
of the Graduate School of Arts and Sciences

COLUMBIA UNIVERSITY

2018

ABSTRACT

HAIR GROWTH IS INDUCED BY BLOCKADE OF MACROPHAGE-DERIVED ONCOSTATIN M AND DOWNSTREAM JAK-STAT5 SIGNALING IN HAIR FOLLICLE STEM CELLS

ETIENNE C.E. WANG

Our lab recently described a role for JAK-STAT signaling in the maintenance of quiescence during the murine hair cycle. Research into signaling pathways and cytokines/growth factors involved in the mammalian hair cycle has not focused extensively on the JAK-STAT pathway. In this thesis, I investigated the upstream effector(s) and downstream mechanisms of JAK-STAT signaling in the HFSC during telogen, using a variety of methods, including murine conditional mutants of the JAK-STAT pathway, pharmacological and immunological techniques. The mechanism through which OSM exerts this effect is via JAK-STAT5 signaling downstream of the OSM receptor, which is antagonized by pharmacological JAK inhibition. Conditional epidermal ablation of OSMR or STAT5 during early- and mid-telogen (P42 – P60) shortens the telogen phase significantly, and inhibition of macrophages by way of neutralizing antibodies, small molecule inhibitors, and genetic ablation (with *Csf1r-CreER::R26-iDTR* mice) during telogen also promotes hair growth. Single-cell RNA sequencing of dermal immune cells across murine telogen identified a distinct subset of TREM2+ macrophages that are enriched for OSM, and gene-set analysis suggests these “trichophages” are similar to the microglia of the central nervous system. I show that this distinct subset of TREM2+ macrophages predominate during early- and mid-telogen, where they produce Oncostatin M (OSM), which is sufficient to maintain quiescence of hair follicle stem cells (HFSCs). Proliferation of HFSCs and hair growth is associated with depletion of this subset of TREM2+ macrophages. Interestingly, macrophage markers and OSM were found to be upregulated in the balding scalp of males with androgenetic alopecia, suggesting that this mechanism is physiologically relevant in the control of human hair cycling.

TABLE OF CONTENTS

List of Figures……...……....iii

List of Tables.....……...v

Acknowledgements……...vi

CHAPTER 1. INTRODUCTION 1

1.1. The mammalian hair cycle..... 2

1.1.1. The murine hair cycle..... 2
1.1.2. The human hair cycle..... 4

1.2. Molecular mechanisms of hair cycle control 5

1.2.1. Catagen..... 5
1.2.2. Telogen..... 6
1.2.3. Anagen 10

1.3. Other cell types during the hair cycle 11

1.3.1. Melanocytes 11
1.3.2. Merkel cell-neurite complexes.....11
1.3.3. The immune system and the hair cycle 12
1.3.4. Immune cells and the telogen-to-anagen transition.....13
1.3.5. Macrophages and the hair cycle 16
1.3.6. Tissue resident macrophages 17

1.4. JAK-STAT signaling and the hair cycle.....18

1.4.1 Effects of JAK inhibitors on the hair cycle 18
1.4.2 The JAK-STAT pathway 18
1.4.3 JAK-STAT3 signaling and the hair cycle 19
1.4.4 JAK-STAT5 signaling and stem cell quiescence 20
1.4.5 Potential effectors of JAK-STAT mediated quiescence in the HFSC 21

1.5. Oncostatin M and the IL-6 family of cytokines.....27

1.5.1. The IL-6 family of cytokines 27
1.5.2. Effects of OSM on the hair cycle.....28
1.5.3. OSM mediates quiescence via JAK-STAT signaling in various cell types 31

1.6. SUMMARY.....32

CHAPTER 2. ONCOSTATIN M IS PRODUCED BY TREM2+ MACROPHAGES AND MAINTAINS HAIR FOLLICLE STEM CELL QUIESCENCE DURING MURINE TELOGEN 33

RESULTS 35
DISCUSSION 66

CHAPTER 3. JAK-STAT SIGNALING IN THE MURINE HAIR CYCLE 73

RESULTS 74
DISCUSSION 90

CHAPTER 4. DISCUSSION 93

SUMMARY 93
FUTURE DIRECTIONS 93

CONCLUSIONS 100

MATERIALS AND METHODS 101

REFERENCES 108

APPENDIX A. KEY RESOURCES TABLE 120

APPENDIX B. LIST OF ABBREVIATIONS 123

APPENDIX C. LIST OF GENES ENRICHED IN CLUSTER 6 127

APPENDIX D: ENRICHR RESULTS 128

LIST OF FIGURES

Figure 1.1. Hair Follicle Morphogenesis progressing into the adult hair cycle in C57BL/6 mice.. 3

Figure 1.2. Interactions of signaling networks during the hair cycle. 7

Figure 1.3. Factors governing quiescence of HFSCs during telogen. 9

Figure 1.4. Summary of immune involvement in the telogen-to-anagen transition. 15

Figure 1.5. Classification of receptors that signal via the JAK-STAT pathway. 23

Figure 1.6. Results from searches performed on Hair-Gel.net. 30

Figure 2.1. OSM prevents HFSC proliferation via OSMR-JAK-STAT5 signaling. 36

Figure 2.2. Supporting Data. 37

Figure 2.3. Spatiotemporal distribution of OSM signaling apparatus during hair cycle. 39

Figure 2.4. Immunofluorescence of OSMRβ and gp130 in telogen HF. 40

Figure 2.5. Validation of OSMRβ and STAT5 conditional KO. 42

Figure 2.6. Early telogen ablation of OSMRβ/STAT5. 43

Figure 2.7. Mid telogen ablation of OSMRβ/STAT5. 45

Figure 2.8. Cellular dynamics following STAT5 epidermal ablation.. 46

Figure 2.9. Laser-capture microdissection of DP and perifollicular dermal tissue 47

Figure 2.10. Identifying the source of OSM as dermal macrophages. 48

Figure 2.11. P45 single-cell RNA sequencing. 50

Figure 2.12. Heat map showing Differentially Enriched genes in macrophage clusters. 52

Figure 2.13. OSM-producing macrophages resemble microglia. 53

Figure 2.14. Pseudotime analysis. 55

Figure 2.15. OSM-producing macrophages are associated with telogen HFs. 56

Figure 2.16. TREM2+ macrophages numbers decrease over telogen. 57

Figure 2.17. Combined scRNA-seq data across telogen. 58

Figure 2.18. Depilation causes decrease in OSM-producing macrophages. 59

Figure 2.19. T-regulatory cell depletion does not affect JAK-STAT induced anagen. 61
Figure 2.20. Macrophage depletion during telogen initiates anagen, and OSM knock-down prevents the inhibitory effects of macrophages on HFSC. 64
Figure 2.21. Schematic of OSM-producing macrophages during telogen. 67
Figure 3.1. Expression of pSTAT3 (both phosphorylation sites) and pSTAT5 across the hair cycle. 75
Figure 3.2. Conditional ablation of STAT5 in various epidermal compartments. 77
Figure 3.3. Analysis of STAT5-response genes and stem cells markers in the bulge and germ (HG) of STAT5-cKO mice.....79
Figure 3.4. Colony forming assay of WT and STAT5-cKO epidermal stem cells.. 80
Figure 3.5. In silico ChIP-seq workflow. 82
Figure 3.6. ID1 as a quiescence factor in HFSCs. 84
Figure 3.7. STAT3 ablation in the skin/HF.....85
Figure 3.8. Assessment of $STAT3^{FL/FL}$ mice. 87
Figure 3.9. Sequencing of loxP sites in introns 17 and 20 of STAT3 locus. 88
Figure 3.10. A. Sequencing of Intron 17 of new $STAT3^{FL/FL}$ mice 89
Figure 4.1. Preliminary lineage tracing of skin macrophages.....96
Figure 4.2. CX3CR1 expression in P45 dermal CD45+ immune cells. 97
Figure 4.3. Macrophages and OSM in human AGA scalp. 98

LIST OF TABLES

Table 1.1. Cytokines and growth factors/hormones that utilize the JAK-STAT signaling pathway……..24

Table 1.2. JAK-STAT signaling, Immune cell involvement and Anagen progression…….26

Box 1. OSM signaling nomenclature……..29

ACKNOWLEDGEMENTS

This thesis could not have been possible without the patience and generosity of my mentor, Dr Angela Christiano. Her welcome of me into her lab provided me with an unparalleled atmosphere that helped to nurture my scientific thinking, and my development as a clinician-scientist.

I would also like to thank Drs. David Owens, Tony Ferrante, Ellen Ezratty and Hans Snoeck for their valuable advice and instruction as my committee, and also for their guidance and encouragement at every step of my Ph.D journey.

I could not have done this without the support and camaraderie of friends and colleagues from my lab, and other labs that I have rotated through, especially the Lumpkin Lab where I learnt the value of meticulous lab records.

I cannot stress how much I appreciate the technical assistance of Ming Zhang, Emily Chang, Jade Huang, Wangyong Zeng and Du Rong. Their help and expertise certainly helped propel my experiments forward in an efficient manner.

I am grateful for funding from the Locks of Love Foundation, which has allowed us to carry out amazing exploratory science. Also for financial support from my home institution, the National Skin Center of Singapore, as well as the National Medical Research Council (NMRC) of Singapore – their foresight and trust in me will not be forgotten.

Also for Roy Chan, who has stood by me the entire way, despite being on opposite ends of the Earth.

CHAPTER 1. INTRODUCTION

The hair follicle (HF) is a complex appendage, exclusive to mammalian skin, that serves thermoregulatory, camouflage and aesthetic functions. The HF as an organ provides tremendous insights into how stem cells interact with their niche, and with the surrounding cells of their dermal macroenvironment (eg. adipocytes). Semi-autonomous, periodic molecular signals within the HF results in a phenomenon known as hair cycling in mammals, which allows for timed shedding and regeneration of hair and fur. These signals are influenced by environmental and systemic cues that may accelerate or inhibit this cycle.

The concept of growth Inhibitory factors in tissues was first put forward by Claude Bernard in 1878 [1]. These factors were given the name “chalones” from the Greek *chalao* that means “to lower” or “to reduce in strength” around 1913, and they have been hypothesized to mediate tissue homeostasis by preventing proliferation and hyperplasia [2]. Their existence in various tissues, in particular the bone marrow and skin, have been illustrated by classic experiments whereby filtrated tissue extracts were able to prevent mitosis of similar cell types *in vitro* [3, 4]. In the skin, chalones have been proposed inhibit hair growth, and dermal extracts during the “rest phase” of the hair cycle was able to inhibit hair growth when injected into another mouse [5]. In this thesis, I explore whether chalones can maintain HF stem cell quiescence via the JAK-STAT (Janus kinase/Signal Transducers and Activators of Transcription) pathway.

1.1. The mammalian hair cycle

The mammalian hair cycle is a tightly coordinated process whereby the hair follicle undergoes distinct phases of growth (anagen), regression (catagen) and rest (telogen) [6-8]. Each phase of the hair cycle requires complex cellular interactions and molecular signals that direct the hair follicle stem cells (HFSCs), their epithelial progeny in the outer and inner root sheaths (ORS/IRS) of the HF, and the instructional mesenchyme (the dermal papilla, DP) to either produce or shed a hair shaft [7, 9].

1.1.1. The murine hair cycle

The hair cycle in the mouse begins at the end of HF morphogenesis (Figure 1.1), which starts with complex epithelial-mesenchymal crosstalk during embryogenesis (E14.5) that creates the epidermal placode that develops into a hair follicle, and lasts until about post-natal day 19 (P19). During morphogenesis, the establishment of the various epidermal and HF stem cell compartments, along with their niches are achieved by a complex combination of Dysplasin A (EDA), Wnt, Bone Morphogenetic Protein (BMP), Fibroblast Growth Factor (FGF) and Sonic Hedgehog (Shh) signaling. Genetic disruption of any of these signaling pathways have profound consequences on HF structure and function [10-14], and many of these pathways have been also shown to be involved in the subsequent phases of adult HF cycling [9]. The DP, which develops via specialized dermal fibroblast condensates during morphogenesis, is comprised of mesenchymal cells that secrete many of the signals that control the activation, proliferation, and differentiation of the HFSCs throughout the life of the mouse [15]. The first two hair cycles in the mouse are tightly coordinated and synchronized across the dorsal skin, whereas they are largely asynchronous in adult humans and guinea pigs [16, 17]. The highly stereotypical

orchestration and synchronization of the hair cycle has been well documented in C57BL/6 mice [6], and provides a valuable tool for the study of HF cycling and control of HFSC activation and quiescence.

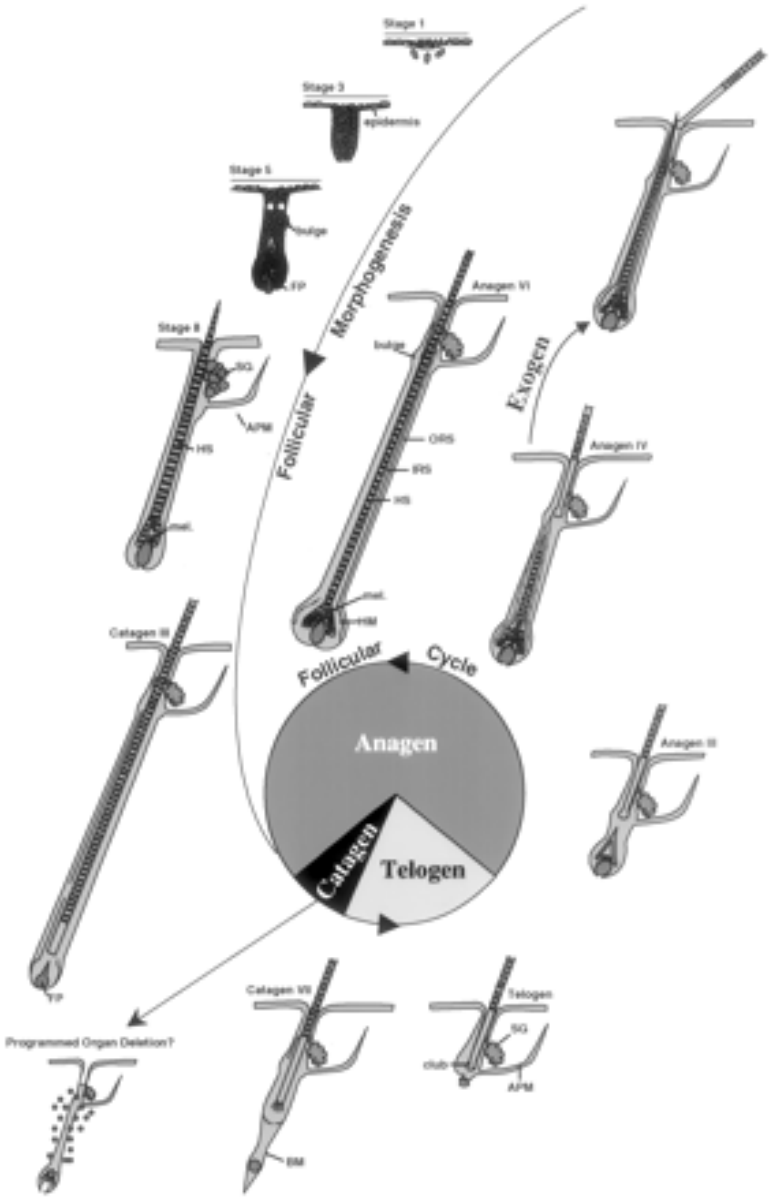

Figure 1.1. Hair Follicle Morphogenesis progressing into the adult hair cycle in C57BL/6 mice. Adapted from Stenn et al, 2001. Epithelial-mesenchymal interactions between the epidermal placode and embryonic mesenchyme leads to downgrowth and invagination of epithelial precursors. Complex patterning and morphogen interactions lead to the establishment of stem cell compartments that persist through adulthood. At around P16-P19, morphogenesis is complete and the newly formed HF undergoes the first catagen (P19-P22), followed by a short first telogen (P22-P28), before entry into the first anagen phase (P28-P42). This proceeds synchronously over the entire dorsal skin of the mouse for the first 2 cycles, after which it becomes patchy and unpredictable. Many of the signaling pathways utilized during morphogenesis are reprised during the hair cycle.

Anagen induction, whereby “resting” telogen follicles enter the next growth phase, may occur spontaneously during the normal hair cycle, or can be induced by depilation, plucking or full-thickness wounding of the mouse telogen skin [18]. Depilation- and plucking-induced anagen synchronizes the hair cycle in murine skin, and are useful techniques for studying anagen progression in the mouse. Several lines of evidence point to differential regulation of spontaneous versus experimentally-induced anagen, and suggest these processes are mechanistically distinct (see section 1.4.3) [19].

1.1.2. The human hair cycle

Human HF morphogenesis occurs entirely during gestation, with epithelial-mesenchymal signaling producing the initial lanugo hairs that cover the body surface of the fetus. The human hair cycle is believed to have a very transient synchronized phase at birth, which may serve to shed the lanugo hairs of the newborn [20]. These hairs are replaced first with vellus hairs, and then with terminal HFs, particularly on the scalp, around the time of birth. Unlike mouse dorsal hair, which spends a large proportion of the hair cycle in telogen, the conspicuous terminal human hairs on the scalp are mostly in the anagen phase. In fact, human scalp hairs may spend up to 7 years in anagen, which accounts for the length that human hair may achieve [21]. Catagen and telogen lasts about 1-2 weeks and 3 months in humans, respectively. As such, studying human hair cycling is very difficult, and computational models [22] or mouse xenograft models [23] have been developed to address this.

Understanding the controls of hair cycling can help clinicians and researchers address disorders associated with arrested or prolonged telogen, which presents clinically as thinning or shedding hair. Telogen effluvium (TE) is characterized by an inverted anagen:telogen ratio, typically after

physical or emotional stress that diverts resources from the hair cycle [24]. TE is common post-partum, or post-surgery, during which alarming amounts of hair is shed 4-6 months after the precipitating event. In androgenetic alopecia (AGA) [25], miniaturized HFs in androgen-sensitive areas of the scalp are unable to enter the anagen phase. At the moment, the distinction between a miniaturized HF of AGA and the vellus hairs of human telogen are purely clinical [26], and their molecular and cellular pathologies are unknown. Although our knowledge of the molecular controls of human hair cycling is limited, we may use mouse models to delineate basic concepts of hair biology that may be extrapolated to humans.

1.2. Molecular mechanisms of hair cycle control

This section describes the molecular signals and mechanisms involved in the control of the murine hair cycle, which has been described in detail by Muller-Rover et al in the C57BL/6 mouse [6].

1.2.1. Catagen

After HF morphogenesis in the mouse is compete (around P16-19), the fully formed HF undergoes its first catagen phase (Figure 1.1), whereby proliferation of the keratinocytes in the ORS and matrix ceases, and the melanocytes and epithelial cells of the HF matrix undergo apoptosis. This process of controlled organ deletion results in the retraction of the non-permanent portion of the HF (ie. the epidermal tissue below the bulge) and the migration of the DP from the deep dermis to a more superficial position nearer the HFSC bulge, separated by the secondary hair germ (HG). The regression of keratinocytes during catagen is an active process, and requires signaling by molecules like FGF-5, parathyroid hormone-related protein

(PTHrp) and IGF-1, amongst others. Genetic disruption of these signaling pathways in mice results in prolonged anagen, failure to enter catagen, and elongated hair shafts [27-31]. In the mouse, FGF-5 mutations are associated with the Angora phenotype, whereby the prolonged anagen phase of the dorsal coat provides these mice with longer, scruffier fur [32]. In humans, mutations in the FGF-5 gene is associated with trichomegaly, whereby a prolonged anagen phase is characterized by longer, thicker eyelashes in affected individuals [33].

The removal of cellular debris of catagen is likely carried out by macrophages [34], which have been observed to cluster around catagen follicles, and have been postulated to be the source of FGF-5 [27]. Recent advances in intravital imaging using two-photon confocal microscopy has also implicated the epithelial cells themselves to be able to clear neighboring apoptotic cells by phagocytosis during catagen [35]. As the HF regresses, it leaves behind a “fibrous tract” of extracellular matrix and macrophages [34, 36], which can be observed on histological sections as a hallmark of catagen follicles.

1.2.2. Telogen

When the DP has migrated up to its position near the bulge following catagen, the “resting” phase of the hair cycle, known as telogen, begins. Telogen is characterized by its lack of proliferation, and has historically been described as a quiescent period of the hair cycle. However, this concept has been challenged in recent years by several groups, who propose that the lack of proliferation does not signify a lack of activity [37]. Indeed, the telogen phase has been shown to be rich in inhibitory signals that maintain the quiescence of HFSCs. Paus et al showed that murine telogen skin contains a factor that could inhibit anagen when extracted and injected into another mouse [5], raising the possibility for the presence of a naturally-occurring

"chalone" or a growth-inhibitory factor [2] of HFSCs. The first telogen phase in a C57BL/6 mouse is short, and lasts about a week from P19 to P28. The second telogen is much longer, and can last from P45 to around P80-P100, making the second telogen more amenable to studying the molecular drivers of telogen.

Immediately after catagen, the skin is in a state known as "refractory telogen", when anagen does not occur spontaneously, and cannot be induced by plucking or depilation. Refractory telogen is associated with high BMP activity, which is a potent inhibitor of HFSC activity [38] (Figure 1.2). BMP levels in the dermis begin to decline during mid-telogen, at which time the skin progresses to "competent telogen", wherein the HFs become receptive to macroenvironmental signals that initiate the next phase of anagen [39]. Using whole-mount *in situ* hybridizations, Plikus et al showed *Bmp2* and *Bmp4* mRNA to have a periodic expression pattern in relation to the hair cycle: being prominently expressed in late anagen/refractory telogen, and absent in competent telogen.

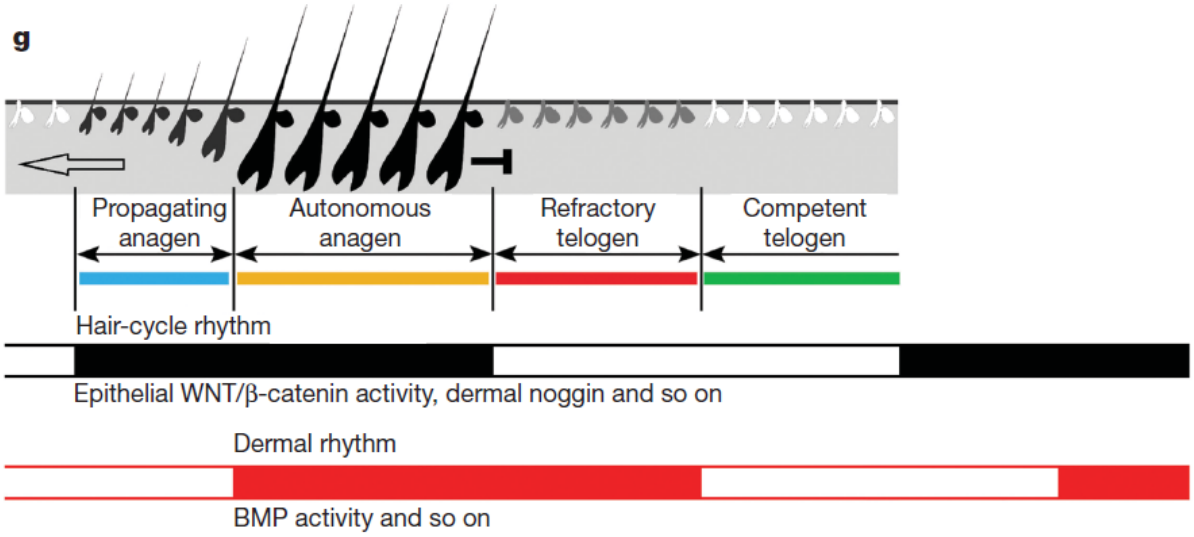

Figure 1.2. **Interactions of signaling networks during the hair cycle.** Adapted from Plikus et al, 2008. Activating signals (Wnt/β-catenin) and inhibitory signals (BMP) are expressed in an overlapping manner to determine the potential of the skin for anagen induction. "Refractory telogen" immediately following catagen is characterized by high BMP activity, which prevents HFSC activation. As BMP declines, "competent telogen" is achieved, allowing the next wave of anagen to propagate through.

Other inhibitory signals are derived from within the HF itself. The K6+ inner bulge was found to produce FGF-18 and BMP6 to maintain quiescence of the outer bulge cells [40]. Intriguingly, the K6+ inner bulge cells were found to be derived from cycling cells in the ORS from the previous hair cycle, and during telogen they provide signals to form the quiescent niche for bulge HFSCs. Hsu et al showed that ablating these cells during telogen with a *Sox9-iDTR* genetic model resulted in shedding of the telogen coat and precocious entry into the next anagen phase. During telogen, the HFSC of the bulge and HG are characterized by pSMAD1/5 signaling (downstream of intrafollicular and dermal BMP signals), as well as Axin2 signaling (likely autocrine Wnt signaling that is essential for stem cell self-renewal) [41].

In addition to Axin2, other molecules have been identified as markers of HF stem cell identity in the bulge and HG during telogen (Figure 1.3). CD34, which is expressed on other stem cells, immune cells and vascular structures, is restricted to the bulge HFSC in the epidermis, and is a reliable cell-surface antigen for fluorescence-activated cell sorting (FACS) of mouse HFSCs [42]. Isolation of bulge HFSCs during various stages of the hair cycle have identified Wnt and BMP signaling to be important in maintaining bulge identity [43]. The Lim-homeodomain transcription factor (Lhx2) is expressed by both the bulge and HG HFSCs, and is co-expressed with other stem cell markers SOX9, Tcf4 and Lgr5 [44]. In the bulge, Lhx2 functions upstream of SOX9 and Tcf4 to *promote* the wound healing capacity of the bulge HFSC, while it *suppresses* proliferation and maintains quiescence of the HG. In both the bulge and HG, Lhx2 also maintains cell polarity and stem cell identity within its niche [45]. NFATc1, which acts downstream of BMP and calcineurin signaling, is also a quiescence factor for the HFSC [46]. FoxC1, which may regulate both BMP and NFATc1 [47], has also been described as a quiescence factor of the bulge HFSCs [48].

While BMPs and FGF-5 exert inhibitory effects on HFs during catagen and telogen, it can be argued that they may not function as true chalones in this system. Criteria for chalones, as defined by Houck in 1973 [2], are 1) Total cell specificity; 2) Lack of species specificity; and 3) Reversibility. BMP signaling has may other roles in HF morphogenesis and cycling. BMP signaling is required for patterning of the HF matrix during anagen [49] and for differentiation of the layers of the IRS [13], and is also required for the inductive properties of the DP [50]. FGF-5, while promoting catagen, is also required for maintenance of HF structure, as Angora mice are described to have dystrophic hair canals with secondary hyperplasia [32]. A true chalone would have negative growth regulatory properties without affecting the overall structure and function of the organ/tissue.

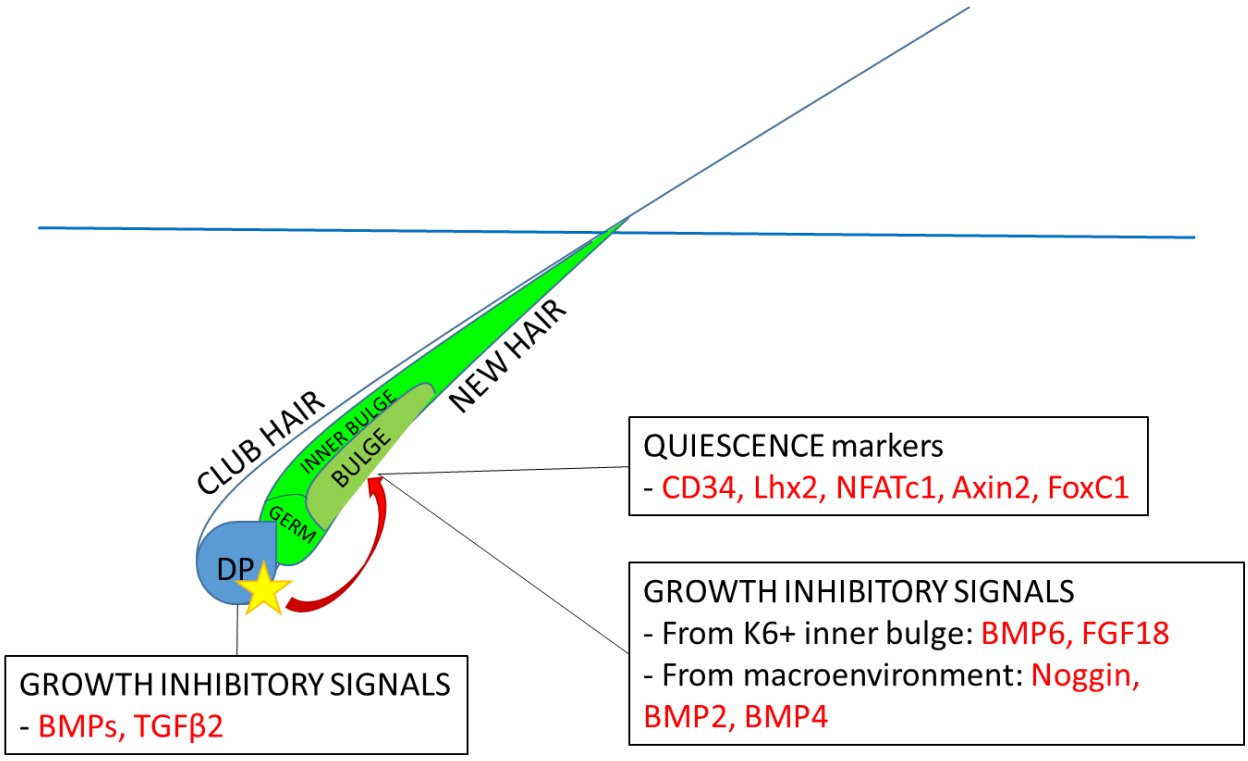

Figure 1.3. Factors governing quiescence of HFSCs during telogen. BMP signaling predominates from the inner bulge, macroenviroment and the DP. The HFSC compartment (bulge and HG) express stem cell markers that are involved in maintaining stem cell identity, self-renewal and quiescence.

1.2.3. Anagen

At the end of telogen, the decline of inhibitory signals (BMPs), coupled with increase in activating signals from the DP, result in activation of the HFSC, making the start of spontaneous anagen. DP-derived Wnt signaling results in stabilization of β-catenin in the adjacent secondary HG [51], leading to proliferation which is first observed in this compartment [52]. In addition to proliferating and differentiating into the ORS, the HG cells also begin to secrete Shh, which in turn activates the bulge HFSCs, which are positioned just above the HG [53]. As the HG proliferates and differentiates into the ORS, it is replenished by less frequent divisions from the bulge. As anagen progresses, and the DP migrates further and further away from the bulge toward the deep dermis, proliferation in the bulge becomes less frequent. Regeneration of the HF is occurs mainly by the proliferative activity of the epithelial cells of the ORS and matrix, which further differentiate to give rise to the concentric layers of the IRS and the hair shaft.

The DP is essential for the initiation of anagen [54]. Precise laser ablation of the DP prevents the HF from entering anagen [55], whereas ablation of HFSC in the bulge or HG does not. It appears that neighboring HFSCs are able to differentiate to fill the space in the niche left by laser ablation of bulge or HG cells [56]. As anagen progresses, the telogen DP enlarges from a small cluster of cells to a large anagen DP that is comprised of up to 3000 cells depending on the hair type. Large anagen vibrissa hairs of the whiskers harbor 3000 cells, while various pelage hairs on the dorsal coat vary in DP sizes. [57]. The cells of the DP are replenished by stem cells found in the dermal cup, which also supplies progeny to the dermal sheath [58, 59]. By the end of anagen, the DP is deep in the subcutaneous adipose tissue, and the fully-developed terminal anagen HF extends through all the layers of the skin. The dermal and subcutaneous adipocytes also proliferate and expand throughout anagen, and contribute to

overall skin thickening during this phase of the hair cycle [60, 61]. Additionally, dermal adipocytes secrete PDGFα that regulates HFSC activity [62], and subcutaneous adipocytes are a source of BMPs that contribute to the macroenvironmental niche for the anagen HF [63].

1.3. Other cell types during the hair cycle

The subcutaneous adipocytes are not the only cell type that interacts with the cycling HF. Other cells types associated with the HF are also involved in the remodeling that accompanies the hair cycle.

1.3.1. Melanocytes

Melanocytes in mammals are found in the basement membrane of the epidermis, and the matrix of the anagen HF, where they produce melanin pigments that are transferred to keratinocytes in melanosomes. In C57BL/6 mice, the epidermis is devoid of melanocytes, which accounts for the pink appearance of telogen skin. Melanocyte stem cells in the bulge are activated by stem cell factor (SCF) secreted by the activated Krox20+ hair matrix [64], which signals via c-kit to initiate proliferation and migration of melanocytes into the HF matrix [65]. This process is very tightly coordinated with the hair cycle, and the darkening of telogen skin due to increased melanogenesis reliably heralds the onset of anagen.

1.3.2. Merkel cell-neurite complexes

Guard hairs, the largest HFs of the mouse pelage which comprise about 1% of the coat hairs, are associated with Merkel cell complexes that mediate sensation derived from pressure and mechanical stimuli [66]. The Merkel cell complex is made up of a touch dome containing 20-50 Merkel cells, and somatosensory afferent innervation. Epidermal innervation and Merkel cell numbers have been described to fluctuate during the hair cycle [67-69], and recently, Marshall et al showed that Merkel cell numbers decrease during anagen, increase before catagen, and maintain their numbers throughout telogen [70]. While the signaling pathways that influence these processes have yet to be described, it is likely that the developmental signaling pathways of the hair cycle (ie. Wnt, BMP, FGF, Shh) may also play a role in neuronal and Merkel cell maintenance and remodeling of touch domes.

1.3.3. The immune system and the hair cycle

The role of the immune system in the maintenance of the stem cell niche has been described in many systems. Besides their given role in the maintenance of the hematological niche in the bone marrow [71], immune cells are widely implicated in processes like embryogenesis [72], post-natal homeostasis and development [73], and regeneration [74].

Paus et al have described the distribution and fluctuations of immune cells associated with the murine adult hair cycle [75]. Langerhans cells and γδ T cells were restricted mainly to the epidermis, where they carry out immunosurveillance. CD4+ and CD8+ T cells were rare in healthy skin and HFs. MHC Class II+ cells, which include macrophages, monocytes and dendritic cells (DCs), were abundant in mouse skin and were found in close proximity to HFs [36], especially during late anagen. Macrophages have been implicated in the clearance of cellular debris during catagen [34].

Mast cells have also been described to be closely associated with murine HFs. Using immunohistochemistry studies, Maurer et al showed that mast cell numbers peaked in late anagen, and degranulated just before spontaneous catagen [76]. The authors proposed that mast cell products like substance P (SP) and adrenocorticotrophic hormone (ACTH) mediate HF involution during murine catagen [77]. SP and other neurotransmitters like brain-derived neurotrophic factor (BDNF) have been implicated in precipitating catagen, and may be linked to HF-associated autonomic innervation [78, 79], which in turn may influence mast cell degranulation.

1.3.4. Immune cells and the telogen-to-anagen transition

The telogen-to-anagen transition reflects the activation of quiescent HFSCs to initiate proliferation and differentiation of ORS and IRS that results in formation and elongation of the hair shaft. The onset of hair growth can be observed readily in the mouse.

The transition from telogen to anagen may occur spontaneously, during the normal unperturbed murine hair cycle, or it can be induced (Figure 1.4, Table 1.2). In the mouse, depilation (with depilatory creams) and plucking (active physical extraction of HFs) during telogen can stimulate the growth of the next hair cycle [80], and is frequently utilized to study the anagen phase in a coordinated and synchronized manner [81]. Plucking of telogen HFs is believed to stimulate CCL2 secretion by the damaged HFs, which recruits macrophages to the vicinity where they release TNF to initiate anagen [82]. This process is dependent on the phase of telogen (refractory vs competent) as well as the number and density of HFs plucked.

Ali et al recently demonstrated that depilation-induced anagen may be mediated by FoxP3+ T regulatory cells via the Jagged1/Notch signaling pathway [83]. Genetic ablation of T regs with a *FoxP3-iDTR* mouse model showed inhibition of depilation-induced anagen, which could be replicated in *FoxP3-Cre::Jag1*$^{FL/FL}$ mice.

During wound healing in rodents, it has been shown that larger wounds regenerate with *de novo* HFs arising from the healed scar tissue by a process called wound-induced HF neogenesis (WIHN) [84]. This process recapitulates HF morphogenesis, and has been shown to depend on FGF-9 produced by γδ T cells [85], which are recruited by factors released by damaged keratinocytes, and are integral in wound repair [86].

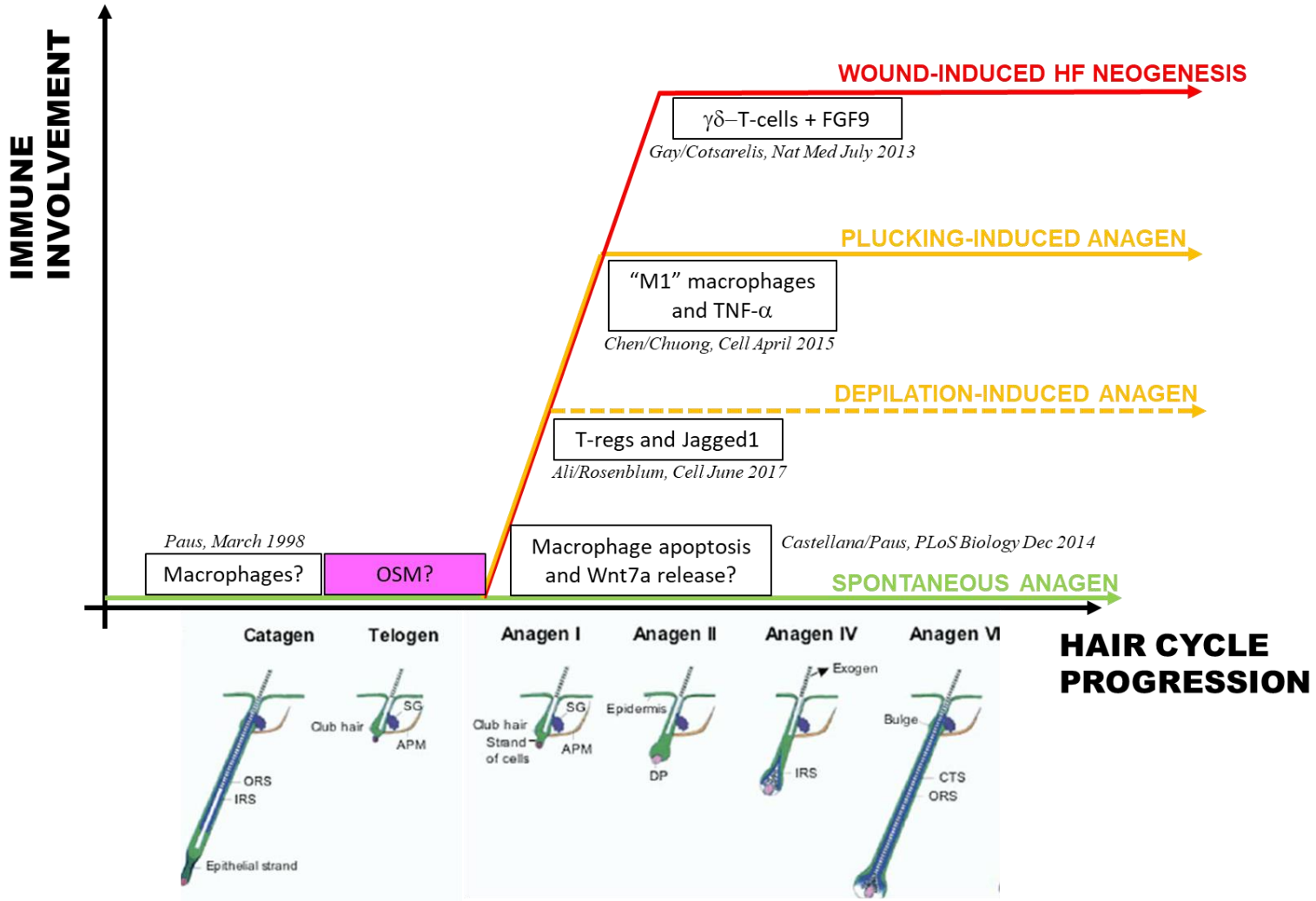

Figure 1.4. Summary of immune involvement in the telogen-to-anagen transition. Horizontal axis represents temporal progression of the hair cycle, and the vertical axis is a representation of degree of physical insult. The green horizontal line (y=0) represents the unperturbed spontaneous anagen, and the various models of anagen induction are layered above it. This model assumes that the physical insult to the skin can be represented as a spectrum. OSM in the purple box represents data presented in this thesis.

1.3.5. Macrophages and the hair cycle

While the role of dermal macrophages during wound healing and psoriatic inflammation have been established [87, 88], their function in non-homeostatic or inflammatory processes in the skin have not been well studied. Their proposed functions during the hair cycle have been inferred from their anatomical associations with HFs, and evidence of their actual function has only recently been uncovered.

Macrophages have been implicated in the control of the telogen-to-anagen transition. Castellana et al showed that macrophage numbers peak during mid-telogen, and declined during late telogen, at which point they underwent apoptosis to release Wnt signals that induced HFSC activation in telogen HFs [89]. The authors also show that macrophage depletion during telogen using clodronate liposomes resulted in anagen initiation.

Several non-immune roles macrophages in various tissues have also been described. In the heart, macrophages have been shown to facilitate electrical conduction [90] In the brain, the microglia (which are innate immune cells with the same ontogeny as macrophages) have essential housekeeping and regulatory functions that maintain synaptic function and neuronal connects. Microglial dysfunction has been associated with neurodegenerative disease like Alzheimer's disease [91]. In the skin, microglia-like cells (expressing the marker Aif-1/Iba-1) have been described to be associated with Merkel cell-neurite complexes, where they have been postulated to participate in remodeling and regeneration of neuronal structures (D. Owens, personal communication). This suggests that dermal macrophages may play a more significant role in tissue homeostasis of the skin and HF than previously appreciated.

1.3.6. Tissue resident macrophages

Dermal tissue-resident macrophages (TRMs) are likely to be heterogenous [92], and are probably mostly unpolarized. The “M1” and “M2” subsets that were described and loosely analogous to Th1/Th2 reactions are unlikely to predominate at steady-state [93]. While M1 “inflammatory” macrophages are believed to be important in dealing with bacterial and viral infections, M2 macrophages are associated with tissue repair and resolution of the inflammatory state [94]. M2 markers like CD163 and CD206 (MRC1) have been used to identify M2-like “anti-inflammatory” macrophages, while MHC Class II expression and production of cytokines like Interferon-γ (IFN-γ), IL-1b and TNF have been used as putative “M1-like” markers. Other than their scavenging function, M2 TRMs may play an anti-inflammatory role by producing IL-4 and IL-10 [95]. Unpolarized TRMs may represent the “M0” subset, characterized by pan-macrophage markers CD68 and Csf1r. Dermal TRMs are dependent on the growth factor Csf1 (signaling via its receptor Csf1r) for maturation [96], and a null mutation in either Csf1 or Csf1r is associated with dramatic loss of dermal TRMs [97].

Unlike the microglia of the central nervous system (CNS) and the Langerhans cells of the epidermis, the dermal macrophages are constantly being replenished by circulating monocytes. Early tissue-resident macrophages like the microglia are seeded during embryogenesis from progenitors in the yolk sac around E8.5, and replenish themselves throughout the adult life [98]. Adult dermal macrophages, on the other hand, are almost entirely made up from circulating monocyte precursors, and only have a minimal contribution from the yolk sac [99]. This may reflect the function of the skin as a barrier organ, requiring a constant flux of immune cell participants, or it may also be related to hair cycling itself, which represents a controlled

regenerative cycle that may require constant macrophage support for the turnover of epidermal cells.

1.4. JAK-STAT signaling and the hair cycle

1.4.1 Effects of JAK inhibitors on the hair cycle

Our previous genetic studies in Alopecia Areata (AA) identified NKG2D+ CD8+ T cells to be the main pathogenic effectors for the disease [100-103]. This led to the interrogation of JAK inhibitors as a novel treatment modality for AA, targeting the JAK-STAT pathways that provide survival signals to the NKG2D+ CD8+ T cells downstream of IL-15 and IFNγ. Intriguingly, in the course of investigating the effects of JAK inhibitors on murine AA, it was observed that topical application resulted in thicker, more robust hair regrowth compared with systemic delivery. This effect was replicated in non-AA C57BL/6 mouse telogen skin [104] where topical JAK inhibitors were found to rapidly induce hair growth, in a manner analogous to physiological, spontaneous anagen. Further, using a qRT-PCR array of mouse dorsal skin throughout the hair cycle, JAK-STAT3 and JAK-STAT5 signaling were the most dynamically expressed, and their activity unexpectedly peaked during telogen. This invited us to postulate whether JAK-STAT signaling is necessary for maintaining of quiescence of HFSCs during telogen.

1.4.2 The JAK-STAT pathway

The JAK-STAT pathway is one of the most ubiquitous and pleiotropic signaling pathways in eukaryotic cells, and is a common downstream effector for many growth factors and cytokines. It was discovered in the late 1980s as a pathway downstream of interferon signaling, and many

of its components were cloned, characterized and named by the mid-1990s [105]. In mammals, the pathway is comprised of four JAKs (JAK1, JAK2, JAK3, Tyk2), and seven STATs (STAT1, STAT2, STAT3, STAT4, STAT5a, STAT5b, STAT6). Ligand binding to cell surface receptors results in a conformational change in the cytoplasmic domain of the receptors, which in turn activates the specific JAK molecules that are associated with the receptor. This leads to trans-phosphorylation of the JAKs, exposure of Src-homology (SH2) domains that recruit specific STAT protein dimers to the receptor complex. The STAT dimers are in turn phosphorylated by the JAKs, which allows for their translocation into the nucleus where they act as transcriptional regulators in various cellular processes. While JAK/STAT interactions are quite promiscuous (ie. all JAKs are potentially able to phosphorylate all STATs), the cell surface receptor and co-receptor structure and stoichiometry dictate the specific combinations of JAK and STAT molecules that are recruited during ligand binding in the particular cell. This gives rise to a remarkable combinatorial diversity of JAK-STAT signaling that is highly cell-type- and context-dependent [106].

Global constitutive knock-out experiments reveal JAK1, JAK2 and STAT3 to be the only embryonic-lethal components of the JAK-STAT pathway [107-109]. Genetic disruption of the other components results in varying degrees of hematological and immune deficiencies [110, 111], but skin and hair morphogenesis appear to be normal. While Tyk2 and STAT3 mutations in humans are associated with innate immune defects, elevated serum IgE and atopic dermatitis [112-114], no distinct hair phenotype has been described in these patients.

1.4.3 JAK-STAT3 signaling and the hair cycle

In order to circumvent the embryonic lethality of STAT3, Sano et al developed a *K5-Cre::STAT3*$^{FL/FL}$ mouse model that restricted STAT3 knock-out to the basal K5+ stem cells of the epidermis from E14.5 (constitutive knock-out) [115]. These mice were viable and underwent normal skin and hair morphogenesis and development, such that epidermal thickness, hair length and thickness were unaffected up to P11. Interestingly, although HF morphogenesis was normal, mutant mice were unable to enter the first spontaneous anagen at around P28. These mice also had delayed wound healing, likely a result of impaired keratinocyte migration. Surprisingly, mutant mice were able to enter anagen after plucking, or after topical application of phorbol 12-myristate 13-acetate (PMA) [19]. As the *K5-Cre::STAT3*$^{FL/FL}$ mice aged, they developed alopecia, scales, crusts and spontaneous ulceration. These set of experiments suggest that while STAT3 is not necessary for skin and HF morphogenesis, it is required for subsequent processes that require keratinocyte motility such as spontaneous hair cycling, wound healing and possibly maintaining proper barrier function and integrity. *K5-Cre::STAT3*$^{FL/FL}$ mice were also protected against epithelial carcinogenesis [116], which appears to be a STAT3-dependent process, and constitutively-active STAT3 mutants developed squamous cell carcinomas (SCC) at a higher rate [117]. These complementary studies conclude that JAK-STAT3 signaling in the HF is central to the activation and differentiation of HFSCs, in HF regeneration during the spontaneous hair cycle, wounding healing, and carcinogenesis. Since JAK-STAT3 signaling is associated with active processes like keratinocyte migration and differentiation, blocking this pathway with JAK inhibitors is not expected to promote hair growth during telogen.

1.4.4 JAK-STAT5 signaling and stem cell quiescence

Global STAT5 knockout mice are growth-stunted with mammary gland development defects, infertile, and have severe immunodeficiencies, but appear to undergo normal HF morphogenesis [118, 119]. However, the effect of STAT5 deletion on the adult hair cycle in these mice were not investigated.

HFSC quiescence in mice resulting from JAK-STAT5 signaling has been previously described in the context of pregnancy by Goldstein et al [120]. Systemic prolactin (PRL) secreted by the pituitary gland during pregnancy and lactation was shown to maintain HFSC quiescence in mice, possibly to divert resources to the developing fetuses. It is possible that the JAK-STAT5 axis utilized to maintain HFSC quiescence has physiological functions outside pregnancy and lactation.

Notably, JAK-STAT5 signaling also maintains the quiescence of stem cells in other systems. Conditional STAT5 knock-out in hematological stem cells (HSCs) using an *Mx-Cre::STAT5a/b*$^{FL/FL}$ mouse model showed increased loss of quiescence, proliferation and subsequent apoptosis of the stem cell compartment [121]. Stem cells of the liver (hepatic stellate cells, HSCs) have also been shown to rely on JAK2-STAT5 signaling to maintain quiescence in response to vitamin A and insulin [122].

In the HF, activated pSTAT5 is prominently expressed in the DP throughout the hair cycle, and may play a role in maintaining DP identity and its ability to initiate each round of anagen [123]. However, we have noticed that pSTAT5 expression in the DP tends to be constant, and does not fluctuate with the phases of the hair cycle [104]. Interestingly, in the HFSCs, pSTAT5 expression is restricted transiently to early- and mid-telogen [104, 124], positioning it as a likely candidate for maintaining HFSC quiescence.

1.4.5 Potential effectors of JAK-STAT mediated quiescence in the HFSC

The signaling pathways employed during HF morphogenesis have mainly been described as significant contributors to the adult the hair cycle. Inhibitory signals during telogen have been attributed to BMP-2 (from the subcutaneous adipocytes), BMP-4 (from within the hair follicle) [39], and BMP-6 and FGF-18 (from the K6+ inner bulge) [40]. However, none of these molecules signal through the JAK-STAT signaling pathway. As stated above, epidermal ablation of STAT3 had no adverse effect on HF morphogenesis, and STAT5-KO mice also seem to undergo normal HF development. This suggests that while JAK-STAT signaling was not essential for HF morphogenesis during embryogenesis, it has been utilized as one mechanism to coordinate the hair cycle in adulthood.

Candidates for the upstream ligand that maintains JAK-STAT signaling in the HFSC are currently unknown. To narrow down the likely candidates, all growth factors and cytokines whose receptors signal through the JAK-STAT pathway were considered (Figure 1.4, Table 1.1). Most cytokines that signal via the common γ-chain (eg. IL-2, IL-15) are involved in T cell development and differentiation [125], and were unlikely candidates for inhibitory effects on stem cells. Growth factors and hormones were also more likely to have activating functions, and most induce differentiation or migration in keratinocytes. This left the fascinating family of cytokines that includes IL-6, whose members have varied and sometimes inhibitory effects on stem cells in different tissues.

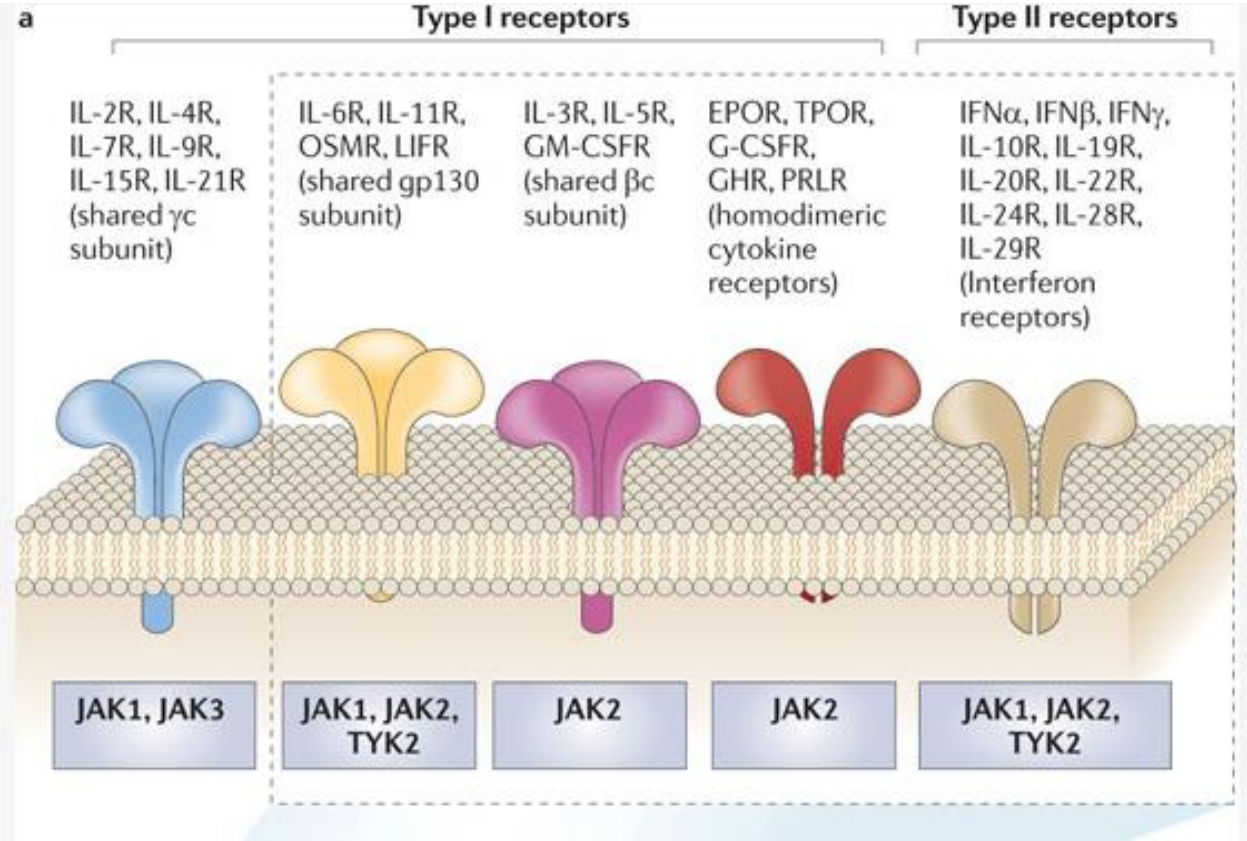

Figure 1.5. Classification of receptors that signal via the JAK-STAT pathway. Adapted from Qunitas-Cardama et al, 2011.

	Class of Receptor		Family members	JAK-STAT utilization										Role in adult skin/HF	Effects on keratinocyte proliferation	Role in quiescence
				JAK			TYK2	STAT								
				1	2	3		1	2	3	4	5	6			
IL-4TYPE 1 CYTOKINE RECEPTORS	Long Type	Heterodimeric α-chains [126]	IL-12											Protective against Th17-mediated skin inflammation	None [127]	N.R.
			IL-23											Mediates Th17 psoriasiform inflammation	+ (via TNF) [128]	N.R.
			IL-27												+ [129]	N.R.
		Shared gp130 co-receptor [130]	IL-6											Pro-inflammatory and induces catagen, promotes keratinization and retards hair growth [131, 132]	+ [133, 134]	Induces mammary gland involution via STAT3 [135]
			Oncostatin M (OSM)											Inhibits melanoma cell line proliferation [136], inhibits plucking-induced anagen [137]	↓ [138]	See section 1.4.3
			Leukemia Inhibitory Factor (LIF)											Induces psoriasiform epidermal hyperplasia [139, 140]	+ [140]	Embryonic stem cells [141]
			IL-11											May mediate UV-mediated loss of facial adipocytes [142]	N.R.	N.R.
			Cardiotrophin-1 (CT-1)											None	N.R.	N.R.
			Ciliary Neurotrophic Factor (CNTF)											None	N.R.	?Sertoli cells [143]
	Short Type	Hormones	Growth hormone (GH)											Promotes keratinocyte migration for wound healing [144]	+ [145]	N.R.
			Prolactin (PRL)											Altered hair cycle [146], induces catagen in cultured HF [147], and maintains HFSC quiescence during pregnancy and lactation [120]	+ [148]	Yes – with sex dimorphism and temporally restriction
			Thrombopoietin											Enhances wound healing through actions on monocytes [149]	N.R.	Hematopoietic stem cells [150]
			Erythropoietin											Enhances wound healing [151], promotes human HF growth in organ culture [152].	+ [152, 153]	N.R.
		Shared γ-chain	IL-2											May prime some SCCs to other inhibitory signals [154]	None [155]	N.R.
			IL-7											Growth factor for DETCs, produced by keratinocytes [156].	N.R.	N.R.
			IL-9											Mediates atopic dermatitis and lichen planus [157, 158]	+ [159]	N.R.
			IL-15											Mediates Th1 an NKT cell activity in skin (ie. psoriasis, AA, CTCL) [160]. Elevated in chronic wounds.	+ [161]	CD4 T cells [162]

	IL-4 family	IL-3	Attracts basophils, involved in urticaria [163].	N.R.	N.R.
		IL-4	Th2 cytokine mediating atopic dermatitis [164], impairs wound healing [88].	+ [165]	N.R.
		IL-5	Eosinophil chemokine in atopic dermatitis [166], bullous pemphigoid [167].	N.R.	N.R.
		GM-CSF	Promotes wound healing [168]	+ [168]	N.R.
TYPE 2 CYTOKINE RECEPTORS	Interferon (IFN) receptors [169]	IFN-α/β	Promotes Th1 inflammation including psoriasis [170] and AA [171].	↓ [172]	N.R.
		IFNγ	Enhanced antiviral response, reduced proliferation and differentiation, induces catagen in culture human HF [173].	↓ [174]	N.R.
		IL-10	Anti-inflammatory cytokine, produced during early phase of wound healing [175].	None [176]	N.R.
OTHERS	G-protein coupled receptors	Leptin	Induces anagen [177].	+ [178]	N.R.
		Angiotensin	N.R.	+ (via EGFR) [179]	N.R.
		Serotonin	Melanogenesis [180], may be increased in allergic skin diseases [181].	+ [182]	N.R.
	Growth factors	EGF	EGF-KO mice have slight delay in first hair cycle [183], EGF enhances keratinocyte migration [184].	+ [184, 185]	N.R.
		PDGF	PDGF from dermal adipocytes may activate HFSC during anagen [62].	+ [145]	N.R.

Table 1.1. Cytokines and growth factors/hormones that utilize the JAK-STAT signaling pathway. Adapted from [186-189]. N.R. = Not reported; + = induces proliferation, ↓ = inhibits proliferation. Note that OSM is the only cytokine in this list that has been reported to inhibit keratinocyte proliferation, and maintain quiescence in stem cells of other systems. **Pink box** represents data from this Thesis.

Table 1.2. Role of JAK-STAT signaling and immune cell involvement during the hair cycle

Phase of hair cycle	Evidence for JAK-STAT signaling	Evidence for immune cell involvement
Telogen (rest)	• Pharmacological JAK-STAT inhibition induces anagen [104]. • Prolactin-JAK-STAT5 signaling maintains HFSC quiescence during pregnancy and lactation [120].	• Macrophages predominate during telogen, and clodronate liposomes induce anagen [89].
Anagen (spontaneous)	• Constitutive epidermal STAT3 ablation inhibits first spontaneous anagen [19], but not plucking induced anagen.	At the end of telogen, macrophages undergo apoptosis and release Wnt7a, which stimulates anagen [89].
Anagen (depilation induced)		T regulatory cells mediate anagen via Jagged1-Notch signaling [83].
Anagen (plucking induced)		Inflammatory “M1-like” macrophages are recruited to plucked HFs by CCL2, and produce TNF-α that stimulates anagen [82].
Wound-induced HF neogenesis (WIHN)		γδ T cells produce FGF-9 that facilitates new HF formation in a regenerating wound [85].
Catagen (regression)	IL-6 induces catagen in anagen HFs [131].	Macrophages are recruited to clear regressing follicles [36], and produce FGF-5 that facilitates catagen [27, 28].

1.5. Oncostatin M and the IL-6 family of cytokines

1.5.1. The IL-6 family of cytokines

The IL-6 family of cytokines include IL-6, Oncostatin M (OSM), Leukemia Inhibitory Factor (LIF), IL-11, cardiotrophin-1 (CT-1) and ciliary neurotrophic factor (CNTF). The receptors for these cytokines require the co-receptor gp130 for signaling transduction via the JAK-STAT pathway, mostly via JAK1, JAK2 and Tyk2, and downstream STAT1, STAT3 and STAT5 [190]. Depending on the cell and tissue type, this family of cytokines are also able to signal via the PI3K-Akt and MAPK pathways. While IL-6 itself is able to induce gp130 homodimerization [191], all other members of the family signal through heterodimerization of their nascent receptor with gp130.

IL-11 and CT-1 are mainly associated with active processes, such as airway inflammation [192] and cardiac muscle hypertrophy [193] respectively, and both have growth-promoting actions on neurons from dorsal root ganglia [194]. However, they have not been shown to have any inhibitory or quiescence-related functions (Table 1.1). Other members of the family have a more varied and pleiotropic range of functions. LIF signaling is essential for the survival and self-renewal of embryonic stem cells (ESCs) in mice and humans [141, 195], and inhibits differentiation and proliferation in the COS-1 cell line via the JAK-STAT3 pathway [196]. Both LIF and CNTF also promote the survival of co-cultured rat Sertoli cells and gonocytes without affecting their proliferation [143].

IL-6 is an acute-phase cytokine that has pro-inflammatory roles in auto-inflammatory diseases like rheumatoid arthritis [197]. In the skin, IL-6 overexpression leads to reduced body weight,

sparse hairs, and increased epidermal keratinization without evidence of hyperproliferation [132]. Levels of IL-6 are increased significantly in lesional psoriatic skin, and IL-6 promotes keratinocyte proliferation *in vitro* [134]. However, Kwack et al showed that IL-6 inhibited HF matrix proliferation in human HF organ cultures, and could induce catagen when injected into the skin mice in anagen [131]. Paradoxically, IL-6 injected into the telogen skin Wistar rats was able to *induce* anagen [198], which may be due to species differences.

1.5.2. Effects of OSM on the hair cycle

In humans, OSM was first discovered as a negative growth regulator of the A375 melanoma cell line [136], at a time when much research was focused on identifying endogenous regulators of cancer cell growth. While OSM was first isolated in the supernatant of histiocytic lymphoma cells [136], it was found to be more reliably obtained from macrophage cell lines [199]. OSM was found to have pleiotropic properties, and (in humans) signals via the Leukemia Inhibitory Factor receptor (LIFRβ) in addition to OSMRβ. Its effects have been shown to be tissue- and context-dependent, acting as a growth inhibitor in some cell lines, and as an activator in others [200, 201]. These receptors were given the suffix -β because they were recruited second to the ligand-gp130 complex [202], unlike the α-receptors of IL-6R which were recruited first.

Yu et al showed that OSM was able to inhibit human HF growth in organ culture, and prevent plucking-induced anagen in C3H/HeJ mice using OSM-soaked beads [203]. Yu et al also showed with immunohistochemistry that in human HFs, OSM was expressed in the IRS, ORS and DP, while its receptor OSMRβ was only localized to the ORS. Using the online resource HairGel.net, developed by the Rendl laboratory who used multicolor FACS to perform RNA-sequencing on almost every cellular compartment in the skin of the mouse at P5 [8, 204],

OSMRβ and the co-receptor gp130 (gene name *Il6st*, see Box 1) are preferentially expressed in the epithelial compartment, particular the HFSCs, whereas OSM has in unknown cellular source in the dermis (Figure 1.5). Whether OSM is expressed in the skin of adult mice during the hair cycle is currently unknown.

Box 1. OSM signaling nomenclature

OSM – Oncostatin M

OSMRβ – β-receptor for OSM, so named because it is recruited *after* OSM binds to gp130, gene name *Osmr*

gp130 – co-receptor used by IL-6 family of cytokines, gene name *IL6 signal transducer*

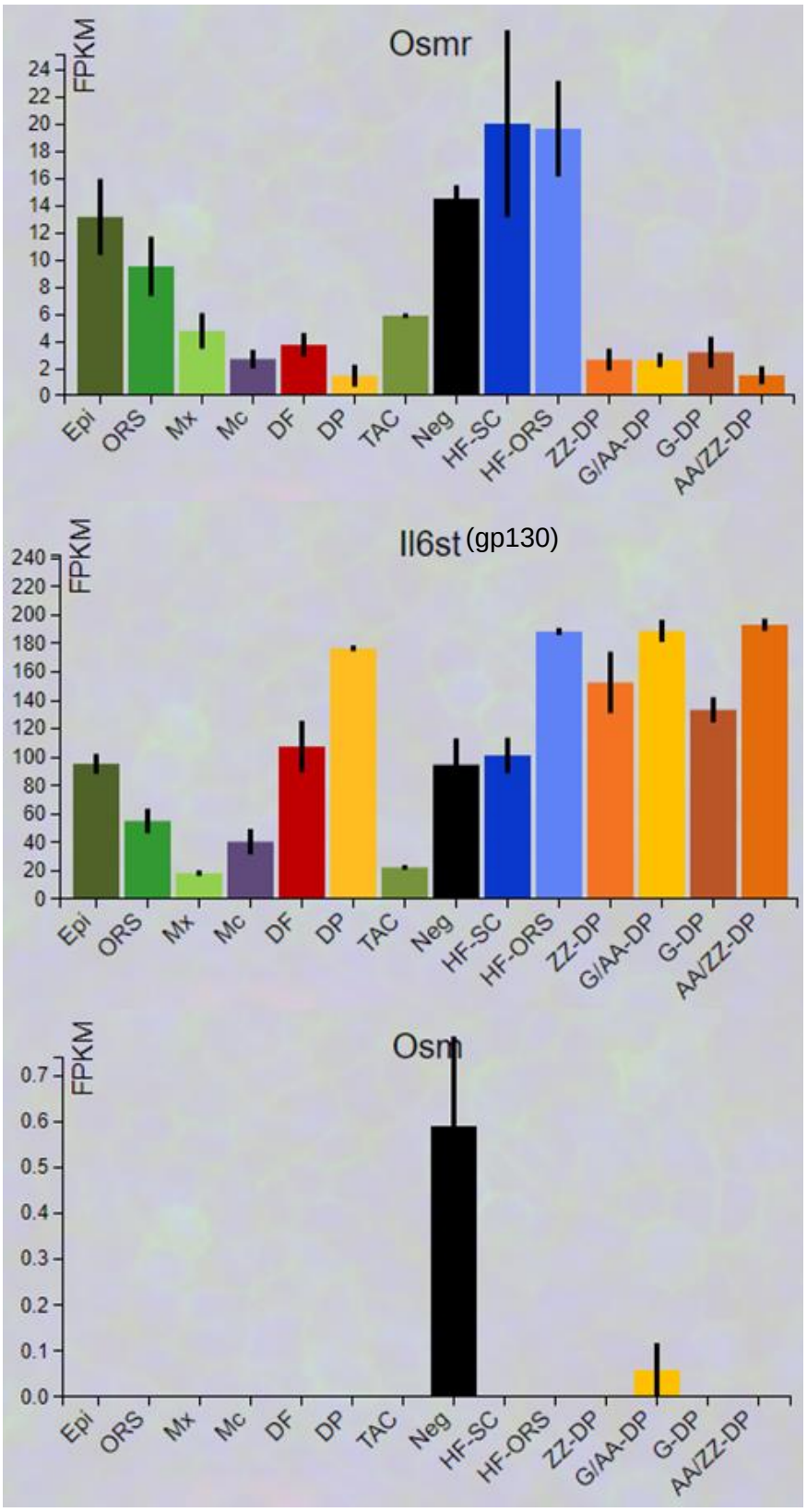

Figure 1.6. Results from searches performed on Hair-Gel.net, an online resource by the Rendl laboratory that catalogues RNA-sequencing data from multiple compartments of mouse skin at E14.5 and P5 (Sennett et al, 2015; Rezza et al, 2016). Data shown represents tissue distribution of OSMR, gp130 (Il6st) and OSM in the skin of a mouse at P5. OSMR is expressed mainly in the epidermal compartment, while OSM is expressed in the "neg" compartment, which includes unlabeled dermal cells that were not actively sorted (ie. immune cells, endothelial cells, smooth muscle cells). The gp130 co-receptor is relatively ubiquitous in expression. Epi = epidermis, ORS = Outer root sheath, Mx = Matrix, Mc = melanocytes, DF = dermal fibroblasts, DP = all dermal papilla cells, TAC = transit amplifying cells, HF-ORS = ORS minus HFSC, ZZ-DP = DP of zigzag hair follicles, G-DP = guard hair DP, AA-DP = awl/auchenne DP.

1.5.3. OSM mediates quiescence via JAK-STAT signaling in various cell types

In addition to its inhibitory properties on melanoma cell lines, OSM has been shown to have inhibitory effects on proliferation and differentiation in other systems. Like LIF, OSM is also able to inhibit differentiation of human ESCs [205]. In skeletal muscle, OSM prevents differentiation of myoblasts via the JAK1-STAT1-STAT3 pathway, and plays role in regulating muscle regeneration [206]. During mammary gland involution, OSM signaling via STAT3 also promotes remodeling by inducing epithelial cell apoptosis [207]. In human mammary gland epithelium, OSM-STAT3 signaling cooperates with Transforming Growth Factor (TGF)-β-SMAD3 signaling to induce senescence [208]. Interestingly, aged and senescent murine skin is also associated with increased JAK-STAT activity [209], although an upstream ligand for this effect has not been identified.

OSM signaling via the JAK-STAT5 pathway inhibits adipogenesis and adipocyte terminal differentiation of 3T3-L1 and mouse embryonic fibroblasts (MEFs) treated with dexamethasone, insulin and 3-isobutyl-1-methylxanthine (IBMX) [210]. OSM also arrests HepG2 cells in the G1 phase of the cell cycle via JAK-STAT5 signaling, which upregulates cyclin-dependent kinase (CDK) inhibitor p27kp1 that in turn reduces downstream CDK2 activity [211]. OSM via JAK-STAT5 signaling also suppresses specific chemokine secretion in T cells [212].

Global OSM-KO mice were found to have hematological discrepancies like anemia and thrombocytopenia, together with increased circulating PBMCs and decreased numbers of HSCs, suggesting a loss of quiescence in the HSC niche [213]. Otherwise, OSM-deficient mice developed normally and appeared indistinguishable from wild-type littermates, suggesting that

there were no gross hair or skin defects, and that OSM is not required for HF morphogenesis. The hair cycle was not closely studied in these mice.

Together, these studies show that OSM signaling via the JAK-STAT pathway is a conserved and often employed for maintaining cellular quiescence in various contexts, making it a potential candidate chalone for HFSCs.

1.6. SUMMARY

Our serendipitous observation that JAK inhibition in mouse skin was sufficient to initiate hair growth invited us to ask whether there is a JAK-STAT signal that mediates quiescence in the HFSCs. This inhibitory signal would fit the criteria for a chalone as described by Houck et al, and would be a potential therapeutic target for hair growth disorders associated with prolonged or arrested telogen. An extensive review of the literature suggests that members of the IL-6 family of cytokines are ideal candidates for this chalone, and that dermal macrophages, which have been suggested to have important roles in the telogen-to-anagen transition, may be a source for this signal.

AIMS OF THIS THESIS

In this thesis, I asked the following questions:

1. What is the upstream effector of JAK-STAT signaling in the HFSC during telogen?
2. What is the source of this “chalone”?
3. What is the downstream mechanism that mediates quiescence in HFSCs?

CHAPTER 2. ONCOSTATIN M IS PRODUCED BY TREM2+ MACROPHAGES AND MAINTAINS HAIR FOLLICLE STEM CELL QUIESCENCE DURING MURINE TELOGEN

The mammalian hair cycle is a tightly coordinated process whereby the hair follicle undergoes distinct phases of growth (anagen), regression (catagen) and rest (telogen) [6]. Each phase of the hair cycle requires complex cellular interactions and molecular signals that directs the hair follicle stem cells (HFSCs), their epithelial progeny in the outer and inner root sheaths of the hair follicle (HF), and the instructional mesenchyme (the dermal papilla, DP) to produce or shed a hair shaft [7]. The keratinocytes of the HFSCs (located in the bulge and secondary hair germ, HG) receive activating signals, such as Wnt and Shh, that promote proliferation during anagen, and inhibitory signals, such as BMP, that promote quiescence during telogen. These signals are received from the microenvironment of the HF and may emanate from the DP or other cells types like the subcutaneous adipose tissue [39], and the K6+ inner bulge [40].

Cells of the immune system have been implicated in regulation of HFSC activity. For example, various classes of immune cells are recruited during depilation- and plucking-induced anagen (Table S1), and although these experimentally-induced anagen models are useful in studying anagen progression in the mouse, they do not give us much insight into immune cell regulation of the spontaneous hair cycle. The normal hair cycle is associated with significant alterations of the local immune cell composition [75], but these associations have been largely descriptive. Recently, macrophages have been shown to increase in numbers during early- and mid-telogen [36, 89], and may play a role in regulating the niche of HFSCs during various stages of the hair cycle.

We have previously shown that pharmacological inhibition of JAK-STAT signaling is sufficient to induce anagen in “resting” telogen follicles in a manner analogous to physiological, spontaneous anagen [104]. This raises the question of whether JAK-STAT signaling is necessary for the maintenance of quiescence of HFSCs during telogen. So far, inhibitory signals during telogen have been attributed to BMP-2 (from the subcutaneous adipocytes) and BMP-4 (from within the hair follicle) [39], as well as BMP-6 and FGF-18 (from the K6+ inner bulge) [40]. However, none of these molecules are known to signal through the JAK-STAT signaling pathway. The upstream signal for JAK-STAT-mediated quiescence during telogen, if any, remains unknown.

Oncostatin M (OSM) has been shown previously to inhibit plucking-induced anagen [137], while interleukin 6 (IL-6) has been shown to induce catagen in anagen follicles [131]. Both OSM and IL-6 belong to the gp130-dependent family of cytokines, which also includes leukemia inhibitory factor (LIF), cardiotrophin-1 (CT-1), ciliary neurotrophic factor (CNTF) amongst others. These cytokines signal via the JAK-STAT pathway, and the MAPK (mitogen-activated protein kinase), mTOR (mammalian target of rapamycin) and PI3K (phosphatidylinositol-3 kinase) pathways, to regulate a variety of biological processes, most notably stem cell maintenance and quiescence in a variety of tissue types [214, 215]. Thus, OSM, and/or the IL-6 family of cytokines, may be a potential *chalone*, or negative growth factor [2], in the mouse telogen skin.

In this paper, we demonstrate that OSM maintains HFSC quiescence via JAK-STAT5 signaling *in vivo*, giving further insight to previous reports that OSM is associated with maintenance of the telogen state [137]. In addition, we identify a distinct subset of TREM2+ dermal macrophages as an endogenous source for OSM in mouse skin.

RESULTS

Oncostatin M maintains hair follicles in telogen via OSMR-JAK-STAT signaling

We first tested OSM and other gp130 cytokines (IL-6 and Leukemia Inhibitory Factor, LIF) on their ability to inhibit anagen induced by topical JAK inhibitors, which has been described to resemble spontaneous anagen [104]. At P60, Ruxolitinib 2% (JAK1/2 selective inhibitor) in DMSO was applied topically to the right dorsal skin of C57BL/6 mice for five consecutive days. This treatment has been established in our lab to induce a robust anagen. Simultaneously, and for 5 additional days (for a total of 10 consecutive days), OSM, IL-6, LIF or PBS control was injected intradermally into a spot on the right dorsum of a P60 (mid-telogen) C57BL/6 mouse, in the middle of the field of topical Ruxolitinib (JAK1/2 selective inhibitor) application. Intradermal OSM was the only member of the gp130-dependent class of cytokines that inhibited anagen locally in the area where it was administered (Figure 2.1A).

Conversely, intradermal injection into the dorsal telogen skin (P60) of neutralizing antibodies to the OSM receptor (OSMRβ) for 2 weeks produced the complementary effect of local anagen induction (Figure 2.1B). This effect was not observed with intradermal PBS or isotype IgG control.

In order to assess the effects of OSM on HFSCs, ITGA6+ Sca-1- epidermal cells were isolated from telogen skin (Figure 2.2A, adapted from [216]), and were cultured and stimulated with increasing doses of OSM. OSM displayed a dose-dependent activation of the JAK-STAT1, JAK-STAT3, JAK-STAT5 and MAPK-ERK pathways in cultured HFSCs *in vitro* (Figure 2.1C). OSM had minimal effects on the PI3K/Akt/mTOR pathway. Localization of pSTAT1 *in vivo* during

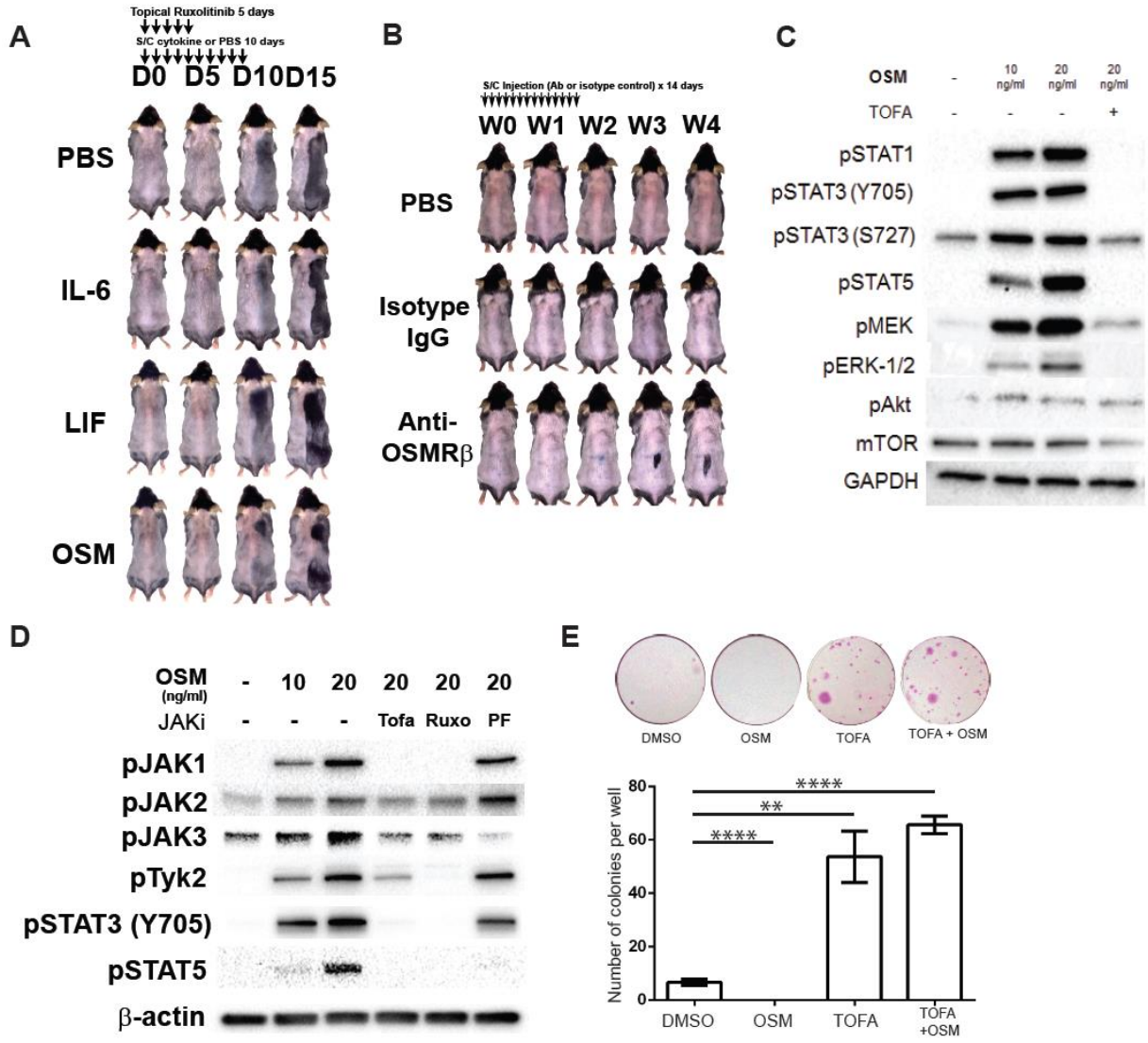

Figure 2.1. **OSM prevents HFSC proliferation via OSMR-JAK-STAT5 signaling. A**. C57BL/6 mice were treated on the right dorsal skin topically with Ruxolitinib 2% in DMSO at P60 for 5 days, recapitulating our previous experiments reported in Harel et al, 2015. This treatment regimen stimulates a robust anagen in the telogen skin that resembles the spontaneous, normal hair cycle. From P60, mice were also injected with control PBS or a gp130 cytokine (IL-6, LIF or OSM) into the middle of the field of topical application for 10 days. OSM was the only member of this family that was sufficient for preventing Ruxolitinib-induced anagen. Note that the lightness seen in the LIF-injected mouse is due to coat sheen rather than bare skin. Data from 2 independent experiments with n = 4 mice per group. **B.** Neutralizing antibodies to murine OSMRβ was injected intradermally into the center of the telogen back skin in P60 C57BL/6 mice for 2 weeks. This was sufficient to induce a local anagen, while PBS and isotype IgG controls did not. Data from 3 experiments with n = 3 mice per group. **C**. Western blots performed on cultured HFSCs (ITGA6+ Sca-1-) exposed to OSM at 10ng/ml and 20ng/ml for 15 minutes. OSM activated JAK-STAT1/3/5 pathways and the MAPK-MEK-ERK pathways in HFSCs, and had minimal effect on the PI3K/Akt/mTOR pathway. Pre-treatment with Tofacitinib inhibited the JAK-STAT and, to a lesser extent, the MAPK-MEK-ERK pathways. Total protein levels were not expected to change with short treatment times, and are not shown. **D.** Western blot of cultured HFSCs stimulated with OSM for 15 minutes, with or without pre-treatment with JAK inhibitors. OSM had a dose-dependent activation of all four JAKs (JAK1, JAK2, JAK3, Tyk2), as well as pSTAT3 and pSTAT5. Tofacinitib and Ruxolitinib pre-treatment inhibited phosphorylation of a variety of JAKs, and inhibited both pSTAT3 and pSTAT5 activation. PF-06651660, a specific covalent inhibitor of JAK3, did not have an effect on JAK1/JAK2/Tyk2 or STAT3 phosphorylation but still inhibited pSTAT5 activation. **E.** Clonogenicity assays of HFSCs. ITGA6+ Sca-1- epidermal stem cells were isolated by FACS, plated in 6-well plates, and cultured for 2 weeks. Addition of OSM 10ng/ml to the culture media completely prevented any stem cell colonies from forming, whereas the addition of Tofacitinib 100nM enhanced HFSC clone numbers, and also reversed the effect of OSM. (Data from 3 independent experiments)

telogen by immunofluorescence places its activity in the isthmus and infundibulum of the HF, and not the bulge/HG (Figure 2.2B).

OSM signaling occurs through all four JAK kinases (JAK1, JAK2, JAK3 and Tyk2) (Figure 2.1D). These pathways were blocked with the addition of Tofacitinib (pan-JAK inhibitor). With the addition of a specific, covalent JAK3 inhibitor PF-06651600, we found that while different JAK inhibitors had varying effects on JAK1/2/3/Tyk2 and STAT3 phosphorylation, all of them resulted in potent pSTAT5 inhibition (Figure 2.1D). Notably, the covalent JAK3 inhibitor was able to initiate anagen with the 5-day topical treatment regimen previously described (Figure 2.2C), without significant inhibition of STAT3 phosphorylation in HFSCs. This suggests that inhibition of STAT5 phosphorylation, and not STAT3, in HFSCs is the common mechanism, and is sufficient to promote anagen initiation in mid-telogen skin.

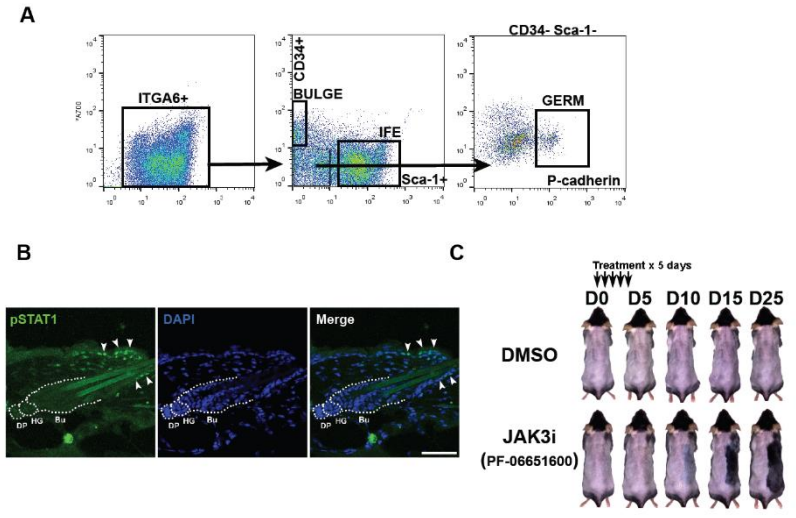

Figure 2.2. **Supporting Data. A**. Flow cytometric strategy for isolating HFSCs in the epidermis. All ITGA6+ cells are included, and Sca-1+ cells are identified as interfollicular epidermis. Sca-1- populations are associated with the HF. Of these, CD34+ cells represent the bulge, and P-cadherinhi cells represent the hair germ (HG). **B.** pSTAT1 immunofluorescence during telogen. STAT1 signaling is not located in bulge (Bu) or (HG) HFSCs, but instead is localized to the isthmus and infundibulum of the HF (arrowheads). DP = Dermal papilla. Scale bar 50µm. **C.** Topical treatment with covalent JAK3 inhibitor PF-06651600 induces anagen in telogen skin.

Colony-forming assays with isolated (ITGA6+ Sca-1-) HFSCs were performed in the presence of OSM (10ng/ml), Tofacitinib (100nM) or both (Figure 2.1E). OSM prevented HFSC colonies from forming *in vitro*, consistent with its inhibitory effect on hair growth. Tofacitinib increased the

colony-forming ability of HFSCs, as well as increasing the colony size, consistent with previous reports [209]. The addition of Tofacitinib was also sufficient to rescue the inhibitory effects of OSM. These results suggest that OSM acts via JAK-STAT signaling, and most likely via activation of STAT5, to prevent proliferation of HFSCs, and is sufficient for maintaining HFSC quiescence during telogen in mouse skin.

OSMRβ and its co-receptor gp130 are expressed on bulge and germ HFSCs, co-localizing with activated pSTAT5 during early- and mid-telogen

In the mouse, OSM binds specifically to its receptor OSMRβ, which requires the co-receptor gp130 for signaling via the JAK-STAT pathway. We next sought to localize the expression of OSM, its receptor (OSMRβ) and co-receptor (gp130). By separating the mouse dorsal skin into the epidermal and dermal compartments with 0.25% trypsin and performing qRT-PCR for OSMRβ and OSM, we showed that OSMRβ was distinctly expressed in the epidermal fraction (which contains the epithelial parts of hair follicles), whereas OSM was located in the dermal fraction (which contains the dermal cells and the dermal papilla, DP) (Figure 2.3A).

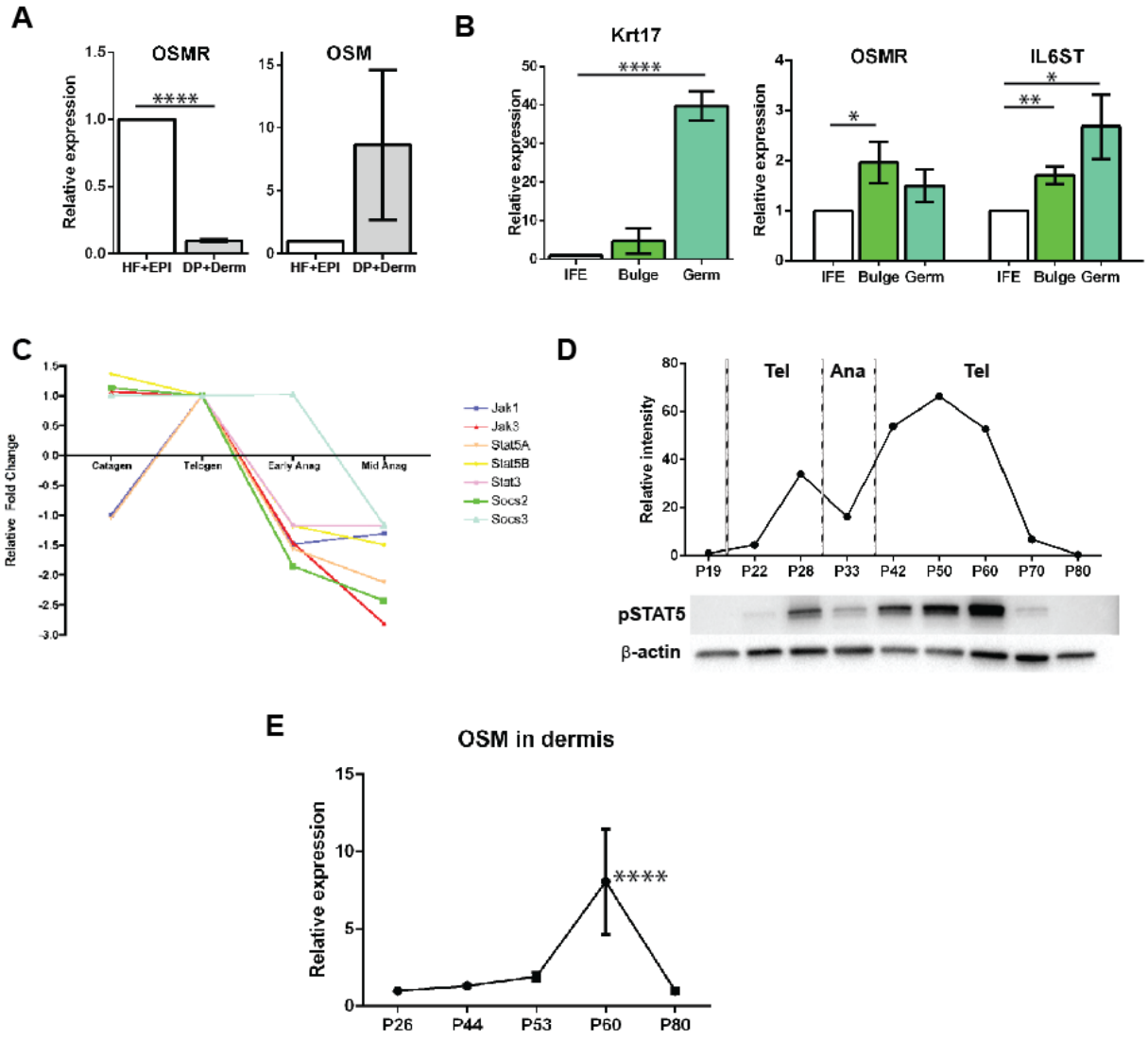

Figure 2.3. Spatiotemporal distribution of OSM signaling apparatus during hair cycle. **A.** Trypsin-dissociated epidermal and dermal tissue from P60 C57BL/6 mice were subjected to qRT-PCR for OSMRβ and OSM. The epidermal sheet contains the hair shafts, whereas the DP was retained with the dermal fraction. The epidermal fraction is enriched for OSMRβ ($p < 0.0001$), while the dermal fraction is enriched for OSM ($p=0.21$). A clear dermal-epidermal signaling axis for OSM is demonstrated. (n = 3 mice) **B.** Flow cytometric analysis of the epidermal ITGA6+ stem cells into IFE (Sca-1+), bulge (CD34+) and HG (P-cadherin+). qRT-PCR for Keratin 17 (hair shaft keratin) was performed to confirm the sorting strategy. OSMRβ and gp130 are expressed at higher levels in the HFSCs of the bulge and HG. (n = 3 mice) **C.** qRT-PCR array of JAK-STAT genes across the hair cycle (adapted from Harel et al, 2015). STAT5a/b and STAT3 expression peak during telogen. **D.** Western blot for pSTAT5 in isolated epidermis across the hair cycle. Consistent with the qRT-PCR array data, pSTAT5 activation peaks during telogen (Tel), more prominently in during early- and mid-second telogen (P42-P60). Ana = Anagen. (n = 1 mouse per timepoint) **E.** qRT-PCR for OSM in isolated dermis across the hair cycle. OSM levels peak from early-mid telogen in C57BL/6 mice. (n = 2 mice per timepoint) Data are mean ± SEM. *$p < 0.05$, **$p < 0.01$, ***$p < 0.001$, ****$p<0.0001$, (A) Student's unpaired t-test. (B) One-way ANOVA between cellular compartments.

To further define the expression of OSMRβ and gp130, the epidermal fraction was separated by fluorescence activated cell sorting (flow cytometry or FACS) into the Sca-1+ interfollicular epidermis (IFE), CD34+ bulge, and the P-cadherin+ hair germ (HG) (Figure 2.2A). qRT-PCR for Keratin 17 (a differentiated HF keratin) validated this sorting strategy with an increasing expression of Krt17 from IFE->Bulge->HG (Figure 2.3B). qRT-PCR confirmed that OSMRβ and gp130 were preferentially expressed in the bulge and HG telogen HFSCs. This was confirmed with immunofluorescence (Figure 2.4A). Of note, gp130 is also expressed in many other cell types in the dermis.

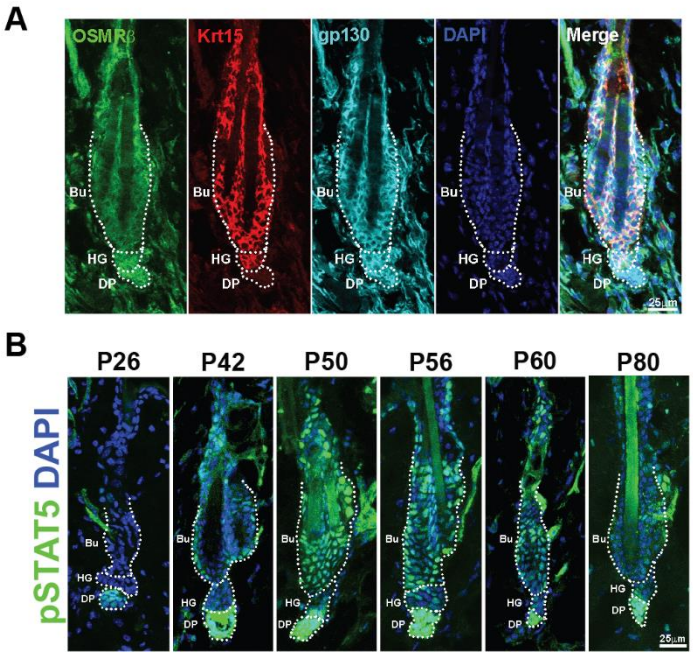

Figure 2.4. Immunofluorescence of OSMRβ and gp130 in telogen HF.

A. Immunofluorescence of P60 telogen hair follicle showing co-localization of OSMRβ and gp130 in the HFSC compartment, marked with the stem cell marker Keratin 15. Note that gp130 expression is ubiquitous, but strong in the HG. OSMRβ expression is also expressed in scattered dermal cells. Scale bar 25μm. **B.** Immunofluorescence of pSTAT5 across the hair cycle. Activation of pSTAT5 localizes to the HFSC compartment particularly strongly from P42-P60, which represents early-to-mid second telogen, and is diminished in the first telogen (P26) and late second telogen (P80), when the hair follicle is ready to enter the next anagen phase.

In keeping with our previous qRT-PCR array data showing dynamic STAT5 activity over telogen (Figure 2.3C) [104], we show with Western blotting of isolated epidermal sheets that activated pSTAT5 protein is also dynamically expressed in the epidermis across telogen, peaking at mid-telogen around P56-P60 (Figure 2.3D). Using immunofluorescence studies, we show that

pSTAT5 during early- and mid-telogen is localized prominently in the bulge and HG HFSCs (Figure 2.4B). pSTAT5 expression in the HFSC decreases by the end of telogen (P80), in agreement with recent publications [124]. This peak of pSTAT5 activity in the HFSC coincides with a peak of OSM expression in the dermis, measured with qRT-PCR (Figure 2.3E). These data show that elevated OSMRβ-pSTAT5 signaling in HFSCs is correlated with early- and mid-telogen, and decreases during late telogen.

Genetic ablation of OSMRβ before early telogen delays and shortens the second telogen

To examine the significance of OSMRβ and pSTAT5 localization to telogen hair follicles, we generated C57BL/6 mice with *K5-CreERT*$_2$ transgenes coupled with either *OSMRβ*$^{FL/FL}$ or *STAT5a/b*$^{FL/FL}$ alleles. Mice were closely shaved with clippers to allow for direct visualization of the dorsal skin, which appears uniformly pink during the synchronized second telogen (P45-P100), and darkens in tandem with the entry into anagen when melanocytes proliferate. Systemic administration of tamoxifen was carried out during early-to-mid telogen to genetically ablate either OSMRβ or STAT5 in epidermal stem cells, including the HFSC. OSMRβ and STAT5 conditional knock-out was confirmed with qRT-PCR, Western blot and immunofluorescence studies (Figures 2.5A-E). Interestingly, epidermal OSMRβ ablation was associated with loss of pSTAT5 in the HFSCs in telogen (Figure 2.5C).

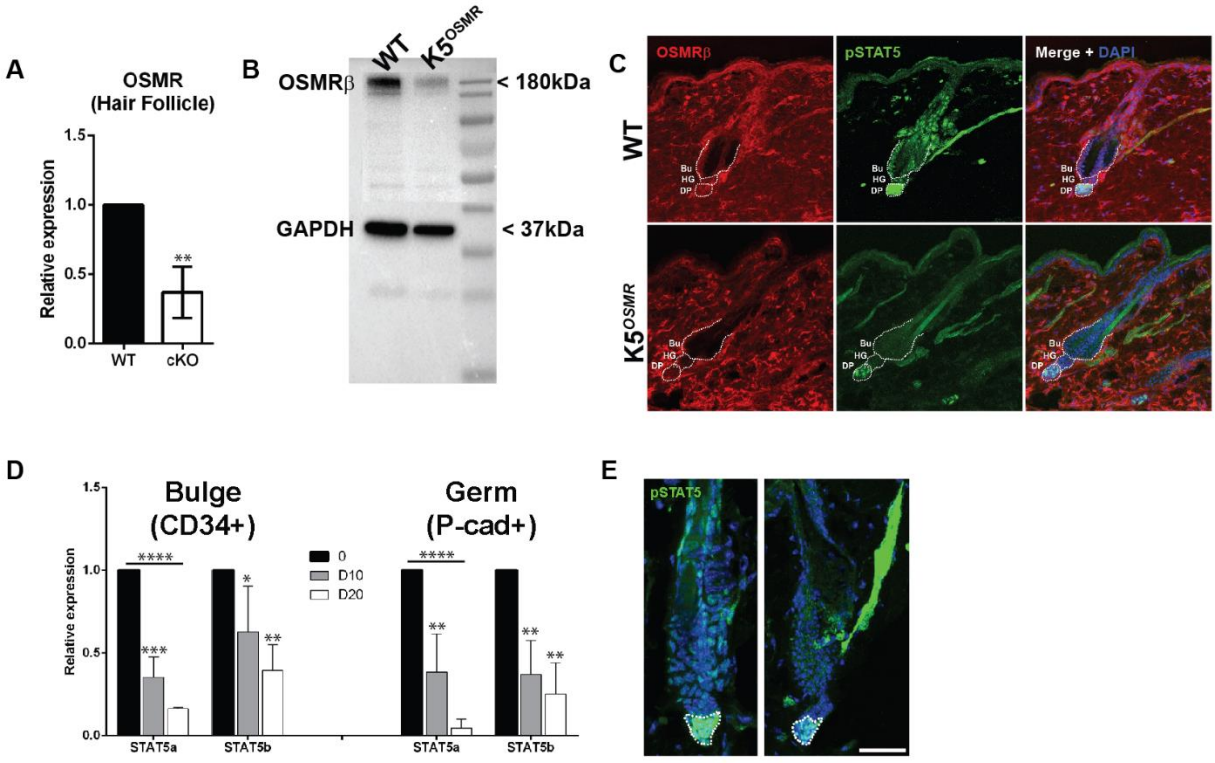

Figure 2.5. Validation of OSMRβ and STAT5 conditional KO. A. qRT-PCR for OSMRβ in the hair follicle of K5-CreERT2::OSMRβ$^{FL/FL}$ mice. HFSCs include bulge and HG cells (ITGA6+ Sca-1-). **B.** Western blot of whole epidermis in K5-CreERT2::OSMRβ$^{FL/FL}$ mice showing reduced expression of OSMRβ after Tamoxifen induction. **C.** Immunofluorescence studies of telogen HFs in WT and K5-CreERT2::OSMRβ$^{FL/FL}$ mice. K5-CreERT2::OSMRβ$^{FL/FL}$ mice had reduced expression of OSMRβ in the bulge and HG, coupled with reduced pSTAT5 activity in the HFSCs. pSTAT5 expression in the DP remained unchanged. Scale bar 50µm. **D.** qRT-PCR for STAT5a and STATb in K5-CreERT2::STAT5a/b$^{FL/FL}$ mice, in the bulge and germ at +10 and +20 days post-tamoxifen. STAT5a/b expression continued to decrease from +10 to +20 days likely because cells with reduced STAT5a/b began to proliferate and predominated the HFSC compartment. **D.** Immunofluorescence studies for pSTAT5 in WT and K5-CreERT2::STAT5a/bFL/FL mice 20 days after Tamoxifen induction. Data are mean ± SEM. *p < 0.05, **p < 0.01, ***p < 0.001, ****p<0.0001. Student's unpaired t-test.

When we ablated OSMRβ or STAT5 at P35-P38 (end of anagen, just before catagen), we found that the upcoming second telogen, which typically lasts 40-60 days in the C57BL/6 mouse, was drastically shortened to less than 2 weeks (Figure 2.6A). Interestingly, in the *K5-CreERT$_2$::STAT5a/b$^{FL/FL}$* mice, despite close shaving, their dorsal skin remained dark and pigmented, suggesting the persistence of the anagen phase (Figure 2.6A – last row). With pigmentation of shaved dorsal skin as a surrogate for anagen, *K5-CreERT$_2$::OSMRβ$^{FL/FL}$* and *K5-CreERT$_2$::STAT5a/b$^{FL/FL}$* mice appeared not to enter full telogen as did their wild-type

littermates (Figure 2.6B). This was confirmed with histology at P60, when control wild-type littermates had small telogen HFs that had retracted entirely within the dermis, both homozygous mutant mice for *OSMRβ* and *STAT5a/b* were in anagen (Figure 2.6C).

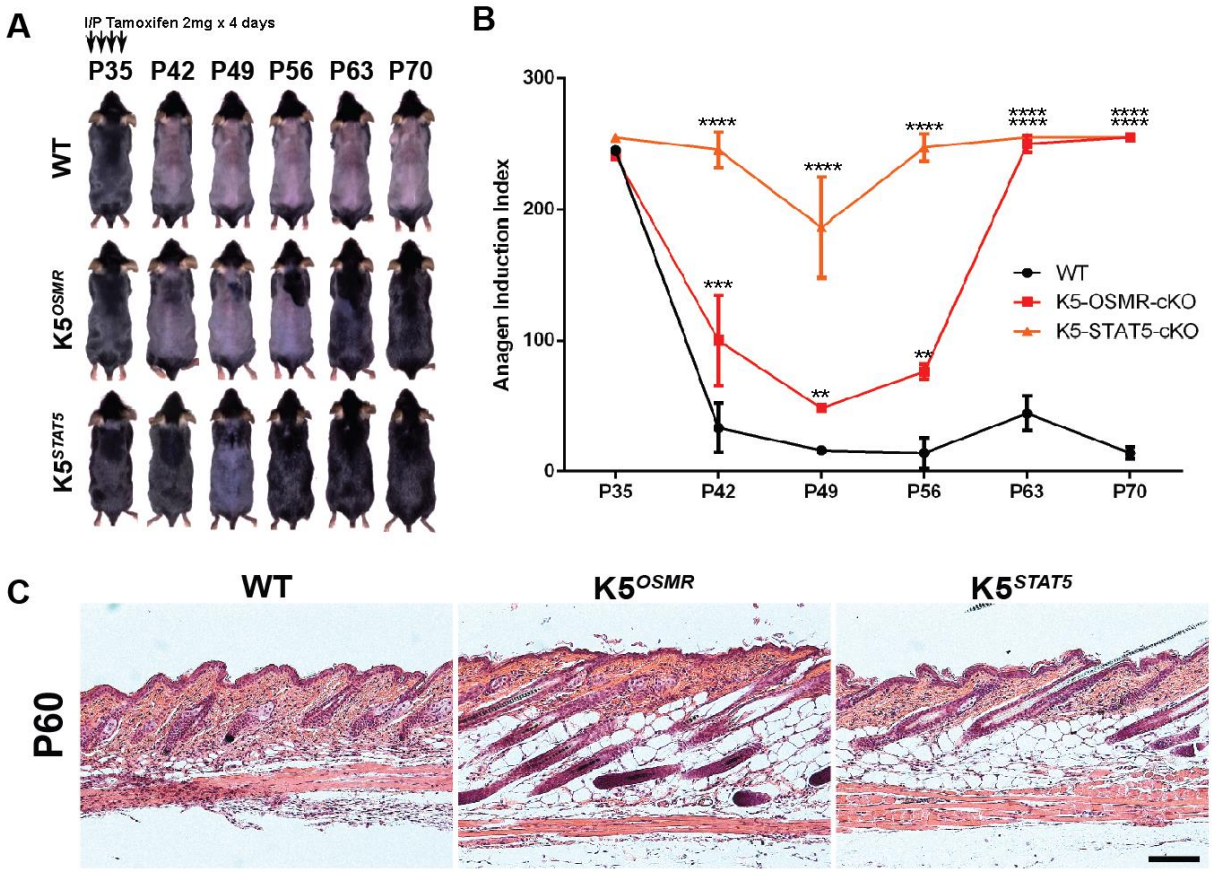

Figure 2.6. Early telogen ablation of OSMRβ/STAT5. A-B. Conditional knock-out of either the OSMRβ or the STAT5 gene using the K5-CreERT2 driver before the early telogen resulted in a much shortened telogen phase. STAT5 ablation during catagen prevented HFSC from reaching full quiescence. Anagen quantification was performed using threshold analysis of the dorsal skin color in ImageJ, since darkening of the skin due to melanogenesis is coupled closely to anagen progression. Mice were closely shaved one day before acquisition of pictures to ensure a close view of the epidermal color. Results are representative of 5 litters for each gene (OSMRβ or STAT5), with 2-5 mice per litter, for a total of 17 mice for OSMRβ (5 homozygous *OSMRβ*$^{FL/FL}$) and 18 mice for STAT5 (5 homozygous *STAT5*$^{FL/FL}$). Data are mean ± SEM. *p < 0.05, **p < 0.01, ***p < 0.001, ****p<0.0001; Two-way ANOVA between genotypes at each respective timepoint **C.** H&E examination of WT, *K5-CreERT2::OSMRβ*$^{FL/FL}$ mice. *K5-CreERT2::OSMRβ*$^{FL/FL}$ mice which underwent Tamoxifen induction at P35-P38. At P60, when WT littermates were well into telogen, mice lacking OSMR or STAT5 in their epidermal compartments were well into their next anagen phase. Scale bar 100µm.

Genetic ablation of OSMRβ and STAT5 during telogen in the epidermis promotes HFSC proliferation and anagen initiation

Using genetic means to recapitulate the pharmacological effect of JAK-inhibition in mouse telogen skin, tamoxifen induction was carried out during mid-telogen (P56-P60) over a period of 4 days to conditionally knock-out either OSMRβ or STAT5 in the epidermis and hair follicle. Both *K5-CreERT$_2$::OSMRβ$^{FL/FL}$* and *K5-CreERT$_2$::STAT5a/b$^{FL/FL}$* mice entered anagen significantly earlier than their wild-type or heterozygous littermates (Figure 2.7A), approximately 3 weeks after tamoxifen induction. Quantification of anagen initiation was carried out by the darkening of the dorsal skin of C57BL/6 mice, an event that is closely coupled to anagen induction (Figure 2.7B) [6]. Genetic ablation of OSMRβ or STAT5 in the epidermis and hair follicle after P60 did not result in significantly earlier anagen induction (data not shown), suggesting OSMRβ-JAK-STAT5 signaling is more physiologically relevant during early- and mid-telogen.

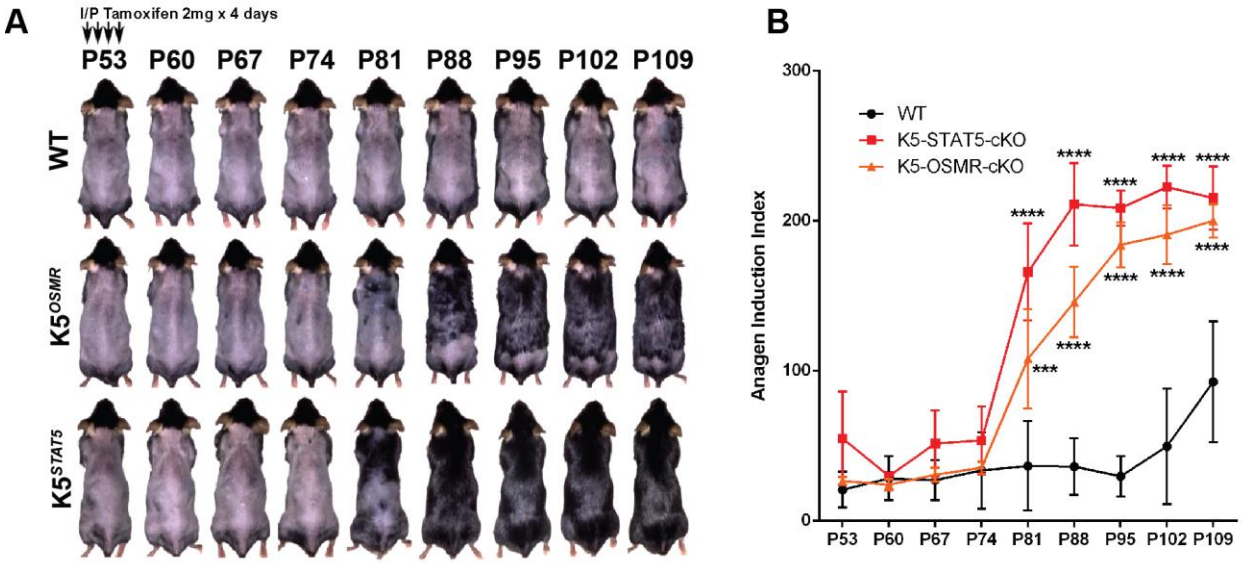

Figure 2.7. Mid telogen ablation of OSMRβ/STAT5. A. Conditional knock-out of OSMRβ or the STAT5 at P56-P60 (mid-telogen) resulted in early anagen initiation (K5OSMR or K5STAT5) compared to control littermates. **B.** Anagen progression was quantified as described earlier. Results are representative of 4 litters for each gene (OSMRβ or STAT5), with 2-4 mice per litter, for a total of 11 mice for OSMRβ (4 homozygous OSMRβFL/FL) and 12 mice for STAT5 (4 homozygous STAT5FL/FL). Data are mean ± SEM. *p < 0.05, **p < 0.01, ***p < 0.001, ****p<0.0001; Two-way ANOVA between genotypes at each respective timepoint

We next studied the cellular dynamics that result from genetic ablation of JAK-STAT5 signaling, since this was the most downstream element of the pathway, and the anagen-inducing effect of STAT5-ablation was stronger in Figure 2.7B. *K5-CreERT$_2$::STAT5a/b$^{FL/FL}$* mice and their control littermates were induced with tamoxifen during mid-telogen. Since anagen initiation in the *STAT5$^{FL/FL}$* mice occurred around 3 weeks after tamoxifen induction, we bisected this period to observe the early responses of the HFSCs with STAT5 ablation. Cellular proliferation was studied at 10 and 20 days post-tamoxifen with EdU administration 24 hours before the mice were sacrificed. At 10 days post-tamoxifen induction, cellular proliferation was observed in the HG, while the bulge remained quiescent (Figure 2.8A). After 20 days, the proliferation in the HG was even more prominent, and EdU incorporation was also seen in the lower bulge, but this latter effect was not significant (Figure 2.8B).

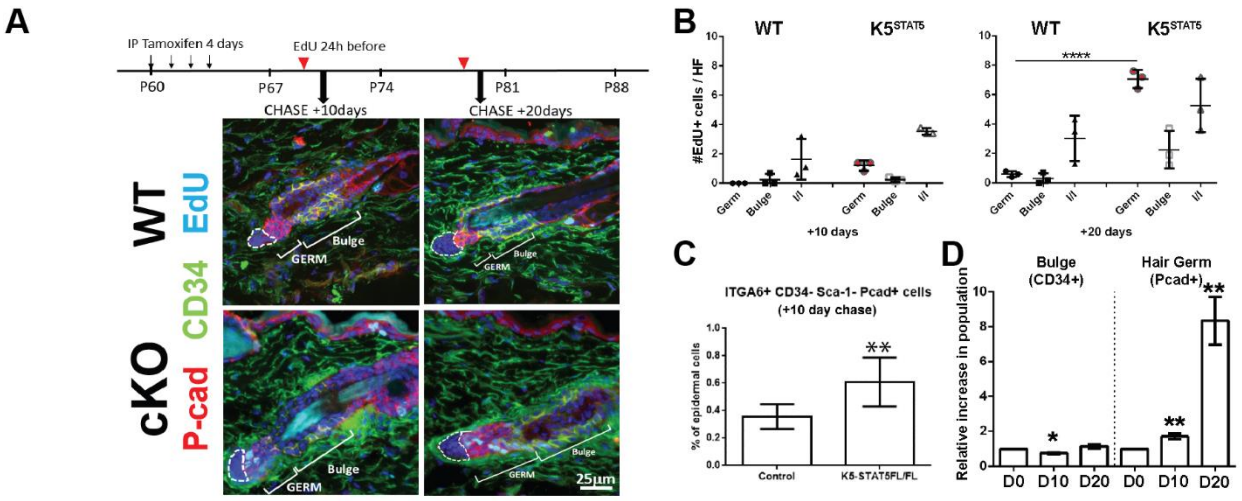

Figure 2.8. Cellular dynamics following STAT5 epidermal ablation. A. EdU incorporation was analyzed +10 and +20 days (D10 and D20) after tamoxifen induction in K5-CreERT2::STAT5$^{FL/FL}$ mice (cKO). EdU (4mg/25g adult mouse) was injected 24 hours before sacrifice. At D10, STAT5 epidermal ablation, EdU incorporation is seen in the HG, while the bulge remained quiescent. At D20, occasional EdU+ cells were seen in the bulge, and the HG was even more proliferative. Scale bar 25µm. **B.** Quantification of proliferative cells (EdU+) in each hair follicle compartment: P-cad+ HG (Germ), CD34+ Bulge or Isthmus/Infundibulum (I/I) after tamoxifen induction of STAT5-ablation in WT and K5-CreERT2::STAT5$^{FL/FL}$ littermates. CD34-negative cells above the bulge but within the HF were considered I/I. EdU incorporation was observed in the HG by D10 (n.s.), which became significant by D20. At D10, bulge proliferation was minimal, and slightly increased at D20. (Data points are mean of 20 HFs per mouse, n = 3 mice per genotype) **C.** Flow cytometric quantification of stem cell populations. At +10 days after STAT5 ablation, the percentage of total ITGA6+ Sca-1- CD34- Pcad+ cells (HG) doubled from 0.3% of total epidermis to 0.6% epidermis. (n = 3 mice per genotype) **D.** While the cell population in the bulge remained relatively constant after epidermal STAT5 ablation, the HG population proliferated and expanded exponentially with the loss of STAT5 signaling. (n = 3 mice per genotype) Data are mean ± SEM. *p < 0.05, **p < 0.01, ***p < 0.001, ****p<0.0001; (B,D) Two-way ANOVA of cellular compartment between genotypes at D10 and D20. (C) Student's t-test.

By FACS, the P-cadherin+ HG cells significantly double (from approximately 0.3% of total epidermal cells to 0.6%) at +10 days post-tamoxifen (Figure 2.8C). Furthermore, comparing the relative increase in cell numbers between the bulge and HG after STAT5 ablation, the HG proliferates up to 8-fold, while the cell numbers of the bulge stay relatively constant (Figure 2.8D). This initial proliferation in the HG is consistent with previous reports of the pattern of HFSC activation during spontaneous anagen [52], as well as the pattern observed with the administration of topical JAK-inhibitors [104]. These genetic data are in agreement with our previous pharmacological inhibition experiment, and further support the hypothesis that

OSMRβ-JAK-STAT5 signaling is necessary for maintaining HFSC quiescence during murine telogen, specifically during the refractory period of telogen (early-to-mid telogen).

Dermal OSM is produced by tissue-resident macrophages during telogen

We next aimed to define the source of OSM, which was shown in Figure 2.3A to be expressed within the dermal fraction (containing the DP). Performing qRT-PCR on isolated dermis tissue collected across the murine hair cycle, we found that *Osm* transcripts peaked in mid-telogen (Figure 2.3E), which is in sync with the expression of pSTAT5 seen in Figure 2C, consistent with its postulated function in maintaining HFSC quiescence. Since previous reports suggested that the human dermal papilla (DP) may be the source for IL-6 [137], we first employed laser-capture microdissection (LCM) to isolate the DP to locate *Osm* transcripts. Perifollicular dermal tissue, primarily containing dermal fibroblasts (DF) but not DP, was used as a control. However, we did not detect any *Osm* transcripts in the DP or DF samples with this method, even though DP-specific LEF1 was found in the DP, and COL1A1 was found enriched in both dermal populations as expected (Figure 2.9).

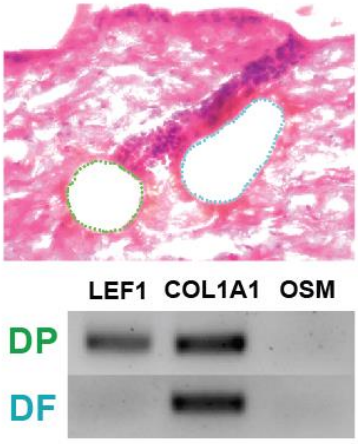

Figure 2.9. Laser-capture microdissection of DP and perifollicular dermal tissue containing fibroblasts (DF) to determine the source of OSM by qRT-PCR. While DP (green dotted line) samples were rich with Lef1 and Col1a1 mRNA, no OSM was detected. DF tissue (blue dotted line) contained Col1a1 mRNA but not Lef1 or Osm.

We next used RNAscope multiplex *in situ* hybridization to localize the source of OSM. In telogen skin, the transcripts for OSMR and its co-receptor (gp130, gene name *Il6st*) were found predominantly within the hair follicle, consistent with previous findings. Since OSM could not be detected in the perifollicular dermal tissue by LCM, we reasoned that OSM must be produced by scattered, possibly migratory cells, of the immune system. Referring to Hair-GEL.net, OSM appeared to be expressed in the “Neg” population of skin cells, which includes immune cells, smooth muscle cells and endothelial cells of the dermis [8, 204]. In agreement with these findings, we found that *Osm* transcripts were found scattered in the dermal tissue adjacent to the hair follicle, rather than within the DP (Figure 2.10A-B).

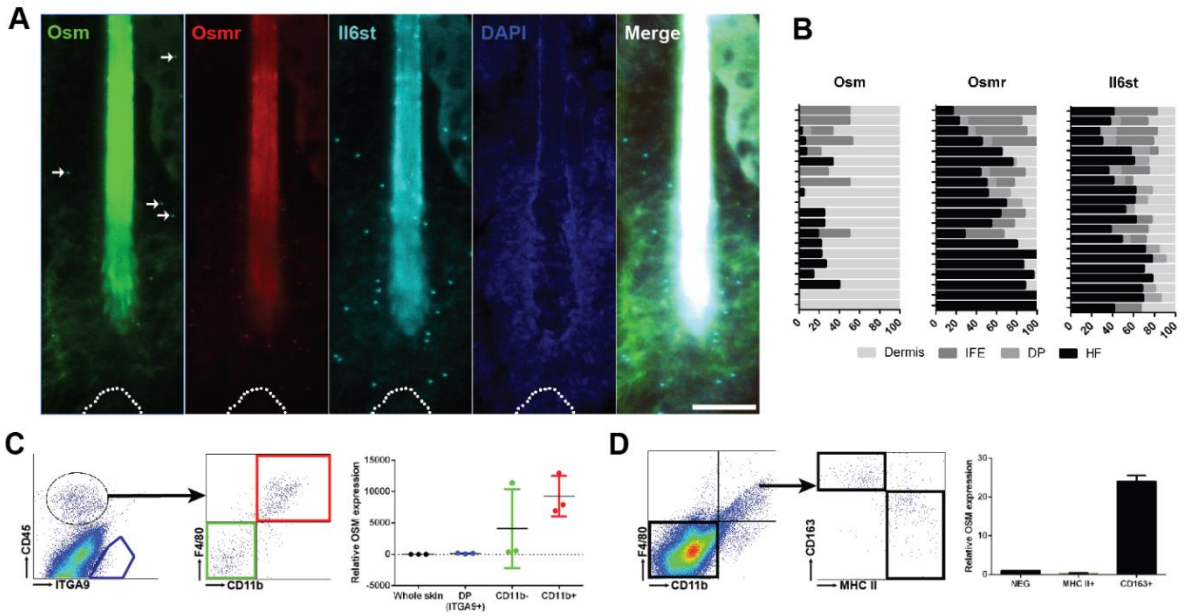

Figure 2.10. Identifying the source of OSM as dermal macrophages. A. Multiplex fluorescence in-situ hybridization (RNAscope) for Osm, Osmr and Il6st (gene for gp130). Osm mRNA was detected most frequently in perifollicular dermal regions (white arrows). Osmr and Il6st mRNA was generally found in the hair follicle keratinocytes. **B.** Quantification was performed over 21 imaged follicles in a 20x field from 2 mice in early-mid telogen. Each row represents one HF, and shaded bars represent the distribution of fluorescent particles within or around the HF as outlined by DAPI nuclear staining of the HF and DP converted to a percentage of total particles in the 20x field. **C.** Flow cytometric analysis of telogen dermis to separate DP (ITGA9+) and macrophages (CD45+ F4/80+ CD11b+). qRT-PCR for OSM revealed that dermal macrophages (F4/80+ CD11b+) were the main source of OSM. DPs and CD11b- immune cells were generally negative for OSM. (n = 3 mice) **D.** Flow cytometric analysis of inflammatory (MHC II+) and non-inflammatory, tissue resident (CD163+) macrophages during telogen. qRT-PCR of macrophage subsets isolated by this FACS strategy confirmed that CD163+ “M2-like” non-inflammatory macrophages were the main source of OSM in the dermis. (n = 3 mice)

Since tissue macrophages were recently reported to have a role in maintaining the second murine telogen [89], we postulated that these cells may be the source of OSM. Using FACS, we sorted the telogen dermis for macrophages (CD45+ F4/80+ CD11b+). Using qRT-PCR, the non-macrophage immune cells (CD45+ F4/80- CD11b-) and presumptive DP (CD45- ITGA9+, identified using the online resource Hair-GEL.net [8, 204]) were mostly negative for OSM. By qRT-PCR, macrophages (CD45+ F4/80+ CD11b+) were found to be the main source of dermal OSM (Figure 2.10C). Using CD163 and MHC II as markers for M2 and M1 markers respectively, we also found OSM to be enriched in the "M2-like" CD163+ MHC II^{low} macrophage subset (Figure 2.10D).

Single-cell RNA-sequencing of dermal CD45+ immune cells

Although we found that "M2-like" macrophages were enriched for OSM-producing cells *in vivo,* we sought to account for the heterogeneity of tissue macrophages by performing single-cell RNA sequencing on the dermal CD45+ immune cells during early (P45), mid (P50, P63) and late (P80) telogen. This provided us with an unbiased survey of the immune cells across telogen. Analysis of CD45+ immune cells during early telogen (P45) revealed 13 distinct clusters, which represent the main components of the immune infiltrate in unperturbed mouse early telogen skin (Figure 2.11A). At P45, macrophages clustered into 5 distinct clusters: 0, 1, 2, 5 and 11 (Figure 2.11A – dotted circle). OSM itself was significantly upregulated in a distinct cluster (cluster 11) (Figure 2.11B).

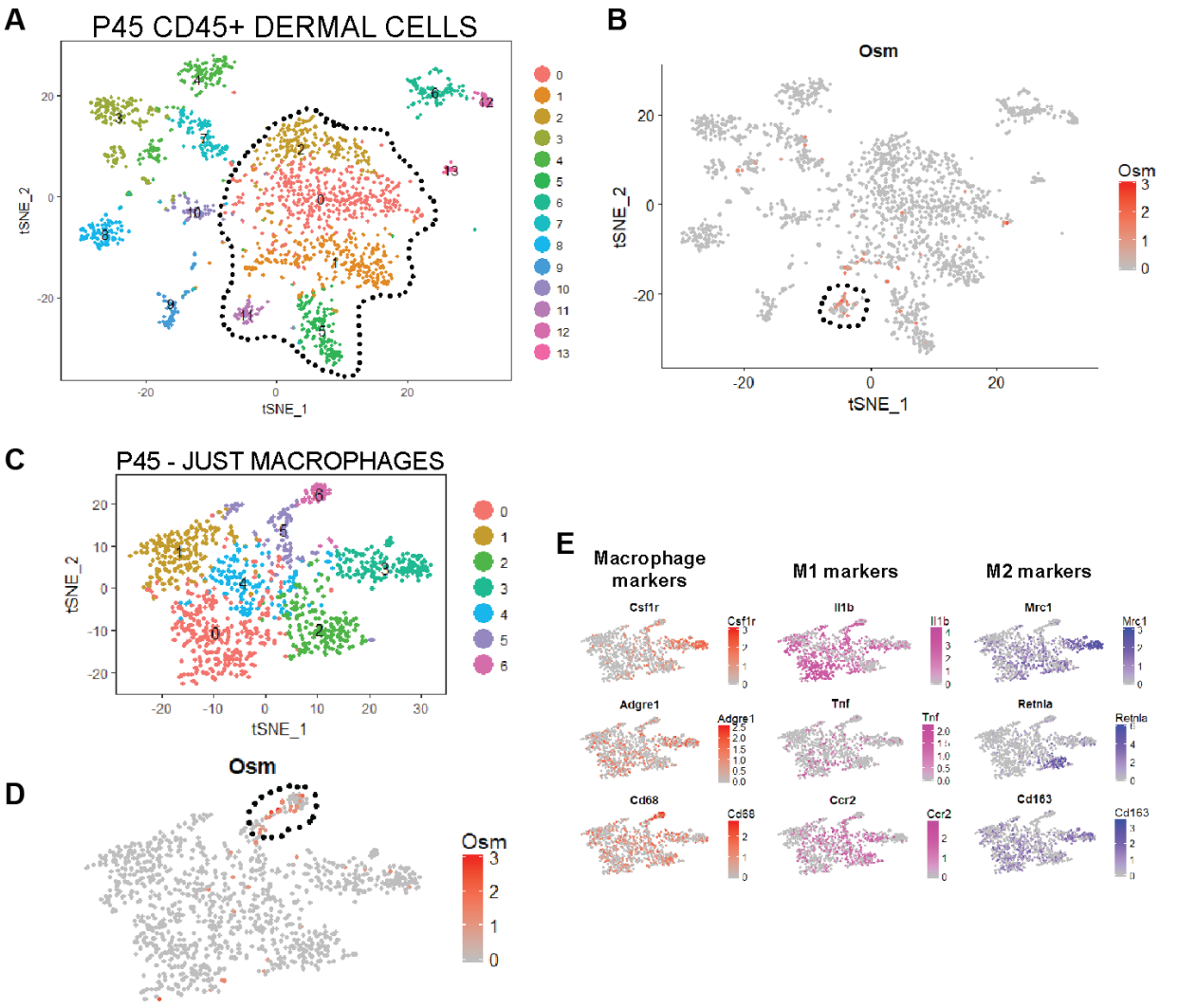

Figure 2.11. P45 single-cell RNA sequencing. A. Single-cell RNA-sequencing of CD45+ dermal immune cells at P45 (early telogen). CD45+ cells were isolated with flow cytometry and 2145 cells were analyzed using the 10x Genomics platform. Macrophages (defined by markers CD68, Csf1r, F4/80) clustered into 5 distinct clusters (0, 1, 2, 5, 11, circled with dotted line in **B**). **B.** OSM was enriched in cluster 11 (circled in G). **C-D.** Clustering of just the macrophage populations yielded seven distinct subsets, with OSM production enriched in cluster 6 of this re-analysis. **E.** Visual inspection of known macrophage markers and M1/M2 markers show that there is significant heterogeneity of macrophages in unperturbed mouse telogen skin. Clusters 0 and 1 tend to express more “M1-like” markers, while clusters 2 and 3 expressed more “M2-like” markers. Cluster 6, where OSM is enriched, does not fall clearly into either M1 or M2 markers based on conventional markers. Note Adgre1 = F4/80; Mrc1 = CD206.

Next, we re-analyzed the data focusing on the macrophage clusters to produce a new set of clusters (Figure 2.11C-D). These macrophage-only clusters showed relatively uniform CD68 expression, but M1 and M2 markers were unevenly expressed amongst the clusters (Figure 2.11E), reflecting the macrophage heterogeneity of the unpolarized and unperturbed dermis at

this stage of the hair cycle. OSM expression was significantly higher in cluster 6 macrophages (Figure 2.11D), which did not conform to a classic M1 or M2 gene expression profile.

OSM-producing macrophages have a distinct gene-expression profile

Comparing the genes expressed by each cluster in a heatmap, cluster 6 macrophages most resemble the “M2-like” macrophages of cluster 3 (Figure 2.12). Interestingly, TREM2 is a distinguishing gene between these two sets, being highly expressed by cluster 6 OSM-producing macrophages, and downregulated in the cluster 3 subset of macrophages.

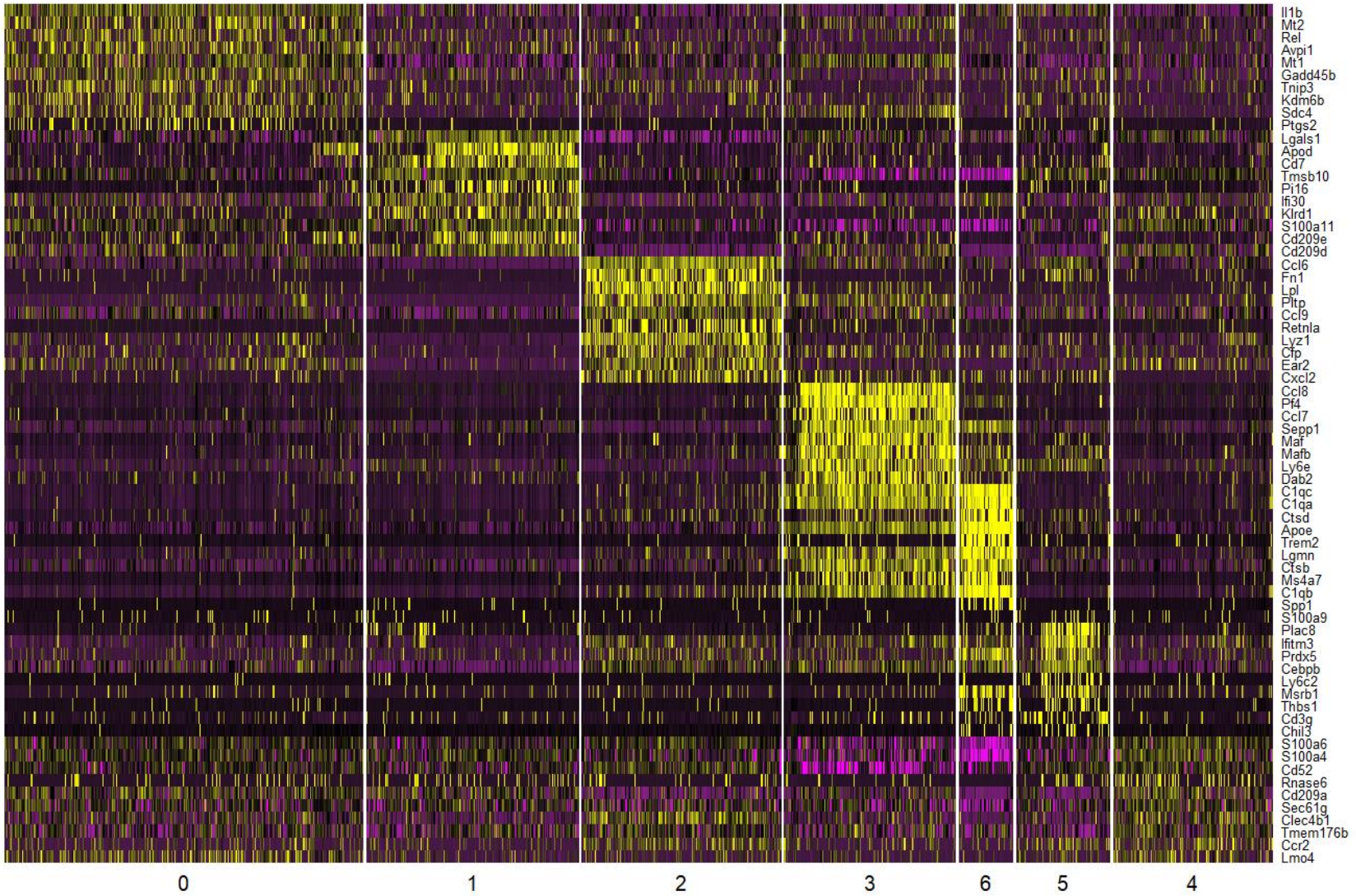

Figure 2.12. OSM-producing macrophages have a distinct gene expression profile. Heat map showing Differentially Enriched genes in macrophage clusters. The gene expression profile of cluster 6 OSM-producing macrophages resembled M2-like macrophages in cluster 3, except for TREM2, which is conspicuously absent in cluster 3. Each column represents a single cell, yellow signifies upregulation, purple signifies downregulation.

Analyzing the enriched genes of cluster 6 (Figure 2.13A, Appendix C) with the online resource Enrichr (http://amp.pharm.mssm.edu/Enrichr/), we found that this set of genes were significantly associated with microglia (Appendix D), which are the long-term tissue-resident macrophages of the central nervous system. Established microglial markers such as Apoe, Aif-1 (Iba-1), Cx3cr1 and Tmem119 were all found to be expressed at varying levels in the OSM-producing macrophages, and TREM2 was found to be the most specific marker for this set of macrophages (Figure 2.13B).

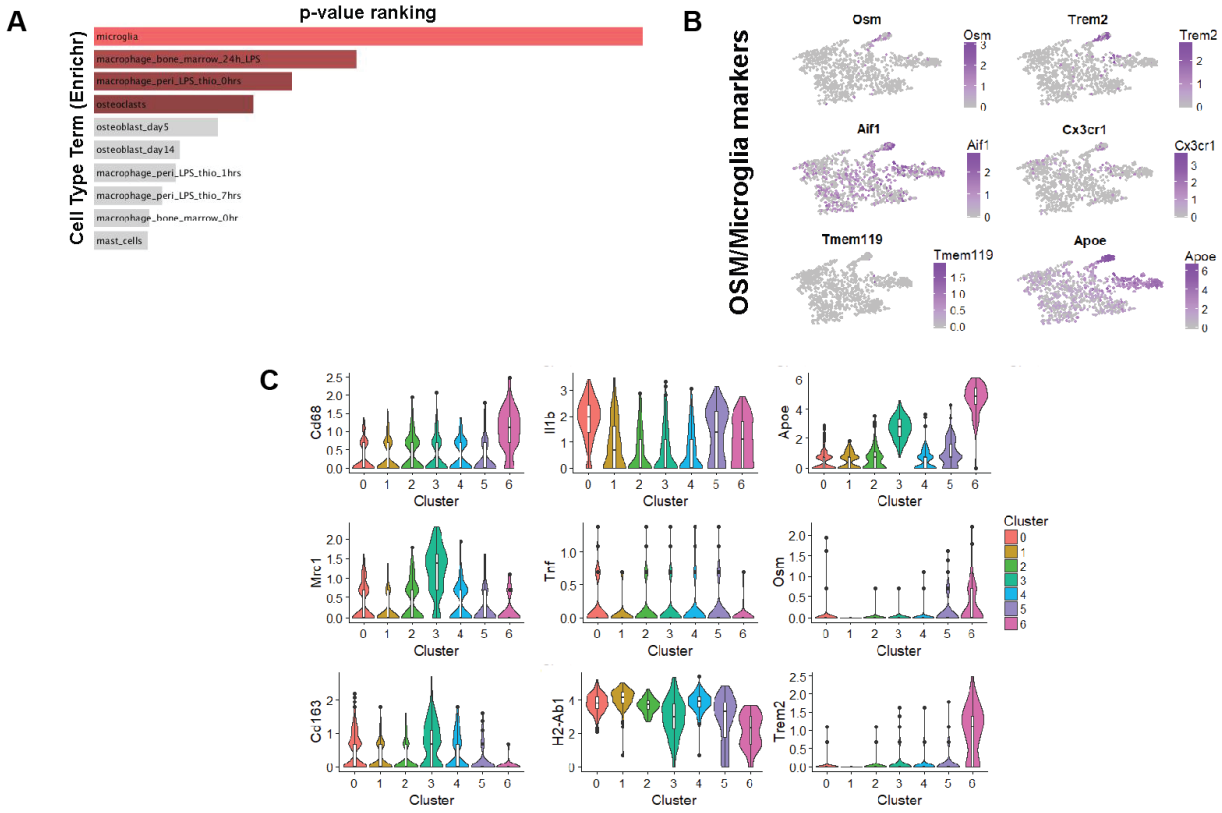

Figure 2.13. OSM-producing macrophages resemble microglia. **A.** Enrichr analysis of most enriched genes in cluster 6 suggest that these genes are also enriched in microglia, according to the Mouse Gene Atlas. **B.** Microglial markers have different distributions amongst the dermal macrophages. **C.** Violin plots of gene expression across macrophage subsets. Cluster 3 tends to have more M2 markers (Mrc1 = CD206; CD163), while clusters 0 and 1 are more enriched in M1 markers like IL-1b, TNF and MHC II (H2-Ab1). Microglial markers ApoE and TREM2 are co-expressed in cluster 6 macrophages along with OSM, with TREM2 being the most specific to this population.

OSM-producing macrophages are TREM2+ and resemble M2 macrophages

Analyzing the macrophage markers in the macrophage clusters, OSM and TREM2 expression were found to be highly specific for cluster 6 (Figure 2.13C). Cluster 3 macrophages were relatively enriched for M2 markers Mrc2 (CD206) and CD163, while clusters 0 and 1 were more enriched for M1 markers like IL-1b and MHC Class II (H2-Ab1).

Due to their similarities in gene expression on the heatmap in Figure 2.12, and their proximity in clustering in Figure 2.11C, clusters 6, 5 and 3 were analyzed further for their relationships in pseudotime. Multidimensional scaling of the clusters was performed, and these clusters formed a potential differentiation trajectory (Figure 2.14A). Microglial markers and OSM were also expressed dynamically across these clusters (Figure 2.14B). Assuming the macrophage heterogeneity in the dermis reflects varying differentiation states of tissue-resident macrophages, this model suggests that TREM2+ OSM-producing macrophages (cluster 6) may differentiate into M2-like macrophages (cluster 3) via in intermediate phenotype (cluster 5) (Figure 2.14C).

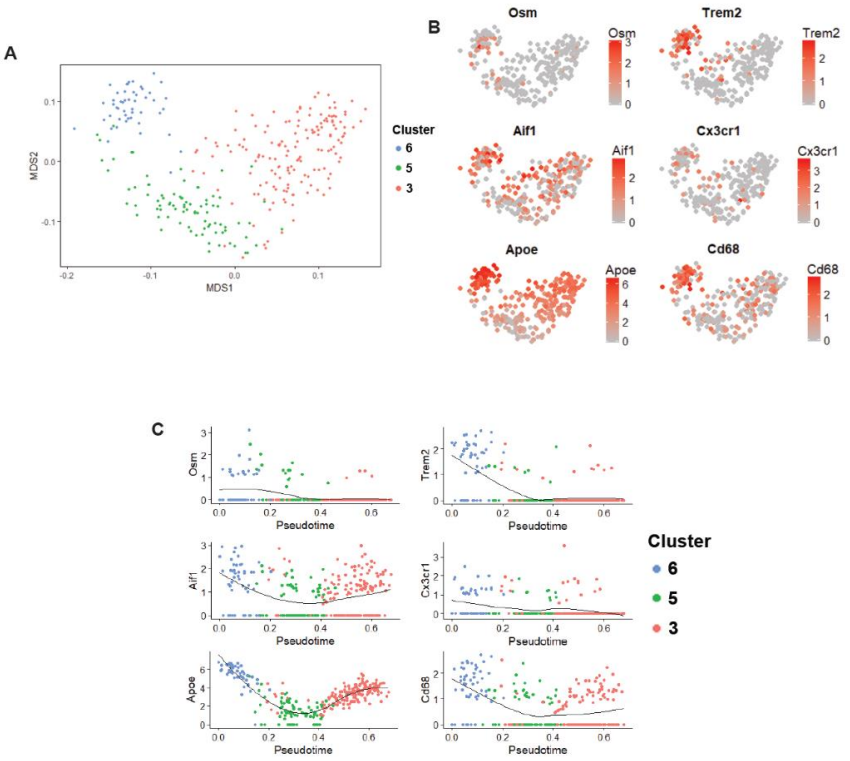

Figure 2.14. Pseudotime analysis **A.** Multidimensional scaling (MDS) of P45 macrophage clusters. Macrophage clusters 6, 5 and 3 were selected due to their proximity on the tSNE plot in Figure 2.11C. Arrangement of clusters in the MDS plot suggests cellular transition from clusters 6 → 5 → 3. **B.** OSM and microglial markers shown according to their expression within this MDS plot. This proposed cellular transition is associated with downregulation of OSM and TREM2, and also a general downregulation of microglial markers. **C.** Pseudotime analysis of OSM and microglial markers in these macrophages suggest a differentiation pathway for TREM2+ trichophages into "M2-like" macrophages, which is accompanied by downregulation of OSM and TREM2.

TREM2+ OSM-producing macrophages are closely associated with HFSC

Immunofluorescence studies were carried out with the microglial markers identified in this distinct subset of macrophages. Aif-1, which were expressed in most macrophages at P45, was found to co-localize with CD11b and OSM, in immune cells that surround the hair follicle at P45 (Figure 2.15A). TREM2, which was specific for the OSM-producing subset, was also found to co-localize with F4/80 and OSM in close approximation to telogen HFSCs (Figure 2.15B). These data strongly suggest that OSM is produced by a distinct subset tissue macrophage that is closely associated with HFs during telogen, which share lineage markers with microglia of the CNS.

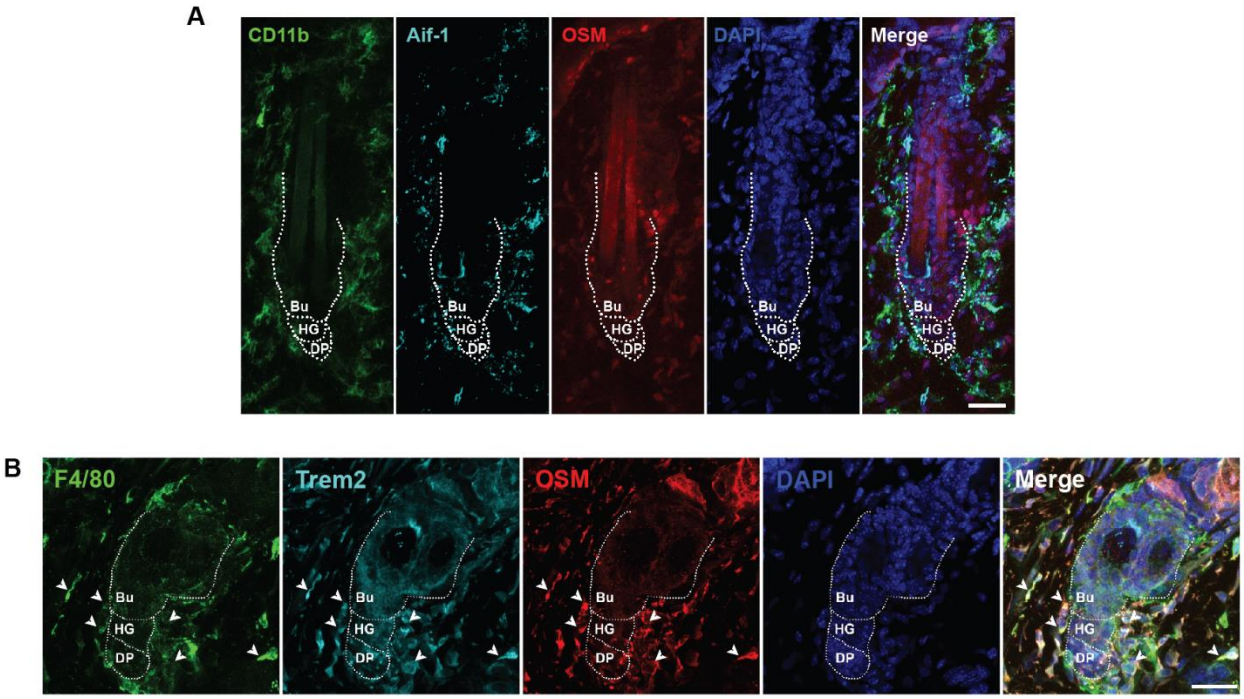

Figure 2.15. OSM-producing macrophages are associated with telogen HFs. A. Immunofluorescence of Aif-1, a microglial marker, that co-localizes with CD11b and OSM, surrounding a telogen HF. **B.** Immunofluorescence of TREM2, a specific marker for the OSM-producing macrophages, co-localizing with F4/80 and OSM, surrounding the HFSC of a telogen HF. Bu = bulge, HG = secondary hair germ, DP = dermal papilla. Scale bars 25μm.

TREM2+ macrophages decrease over telogen

Dermal tissue was collected from C57BL/6 mice at 3 other timepoints during telogen, and analyzed with single-cell RNA sequencing (Figure 2.16A). The CD45+ immune cell diversity in the dermis decreases as telogen progresses, starting with 13 distinct clusters at P45, and falling to 3 clusters by P63. The OSM-producing cluster, while distinct at P45, becomes less distinct at P50, and is greatly diminished by P63 and P80 (Figure 2.16B).

Using FACS, TREM2+ macrophages in the dermis were found to be prominent during early- and mid-telogen, and were greatly reduced in number by late-telogen (Figure 2.16C), consistent with our observations of the scRNA-seq data.

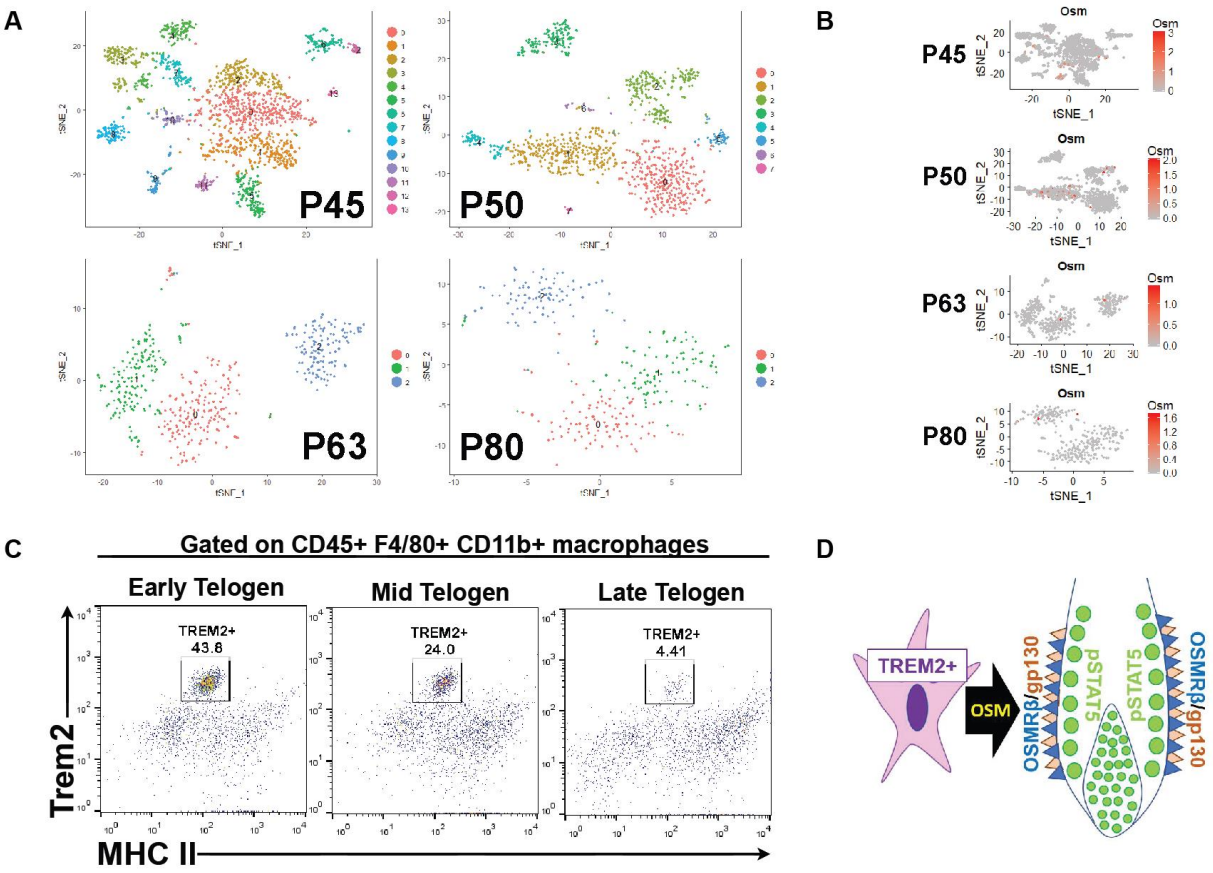

Figure 2.16. TREM2+ macrophages numbers decrease over telogen. A. Single-cell RNA sequencing was performed at 3 further timepoints in telogen (P50, P63, P80). Number of cells at each time point analyzed were 1497 (P50), 592 (P63) and 497 (P80). Immune cell diversity becomes less diverse as telogen progresses. **B.** The OSM-producing cluster becomes less distinct as telogen progresses. At P50, OSM producing macrophages are dispersed in the main macrophage cluster, and by P63, very few cells express OSM. **C.** Flow cytometry of dermis across telogen using TREM2. Macrophages (gated on CD45, F4/80 and CD11b) were further analyzed according to their TREM2 and MHC II expression. TREM2+ macrophages tend to be MHC IIlow, as expected, and their numbers decrease from early to late telogen. **D.** Schematic of telogen HF with TREM2+ macrophages that produce OSM, which signals via OSMRβ/gp130-JAK-STAT5 on HFSC to maintain stem cell quiescence.

When cells from all telogen timepoints are pooled and analyzed together, the microglia-like cells from P45 cluster distinctly (Figure 2.17A-B), suggesting that these cells are unique to early telogen, and are somehow lost as telogen progresses. When the pooled data is labelled according to the 4 telogen timepoints, early, mid and late telogen have overlapping but quite distinct immune cell profiles (Figure 2.17C). While this dynamism of immune cells across telogen has been described anatomically [75], this is the first functional correlation of this phenomenon.

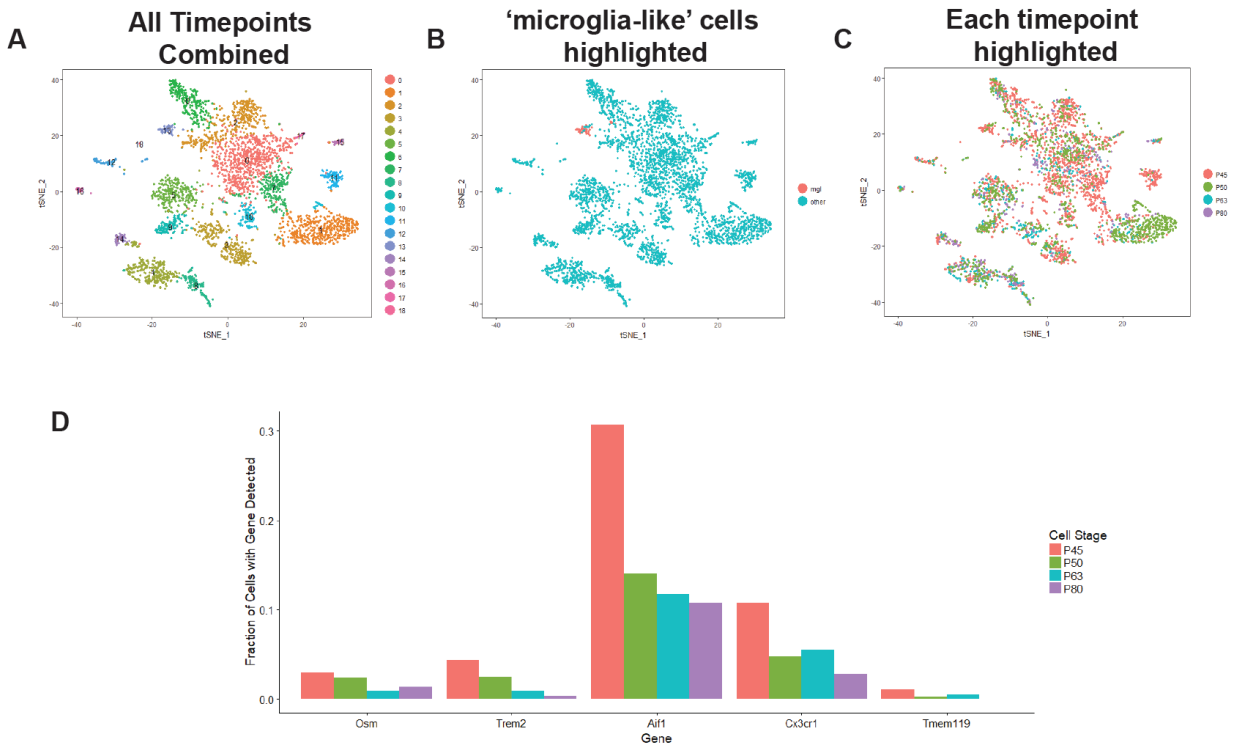

Figure 2.17. Combined scRNA-seq data across telogen. A. tSNE plot of pooled data from CD45+ dermal cells of C57BL/6 mice at P45, P50, P63 and P80. **B.** Cluster 6 macrophages (microglia-like cells, mgl) cluster distinctly when pooled with all timepoints. **C.** Same plot highlighting the different timepoints. The profiles of CD45+ immune cells in the dermis throughout telogen is dynamic and shifts with time. **D.** OSM, TREM2 and other microglial markers decrease across telogen in the dermis.

Analyzing the trajectories of OSM and microglial markers across telogen, we find that all these genes decrease with time (Figure 2.17D), being most prominent at early-to-mid telogen. Along with our FACS data, these data support the disappearance of the TREM2+ subset of macrophages by late telogen, just before the next anagen phase.

Depilation during telogen causes loss of TREM2+ macrophages

As depilation during telogen is known to induce synchronized anagen across the dorsal skin, we next interrogated the effect of depilation on TREM2+ macrophages. P50 C57BL/6 mice were treated with depilatory cream, and dermal CD45+ immune cells were analyzed by scRNA-seq 5 days later, before any darkening of the dorsal back skin is evident (Figure 2.18A). While the diversity of immune cells at this timepoint (P50 depilation + 5D) was comparable to that of unperturbed P50 immune cells, the fraction of TREM2+ macrophages and OSM expression was reduced to the levels of late telogen P80 skin (Figure 2.18B-C). These data further support the hypothesis that downregulation of OSM, and reduction in the number of TREM2+ macrophages, are associated with anagen initiation.

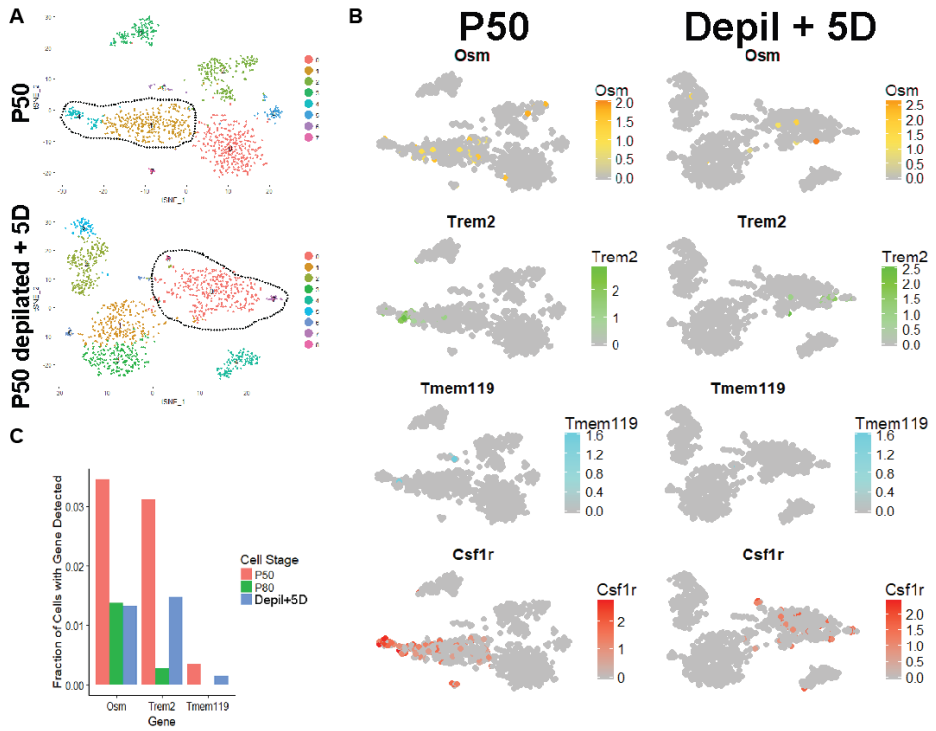

Figure 2.18. **Depilation causes decrease in OSM-producing macrophages. A.** tSNE plots of CD45+ dermal immune cell clusters of P50 skin before depilation, and P50 skin 5 days after depilation. Dotted lines encircle macrophage clusters. **B-C.** OSM, TREM2 and Tmem119 expression in dermal immune cells are reduced 5 days after depilation (n = 1502 cells). Levels of OSM are reduced to levels comparable with late telogen P80 skin. Unlike at the P45 timepoint, most TREM2+ macrophages at this time point appear to have downregulated OSM production.

T regulatory cells (T regs) have recently been shown to play a role in depilation-induced anagen [83], were dispensable for these effects (Figure 2.19A-B). Interestingly, while spontaneous anagen was associated with a decrease in FoxP3- and TNF-producing cells in our single-cell RNA-seq data (the latter being implicated in plucking-induced anagen [82]), depilation of telogen skin did not significantly reduce the expression of these cell populations (Figure 2.19C). These data suggest that while both experimentally-induced and spontaneous anagen are associated with loss of OSM and TREM2+ macrophages, they are mechanistically distinct with respect to the involvement of other immune cells.

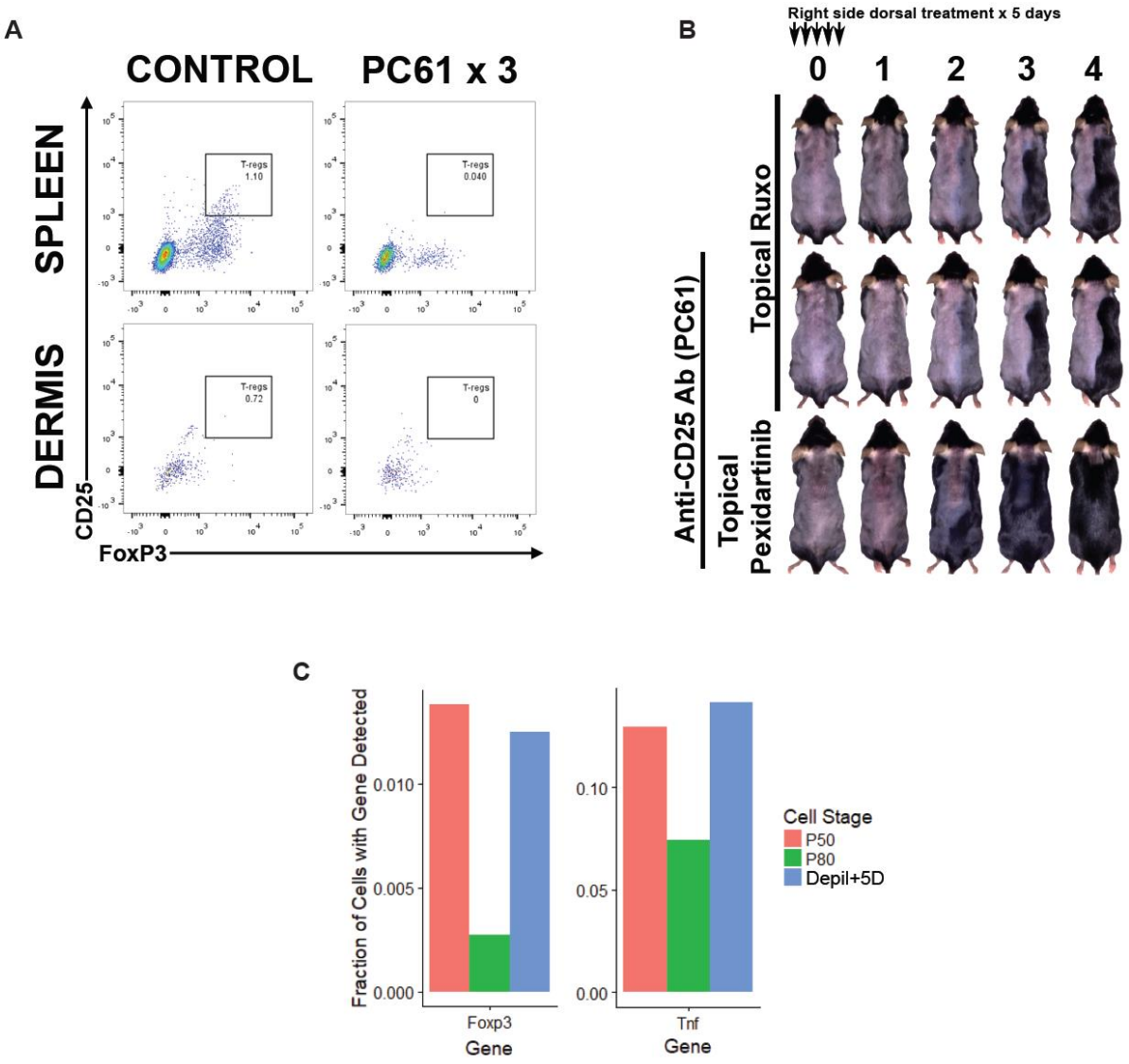

Figure 2.19. T-regulatory cell depletion does not affect JAK-STAT induced anagen. **A.** T reg depletion with anti-CD25 neutralizing monoclonal antibody (PC61). C57BL/6 treated with 3 intraperitoneal injections of PC61 exhibited marked T reg depletion in the spleen and dermis. **B.** Mice treated with PC61 underwent JAK-inhibitor initiated anagen with the same kinetics as WT mice. Likewise, mice treatment with the small molecule Csf1r tyrosine kinase inhibitor Pexidartinib to target macrophages also underwent anagen initiation. Together, these data demonstrate that these processes are not dependent on T regs. **C.** Depilation does not affect the levels of FoxP3 or TNF expression in the dermal immune cells. FoxP3+ T regs and TNF-producing macrophages have been implicated in experimentally-induced anagen. These cell populations decrease at unperturbed P80 skin, highlighting differences between experimentally-induced and spontaneous hair cycling.

Macrophage inhibition during telogen leads to anagen initiation

We used three independent methods of macrophage inhibition during telogen to initiate anagen in C57BL/6 mice. Neutralizing antibodies to Csf1r (AFS98) and F4/80/EMR1 (CI:A3-1) have been shown to preferentially deplete tissue resident populations of macrophages [217, 218]. Neutralizing antibodies to Csf1r and F4/80 (Figure 2.20A), topical and subcutaneous Pexidartinib (PLX3397, Csf1r tyrosine kinase inhibitor) (Figure 2.20B) were both successful at initiating anagen when administered during mid-telogen.

We also bred a *Csf1r-CreER* mouse with *Rosa26-iDTR (R26-iDTR)* mice, producing offspring that will express the diphtheria toxin receptor on Csf1r+ cells upon tamoxifen induction. Tamoxifen was administered for 4 days in mid-telogen, followed by 7 days of intradermal diphtheria toxin (DTA) injections. This treatment led to ablation of dermal macrophages, and resulted in local anagen initiation that preceded their the wild-type littermates that received the same DTA injections (Figure 2.20C). Introduction of the *R26-TdTomato* reporter allowed us to demonstrate macrophage ablation in these mice. Analysis of biopsies of the dorsal skin 10 days after intradermal DTA show a drastic reduction in perifollicular TdT+ macrophages in the area of intradermal DTA injection, and this was associated with increased EdU incorporation of HFSCs (Figure 2.20D). Ablation of HF-associated macrophages was strongly correlated with increase HFSC proliferation (Figure 2.20E). Flow cytometry of the dermis dissected from these areas also show preferential ablation of the F4/80+ TREM2+ subset of macrophages (Figure 2.20F), which correspond to the OSM-producing subset.

These data, along with previously published findings by others [89], strongly support the hypothesis that macrophages are necessary for the maintenance of an inhibitory environment on the HFSCs during telogen, likely by producing OSM.

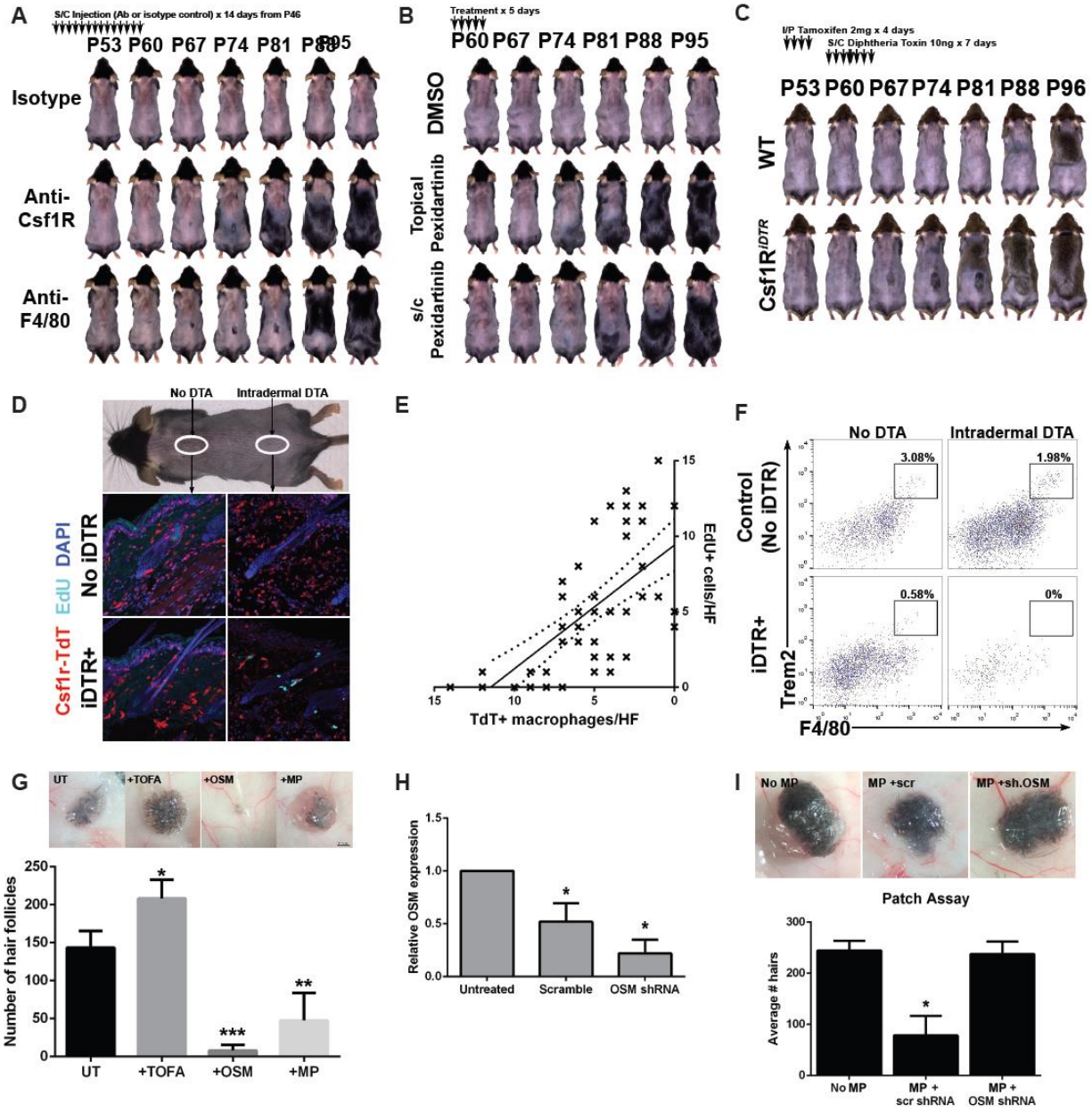

Figure 2.20. Macrophage depletion during telogen initiates anagen, and OSM knock-down prevents the inhibitory effects of macrophages on HFSC. **A.** Neutralizing antibodies to Csf1r and F4/80 injected intradermally into the middle of the dorsal skin of C57BL/6 mice for 14 days were sufficient to initiate a local anagen at the site of injection. **B.** Pharmacological inhibition of Csf1r (5 day treatment) with the small molecule Pexidartinib was similarly successful at initiating anagen when administered both topically and subcutaneously. **C.** Genetic ablation of macrophages using Csf1r-CreER::R26-iDTR mice. Tamoxifen was administered systemically for 4 days from P53-P56, and 10ng diphtheria toxin (DTA) was injected intradermally for 7 days from P60. A local anagen was initiated at the site of injection. **D-E.** Csf1r-CreER::R26-TdTomato::R26-iDTR mice and littermate controls (no R26-iDTR) underwent Tamoxifen induction and DTA administration as described. Dermis from area of injection, and a remote area on the dorsal skin, were collected and examined with IF and FACS. Intradermal DTA was associated with loss of perifollicular macrophages in mice expressing iDTR on macrophages, which in turn was associated with increased proliferation of HFSCs highlighted by increased EdU incorporation. (Quantification of 50 HFs in a 20x field across 2 mice. $R2 = 0.4674$, $p<0.0001$. Dotted lines represent 95% CI.) **F.** FACS of dorsal skin at the site of intradermal DTA treatment compared with remote areas, and with control mice (no R26-iDTR). Local DTA injection resulted in reduction of all macrophages (with reduced density seen in the FACS plot), and specific ablation of the F4/80+ TREM2+ subset of macrophages. Reduction of TREM2+ macrophages in the remote area (0.58%) of Csf1r-CreER::R26-TdTomato::R26-iDTR mice might be a reflection of DTA diffusion. Data representative of 2 experiments. **G.** Patch assay for hair reconstitution. Neonatal epidermis and dermis were recombined to assess the effect of macrophages and OSM on hair reconstitution. Addition of Tofacitinib 100nM enhanced hair regeneration in this model. Addition of OSM 20ng/ml completely inhibited hair regeneration. F4/80+ CD11b+ macrophages (MP) sorted from adult telogen dermis also inhibited hair regeneration. Data from 3 patches per condition, across 2 independent experiments. **H.** shRNA knockdown of OSM in cultured peritoneal macrophages. Macrophages were obtained from murine peritoneal cavity with gavage and cultured in the presence of M-CSF to skew them to an anti-inflammatory phenotype. Plasmids containing shRNA (scrambled or OSM-specific) were transfected into the macrophages and OSM knock-down was confirmed by qRT-PCR. Data from 2 independent transfections. **I.** Patch assay with OSM knock-down. While macrophages transfected with scrambled shRNA were still able to inhibit hair reconstitution in the patch assay, this was rescued by OSM knock-down. Data from 3 patches per condition, across 2 independent experiments.Data are mean ± SEM. *$p < 0.05$, **$p < 0.01$, ***$p < 0.001$, ****$p<0.0001$, (G-I) Student's unpaired t-test

Macrophage OSM inhibits hair regeneration

To examine the interactions between macrophages and HFSC in more detail, we used hair reconstitution assays to show that macrophages had an inhibitory effect on hair regeneration. Neonatal keratinocytes and dermal cells were injected intradermally in a 1:2 ratio in the patch assay, which recapitulates the epithelial-mesenchymal interactions required for HF regeneration. While tofacitinib enhanced the hair follicles generated in this assay, consistent with our previous findings [104], addition of OSM was sufficient to nearly completely inhibit hair reconstitution. Macrophages sorted from the P60 telogen dermis were recombined with the neonatal cells, and these were also found to inhibit hair reconstitution (Figure 2.20G).

In order to determine whether OSM in the macrophages were responsible for their inhibitory effects, we cultured murine peritoneal macrophages in the presence of M-CSF to skew them to a tissue-resident, anti-inflammatory phenotype [219]. shRNA was utilized to knock-down OSM expression (Figure 2.20H). While macrophages with scrambled shRNA were still able to inhibit hair reconstitution, knock-down of OSM in macrophages attenuated the inhibitory properties of the macrophages, and restored the original hair reconstitution of this assay (Figure 2.20I). These data show that OSM produced by the macrophages is the cytokine that inhibits proliferation and activation of HFSCs (Figure 2.16D).

DISCUSSION

Here, we uncover a new mechanism for JAK-STAT signaling in the maintenance of HFSC quiescence. We identify a distinct subset of TREM2+ tissue macrophages in the dermis that secrete OSM, which prevents proliferation of HFSC, particularly during the second telogen (Figure 2.21A). Our findings add to the growing literature in support of immune cells having direct effects on tissue stem cell regulation and control. We propose the name “trichophages” to refer to these specialized macrophages that maintain HFSC quiescence.

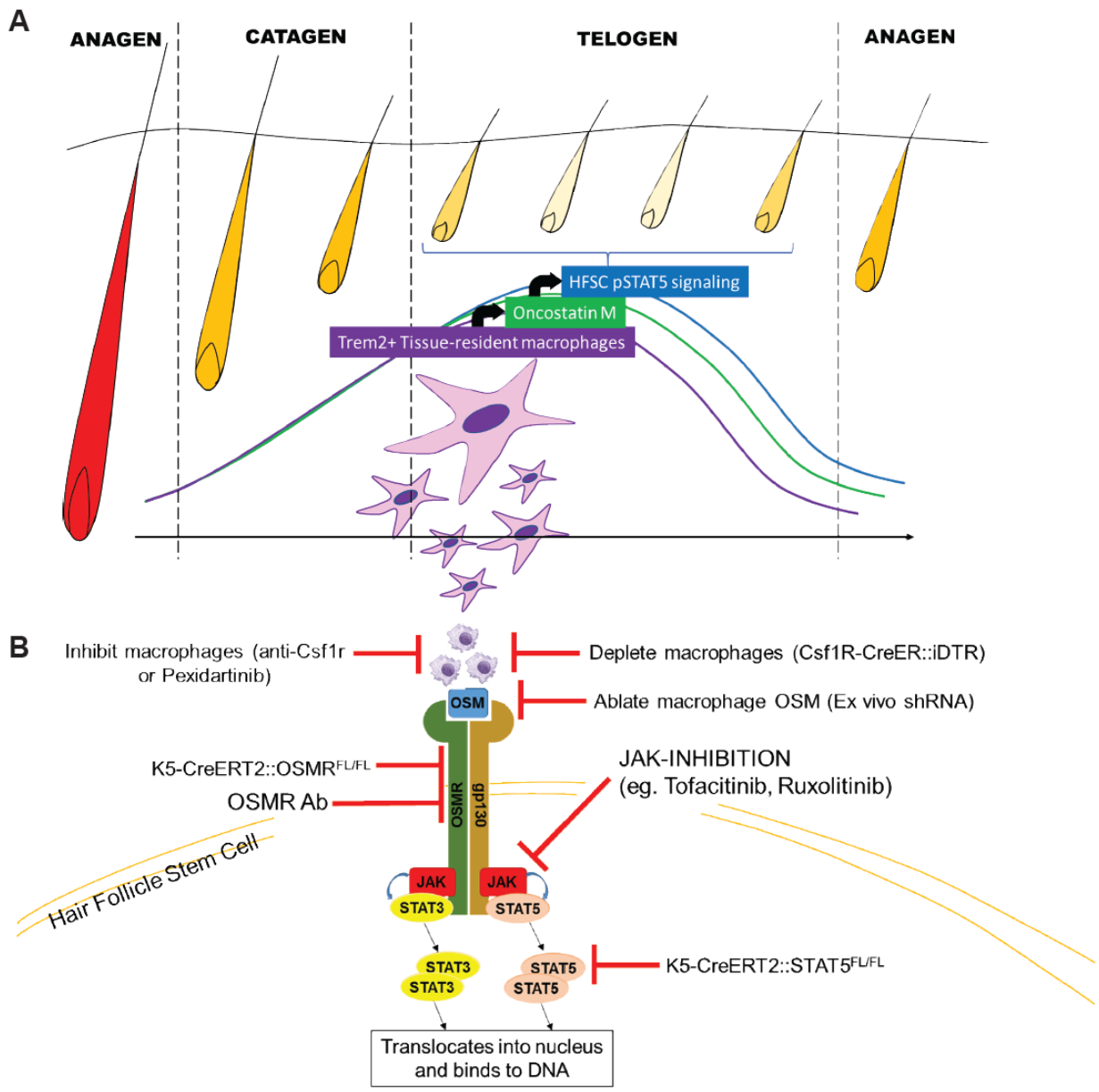

Figure 2.21. Schematic of OSM-producing macrophages during telogen. A. Tissue resident TREM2+ macrophages with an anti-inflammatory phenotype produce OSM during early- and mid-telogen, which signals via JAK-STAT5 in HFSC to maintain their quiescence. These "trichophages" predominate during early and mid telogen, and lose their OSM-producing ability as telogen progresses, which allows the HFs to enter the next anagen stage. **B.** Summary of experiments reported in this paper that successfully initiated anagen in telogen skin. Targeting multiple steps of the OSM-OSMRβ-JAK-STAT5 pathway in the telogen dermis and HFSCs were sufficient to initiate anagen in C57BL/6 mice.

Macrophages have previously been shown to have intimate interactions with HFSCs.

Macrophages have been described to cluster around hair follicles [36], and may secrete FGF-5

that promotes catagen [27, 28]. Castellana et al showed that macrophages numbers fluctuate during the second telogen, and peak during mid-telogen, whereby their inhibition by clodronate liposomes was sufficient to induce anagen [89]. We corroborate their data molecularly (with neutralizing antibodies), pharmacologically (with Csf1r antagonists) and genetically (with *Csf1r-CreER::iDTR* mice) (Figure 2.21B). We also showed that knocking down OSM in cultured macrophages removes their ability to inhibit hair regeneration in a patch assay (Figure 2.21B). The importance of “trichophages” in the maintenance of telogen reflects the understanding that macrophages have a significant and integral non-immune role in many tissues, including the brain, where they perform essential developmental and homeostatic functions like synaptic pruning [220], and also the heart where they facilitate electrical conduction [90].

Our single-cell RNA-sequencing data uncovered a small, yet distinct subset of macrophages that secrete OSM during telogen. These trichophages appear to be genetically similar to microglia, and might perform similar functions with respect to the hair cycle. Microglia are important supportive cells of the brain and CNS, where they carry out innate immune functions, clear cell debris, and participate in homeostasis and pruning of neurons [221]. TREM2-DAP12 signaling in microglia have been functionally linked to their survival [222] and role in phagocytosis [223]. This may be analogous to the proposed role of trichophages in the hair cycle, where they modulate HFSC activity and coordinate the cyclical growth and regression of hair follicles. In the CNS, dysfunctional microglia have been implicated in the pathogenesis of Alzheimer’s disease, and mutations in TREM2 have been associated with neurodegenerative disease in humans [91, 224]. Whole exome sequencing has implicated TREM2 in diseases such as polycystic lipomembranous osteodysplsia (PLOSL) [225] and frontotemporal dementia (FTD) [226], but a distinct hair pathology has not been described in these patients. Whether trichophage dysfunction may lead to hair disorders associated with hair cycle abnormalities (eg.

Telogen effluvium, androgenetic alopecia) is an interesting avenue for future translational research.

Macrophage heterogeneity in the skin likely reflects the constant remodeling that occurs during the hair cycle. This is important when considering macrophage involvement in other anagen-inducing processes (Table S1). For example, in plucking induced anagen, damaged hair follicles release CCL2, which attract TNF-producing “M1-like” inflammatory macrophages that *initiate* anagen in surrounding follicles [82], a function that is opposite to the proposed role of the trichophage. This pathway may have evolved to maintain a coat of fur in rodents following environmental or predator-inflicted damage. Other fluctuations of the immune system with the hair cycle have been described [227, 228], and parts of it have been elucidated. For example, depilation-induced anagen is mediated by Jag1-Notch signaling from T regulatory cells [83, 229], and wound-induced hair follicle neogenesis (WIHN) involves recruitment of FGF9-secreting γδ T cells [85]. T regs do not appear to be involved in the spontaneous anagen initiated by JAK inhibition, or macrophage inhibition/depletion in our study, as they do in anagen resulting from depilation. From our observation that the TREM2+ trichophages decrease as telogen progresses, along with the pseudotime analysis of TREM2+ macrophage differentiation trajectories, it can be hypothesized that the trichophages differentiate into a M2-like, tissue-resident phenotype over time. Whether the TREM2+ trichophages can also differentiate into “M1-like” macrophages in response to plucking, or whether they produce chemokines or factors that recruit other cell types that influence the hair cycle, are intriguing questions for future studies.

In the mouse, administration of recombinant OSM was shown previously to be a potent inhibitor of anagen [137], but until now, its source and physiological contribution to the hair cycle

remained undefined. In humans, OSM was first discovered as a negative growth regulator of the A375 melanoma cell line [136], at a time when researchers were hunting for endogenous regulators of cancer cell growth. While OSM was first isolated in the supernatant of histiocytic lymphoma cells [136], it was found to be more reliably obtained from macrophage cell lines [199]. OSM has roles in development, inflammation and hematopoiesis [230, 231]. OSM appears to play a pro-inflammatory role in human keratinocytes [232, 233], causing epidermal hyperplasia in the context of some diseases, but also having inhibitory effects on keratinocyte differentiation under other conditions [138]. Lately, OSM is emerging as an important cytokine in tissue remodeling and regeneration in humans. OSM produced by M2-like macrophages during acute hepatic injury in mice was associated with a pro-fibrotic phenotype [234] . Macrophage OSM has also been shown to induce bone formation by mesenchymal stem cells during physiological osteogenesis [235], as well as in pathological Ewing sarcoma [236]. OSM has also been shown to be secreted in excess by mononuclear cells of patients with systemic sclerosis [237], and has pro-fibrotic effects in the skin and lung [238, 239]. Monoclonal antibodies against OSM are currently undergoing Phase I and II trials for the treatment of systemic sclerosis (Clinical Trial # NCT03041025). Whether there is an analogous subset of OSM-producing trichophages in humans that is involved in the hair cycle is an open question.

Murine HFSCs of the bulge and HG express both the receptor (OSMRβ) and co-receptor (gp130) necessary for OSM signaling, which occurs via the JAK-STAT and MAPK signaling pathways. We show here that STAT5 is the most likely downstream mediator of quiescence in HFSC, since the activated phosphorylated form of STAT5 in the HFSC coincides with the early-to-mid second telogen, and its genetic ablation was sufficient for initiating anagen during telogen. OSM signaling via the JAK-STAT5 pathway inhibits adipocyte terminal differentiation [210], delays cell cycle entry in HepG2 cells [211], and suppresses cytokine secretion in T cells

[212]. Further, the murine OSMRβ subunit is believed to directly recruit JAK2 to phosphorylate STAT5 in response to ligand binding [240].

The maintenance of quiescence via JAK-STAT signaling is emerging as a common theme, where its role is evolutionary conserved. JAK-STAT signaling in the Drosophila testis is mediated by the ligand *Unpaired*, which is the fly homologue of IL-6, and signals via STAT92E to prevent differentiation of the germline stem cells [241]. JAK2-STAT5 signaling in murine hepatic stellate stem cells mediates quiescence signals from vitamin A and insulin [122]. In the murine mammary gland, another organ that undergoes controlled cycles of growth and involution, JAK-STAT3 transmits signals via LIF (another gp130-dependent cytokine) to mediate involution [242], while JAK-STAT5 transmits signals from Prolactin (PRL) during lactation to increase milk production [243]. Interestingly, during pregnancy and lactation, PRL signaling occurs via JAK-STAT5 in the HFSC to maintain quiescence of the hair follicles, perhaps to conserve nutritional resources during pregnancy [120, 147]. Here, we show that the JAK-STAT5 pathway downstream of OSM to maintains HFSC quiescence is physiologically relevant during telogen in male and female mice, and may represent a novel paradigm in the control of stem cell quiescence.

In mice, JAK-STAT3 signaling has been shown to be required for the initiation of spontaneous anagen, but not for plucking-induced anagen [19]. We showed that both STAT3 and STAT5 signaling is dynamically expressed across telogen, but only pSTAT5 is specific for the HFSC during this phase. Further, using the covalent JAK3 inhibitor PF-06651600, we show that inhibition of the JAK3-STAT5 signaling axis alone in HFSCs is sufficient to initiate anagen. The role of STAT3 in keratinocyte differentiation and migration is distinct from the role of STAT5 in maintaining HFSC quiescence. STAT3 and STAT5 signaling likely contribute to complementary

forces of quiescence and proliferation/migration, and may interact in the coordination of the induced hair cycle (ie. in response to plucking, depilation and wounding).

Our findings may potentially expand the indications of JAK inhibitors in the treatment of skin and hair diseases. JAK inhibitors have been FDA approved for the treatment of rheumatoid arthritis (RA) (Tofacitinib), and myelofibrosis (Ruxolitinib). Both these drugs have been shown to be efficacious in the treatment of alopecia areata (AA), an autoimmune form of hair loss [244, 245], where their mode of action likely lies in the inhibition of pathogenic NKG2D+ CD8+ T cells. In our mouse models, topical JAK inhibitors induced a more robust anagen than systemic treatment [102, 104], in agreement with our findings that the local effect on the HFSCs is important for anagen initiation. Topical formulations of JAK inhibitors are currently being developed for AA, and may potentially have a more potent effect on the HFSCs to stimulate regrowth after the autoimmune attack has been treated. The role of topical JAK inhibitors in the treatment of other alopecias, particularly those associated with arrested or prolonged telogen, will be a fascinating avenue for future research.

CHAPTER 3. JAK-STAT SIGNALING IN THE MURINE HAIR CYCLE

Our interest in JAK-STAT signaling in the hair cycle stemmed from the serendipitous observation that JAK inhibitors were more potent at reversing the mouse model of Alopecia Areata (AA) when applied topically, compared with systemic administration [102]. This led to further investigation into the role of JAK inhibitors in the hair cycle of normal C57BL/6 mice (without AA), and the conclusion that JAK inhibition stimulated anagen in a manner that resembled spontaneous anagen [104]. In addition to JAK-STAT5 signaling (discussed in the previous chapter), at the start of this project, we were also interested in examining the contribution of JAK-STAT3 signaling in the murine hair cycle.

Unlike JAK-STAT5 signaling, the role of JAK-STAT3 signaling pathway in the skin and hair follicle is better documented. STAT3 is essential in embryogenesis, and is the only STAT family member that is embryonic lethal when knocked out globally [109]. STAT3 in the epidermis has been extensively studied with respect to its role in cellular functions like differentiation, migration, epithelial-to-mesenchymal transition, and carcinogenesis [246-248]. With respect to the hair cycle, Sano et al showed that constitutive STAT3 ablation in the epidermis (with a K5-Cre driver) did not have an effect on HF morphogenesis. The major effect was on hair cycling, and it was shown that hair follicles (HFs) were arrested in the first telogen phase and unable to spontaneously enter the next anagen [115]. Interestingly, while STAT3 appeared to be required for spontaneous anagen entry, it was shown to be dispensable for plucking-induced anagen, which was postulated to occur via the PI3K-Akt signaling pathway [19]. Thus, the role for STAT3 in anagen initiation is essentially the opposite of the role for STAT5 in maintaining HF quiescence.

In this section, we examine further the role of STAT3 in the murine hair cycle, and we review negative data and experiments that did not succeed. The early decision to focus on the role of STAT5 during hair cycling allowed us to more fully interrogate its role in hair cycling, which was reported and discussed in the previous chapter.

RESULTS

Activated pSTAT3 distribution in the HF

Unlike pSTAT5, whose expression is restricted to the DP and the HFSC particularly during telogen (Figure 2.4B), pSTAT3 has a less well-defined distribution in the skin and HF. There is a constitutive activation of STAT3 on serine 727 (S727), and nuclear pSTAT3-S727 is observed in the epidermis, HF and DP at all stages of the hair cycle. The other phosphorylation site for STAT3 (tyrosine 705, Y705), which has a more restricted pattern of activation, and appears in the outer root sheath (ORS) at P22 and at the DP-HG junction during telogen. This expression becomes more prominent in the bulge and the isthmus HFSCs by the end of telogen at P80 (Figure 3.1), suggesting that pSTAT3 may have pleiotropic and diverse functions during the hair cycle.

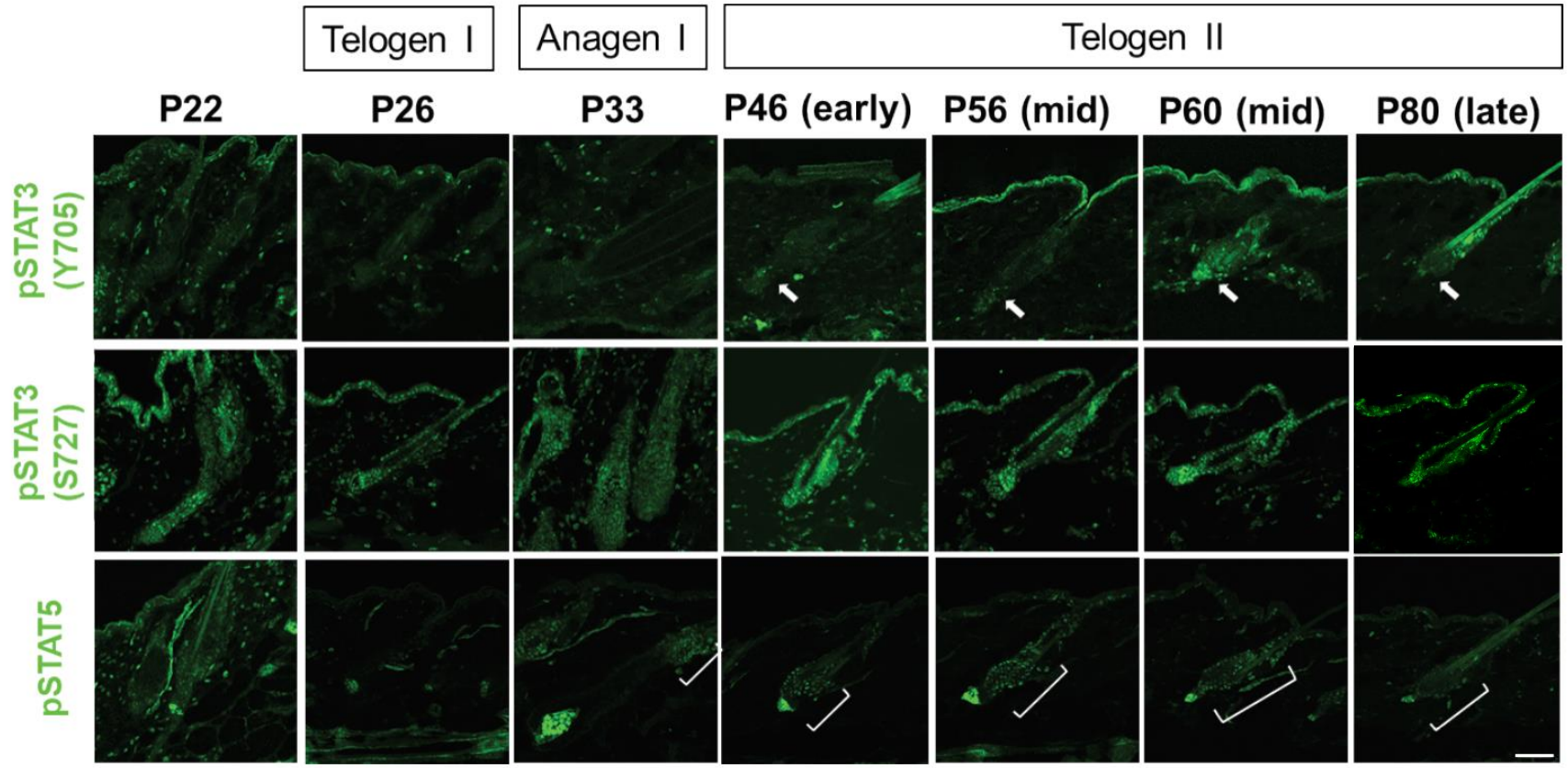

Figure 3.1. Expression of pSTAT3 (both phosphorylation sites) and pSTAT5 across the hair cycle. pSTAT3(S727) is ubiquitous and is seen throughout all cell types at every time point. pSTAT3(Y705) is more restricted to the DP-HG junction during telogen (arrows), and is present during late telogen. pSTAT5, as discussed in Chapter 2, is dynamically expressed in the HFSC across telogen (brackets), and is persistently activated in the DP, even in anagen. Images are representative of 3 mice at each timepoint. Scale bar = 50μm.

Ablation of STAT5 using multiple Cre-drivers induces anagen

In addition to the *K5-CreERT_2* driver transgene discussed in the previous chapter, we also introduced *K14-CreER, K15-CrePR* and *K17-CreERT_2* driver transgenes into *STAT5$^{FL/FL}$* mice. We successfully induced anagen with STAT5 ablation using the K14 and K17 drivers during mid-telogen (Figure 3.2), similar to the results with the *K5-CreERT_2* driver. Since K14 is expressed in the entire epidermis, and K17 is restricted to the HF, all three drivers are expected to target the HFSCs in both the bulge and HG. Surprisingly, when genetic ablation of STAT5 was performed with the *K15-CrePR* driver during mid-telogen, which targets Cre recombinase expression to just the bulge HFSC (but not the HG), anagen was not initiated. This finding suggests that JAK-STAT5 mediated quiescence is most crucial in the HFSCs of the HG, rather than the bulge. Indeed, we have shown that STAT5 ablation results in proliferation of the HG before the bulge (Figure 2.8)

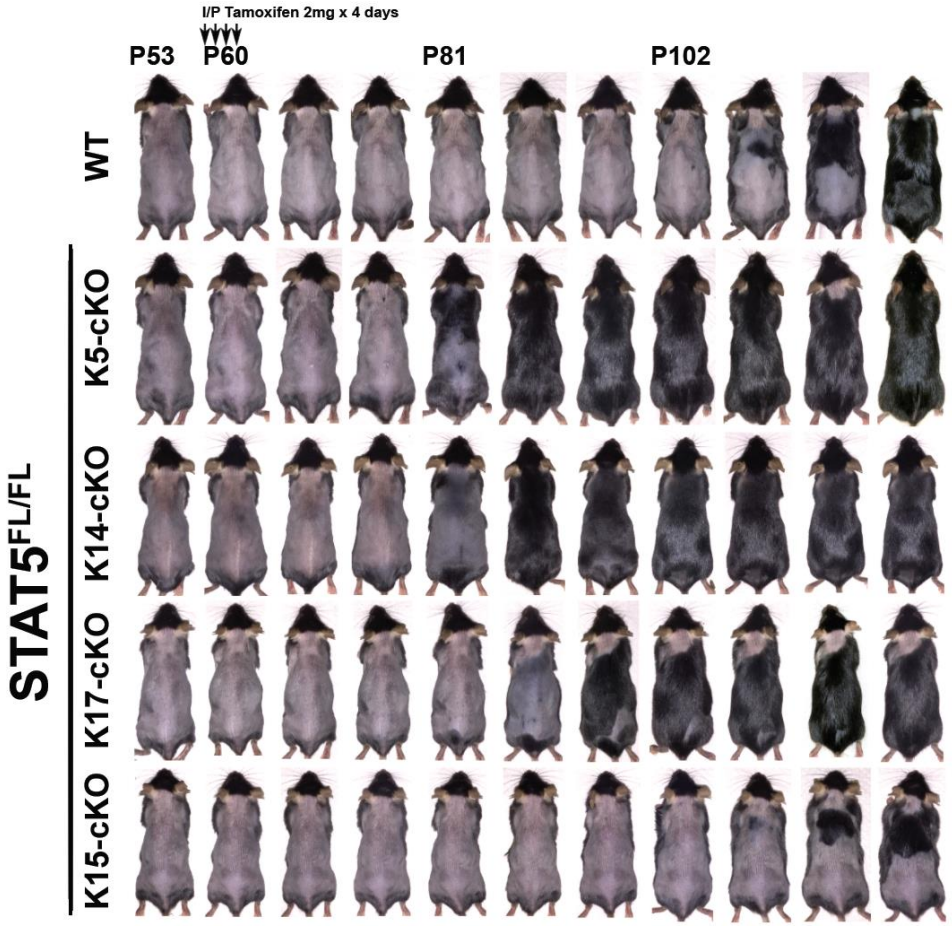

Figure 3.2. Conditional ablation of STAT5 in various epidermal compartments. Using Cre-drivers expressed under the K5/K14 promoters (entire epidermis and HF), and the K17 promoter (just the HF), STAT5 ablation successfully initiated anagen in STAT5a/b$^{FL/FL}$ mice earlier than littermate controls. Interestingly, targeting STAT5 ablation to the bulge with K15-CrePR did not induce anagen. This suggests that the HG (a compartment that is in the HF, and not the bulge) is the likely responsive target of STAT5 ablation. Results are representative of at least 5 litters per Cre driver, with at least 1 homozygous STAT$^{FL/FL}$ mouse in each litter.

Epidermal ablation of STAT5 has minimal effect on HFSC stem cell identity

To determine the downstream effects of JAK-STAT5 inhibition on HFSCs, qRT-PCR was performed on flow-sorted bulge cells (CD34+) and HG cells (P-cad+), 10 and 20 days after systemic Tamoxifen induction in *K5-CreERT$_2$::STAT5a/b$^{FL/FL}$* mice . These time points correspond to those used to analyze HG proliferation in Section 2.XX. Known STAT5-response genes (*CCDN1, CDKN1a, IRF-1, IL2ra, PIM1, Cish*) and HFSC stem cell markers (*NFATc1, Lhx2, Axin2, Tcf3, Tcf4, SOX9)* were selected from the literature [43, 249-253], and their relative expression in the HFSC was analyzed after STAT5 ablation.

Ten days after tamoxifen induction (D10), there was no significant suppression of putative STAT5-response genes in either the bulge or HG. However, by D20, the pattern of suppression of these genes in the bulge and HG were strikingly different (Figure 3.3A). In the bulge, significant suppression of CCDN1, IL2ra and PIM1 was observed 20 days after STAT5 conditional ablation, whereas CCDN1, CDKN1a, IRF-1 and IL2ra were suppressed in the HG. Although these target genes were identified in other cell types (mainly immune cells), their role in epithelial stem cells remains undefined. The change in their expression in bulge vs HG cells following STAT5 ablation suggests that downstream effectors of JAK-STAT5 signaling in the bulge vs HG are fundamentally different, likely due to differences in stem cell identity, chromatin structure, and the presence of co-factors and other transcription factors.

We next investigated the stem cell markers, which tend to be associated with quiescence and self-renewal of the HFSCs. STAT5 ablation had little effect on bulge stem cells markers at D10, but significantly perturbed these genes in the HG. By D20, stem cell markers were generally repressed in both bulge and HG HFSCs, except for Tcf3 expression in the HG, which was upregulated in the HG by D10. Tcf3 is a downstream element of Wnt/β-catenin signaling, and is consistent with the observation that proliferation is first observed in the HG.

These results were corroborated with immunofluorescence studies of telogen HFs performed ten days after STAT5 ablation (Figure 3.3B). The level of pSTAT5 in both bulge and HG was markedly decreased, but the expression of NFATc1, Lhx2, SOX9 and FoxC1 were unchanged. FoxC1 is a newly described quiescence factor in murine telogen HFs [48]. Increased nuclear Tcf3 was observed in the HG of *K5-CreERT_2::STAT5a/b$^{FL/FL}$* mice.

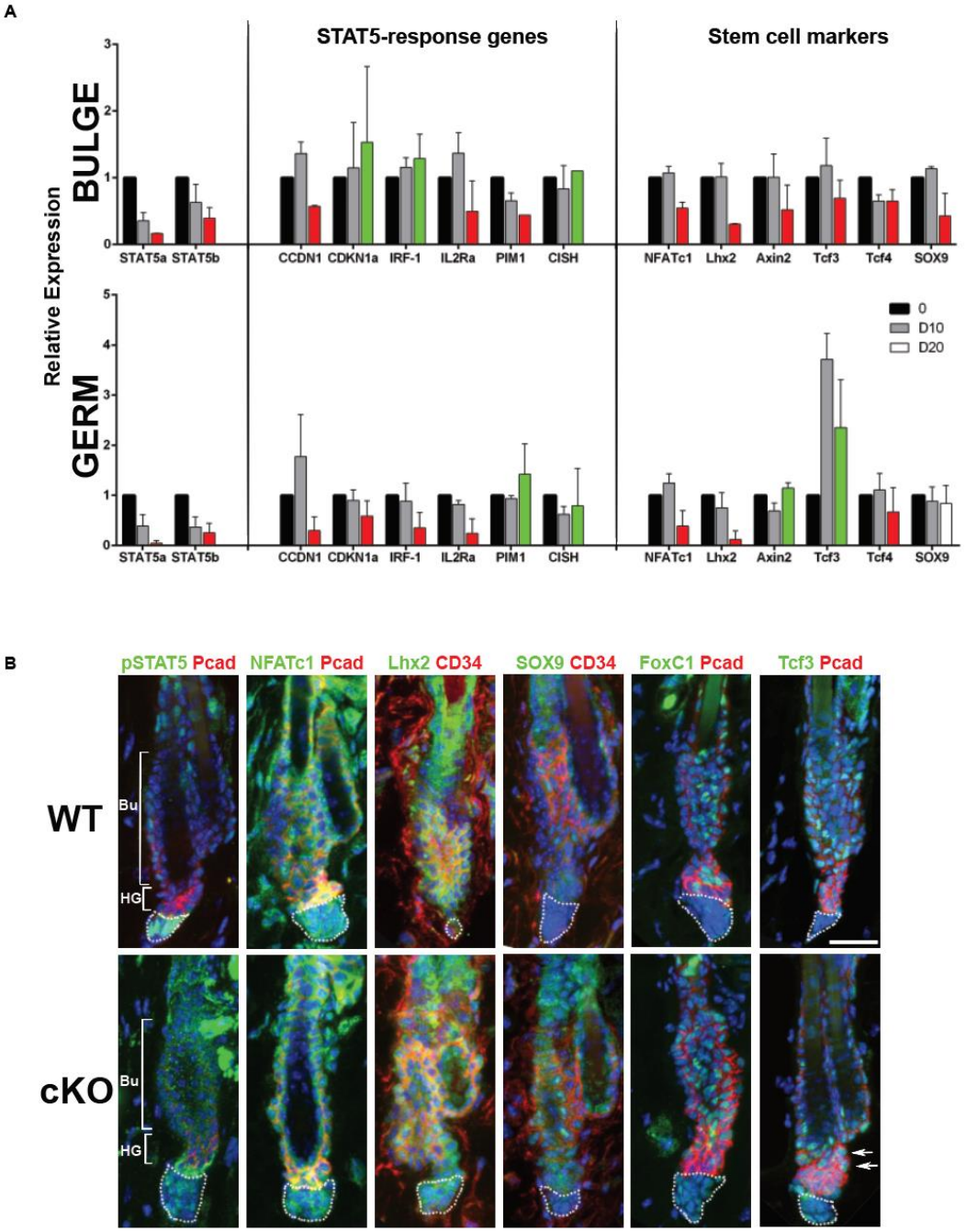

Figure 3.3. Analysis of STAT5-response genes and stem cells markers in the bulge and germ (HG) of STAT5-cKO mice. **A**. qRT-PCR of STAT5a/b, STAT5-respones genes, and stem cell markers in CD34+ bulge and P-cad+ HG at D10 and D20 days after tamoxifen induction. Expression normalized to GAPDH and WT littermates at each timepoint. n = 3 pairs of mice per timepoint. Data are mean ± SEM. At D20, green bars represent increased expression, while red bars represent decreased expression. **B.** IF studies of D10 telogen HFs in WT and STAT5-cKO mice. Note slightly increased Tcf3 expression in HG of STAT5-cKO mice (arrows). Scale bar 25µm.

STAT5 ablation has different effects on bulge and germ proliferation

In order to determine the effects of STAT5 ablation in the different stem cell compartments of the skin, colony forming assays were performed on epidermal stem cells sorted by FACS. Interfollicular epidermal (IFE), bulge and HG stem cells from WT or *K5-CreERT$_2$::STAT5a/b$^{FL/FL}$* mice were plated and cultured for 2 weeks, with or without the addition of Tofacitinib. Tofacitinib had little effect on IFE stem cells, but increased the colony-forming ability of both bulge and HG cells (Figure 3.4). Intriguingly, STAT5-ablation had very little effect on bulge stem cells, even *in vitro*, but was associated with increased colonies of HG stem cells, to the level of Tofacitinib treatment. Thus, while JAK inhibition was able to enhance proliferation of bulge stem cells, it does not do so via STAT5. Further, in keeping with our observations *in vivo*, the loss of STAT5 primarily resulted in HG proliferation, consistent with the two-step hypothesis of anagen initiation.

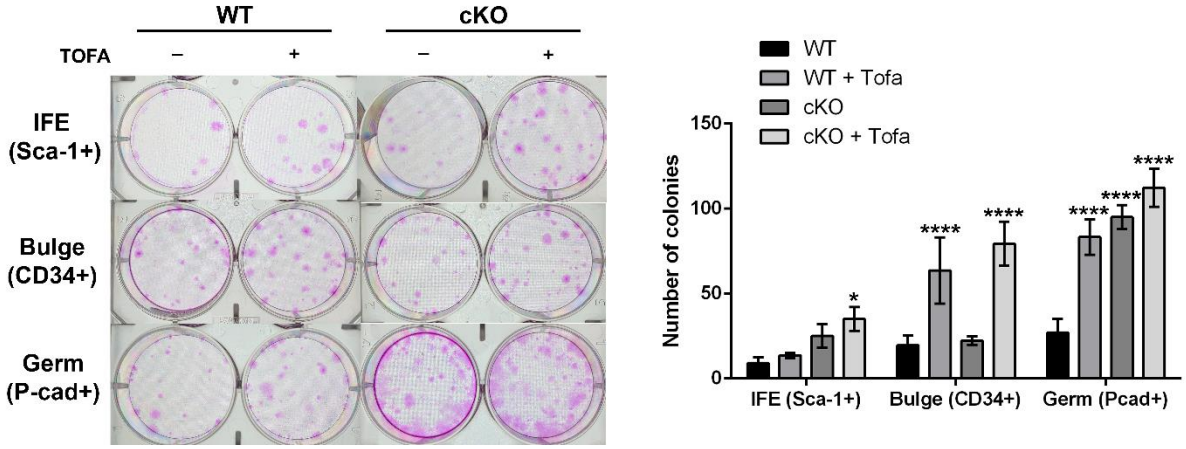

Figure 3.4. Colony forming assay of WT and STAT5-cKO epidermal stem cells. JAK-inhibition has minimal effects on IFE cells, while Tofacitinib treatment increased colony-forming abilities of bulge and HG stem cells. While STAT5-KO had no effect on bulge proliferation, it was associated with increased HG proliferation. IFE = Interfollicular Epidermis, HG = Hair Germ. Data are mean + SEM. *p < 0.05, **p < 0.01, ***p < 0.001, ****p<0.0001Two-way ANOVA of genotype, followed by Tofacitinib treatment.

In silico analysis of STAT5 response elements and target genes

In order to identify downstream quiescence genes that may be affected by STAT5 ablation, we used published datasets to identify STAT5-response genes whose expression changes in a pattern that correlates with that of pSTAT5 activation in HFSCs. Greco et al performed RNA-sequencing on flow-sorted bulge, HG and DP cells from early (P43), mid (P56) and late (P69) telogen in wild-type C57BL/6 mice [52]. Their data showed that telogen HG cells were more transcriptionally active than the bulge. They also showed upregulated Wnt/β-catenin signaling at late telogen, which supports our findings in the previous section.

Using published ChIP-seq information on STAT5a/b binding elements [249, 250, 254], we performed an *in silico* ChIP-seq to identify likely STAT5-response genes in the HG of the Greco dataset (GSE15185). Next, we filtered this list of STAT5-response genes to find those that had relative expression levels that matched the pattern of pSTAT5 activation in the epidermis (ie. highest during mid-telogen) (Figure 3.4, inset). When viewed on a heatmap, we observed that putative STAT5-response genes were more dynamically expressed in the HG across telogen, in agreement with findings by Greco et al. This *in silico* experiment suggested that JAK-STAT5 signaling in the HFSC of the HG is dynamically regulated across telogen. The gene that best matched our criteria in this experiment was *Id1* (Figure 3.4).

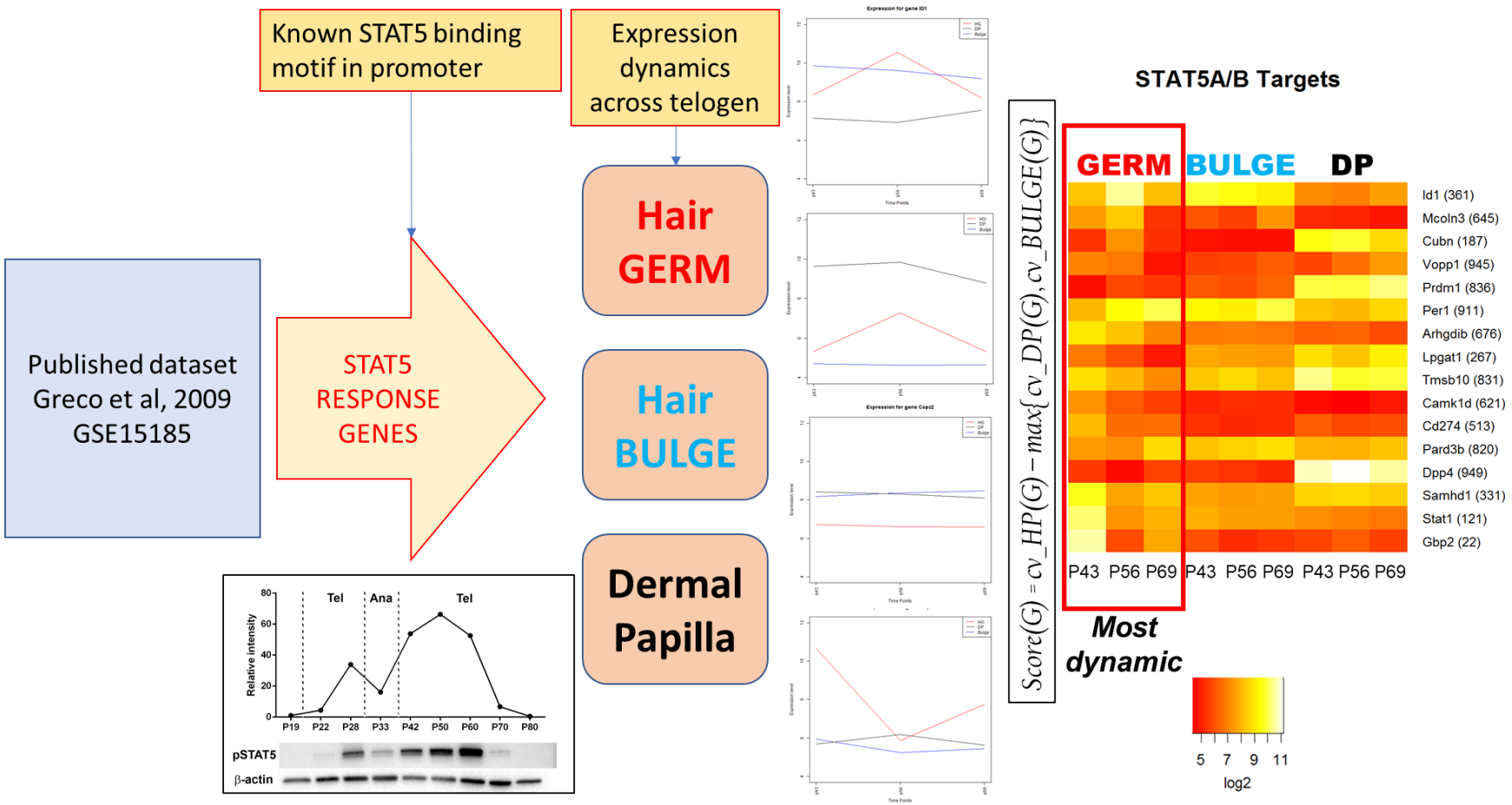

Figure 3.5. **In silico ChIP-seq workflow**. STAT5-response elements identified in published ChIP-seq data (Basham et al, 2008; Kanai et al, 2014) were used to identify potential downstream STAT5-response genes. Microarray data from telogen bulge, HG and DP (Greco et al, 2009) were used to find STAT5-response genes that fluctuated in a pattern that matches pSTAT5 activated in the murine skin during telogen (inset). HG genes were the most transcriptionally dynamic across telogen. ID1 was identified as a gene that best matched pSTAT5 activation.

ID1 is a marker of quiescence downstream of JAK-STAT5 signaling

ID1 (Inhibitor of DNA-binding, or Inhibitor of Differentiation) is a transcriptional repressor that has been identified to be downstream of BMP-SMAD1/5 signaling in the HFSC [13]. ID1 has also been shown to be upregulated in myoblasts in response to OSM stimulation, where it inhibited differentiation of myoblasts [206]. Using our *in silico* ChIP-seq data, we found that ID1 expression in the HG is dynamic, and peaks during mid-telogen (Figure 3.5A). In contrast, ID1 expression in the bulge and DP does not change throughout telogen. Using immunofluorescence studies, we found nuclear ID1 to be most prominent in HFSCs during early telogen, and its expression is reduced in the HG by late telogen. During anagen, ID1 expression is maintained in the bulge, but is absent from the ORS and matrix keratinocytes, consistent with the known role of ID1 in maintaining HFSC quiescence (Figure 3.5B).

We next performed qRT-PCR on flow-sorted HG cells at D20 after tamoxifen induction of *K5-CreERT$_2$::STAT5a/b$^{FL/FL}$* mice and control littermates. We found that STAT5 ablation is associated with a significant downregulation of the ID1b isoform (Figure 3.5C), which has been shown to be a mediator of stem cell quiescence and self-renewal [255]. Using immunofluorescence, we showed that STAT5 ablation is also associated with loss of nuclear ID1 in both the bulge and HG as early at D10. This is accompanied by increased EdU incorporation in the HG by both D10 and D20 (Figure 3.5D).

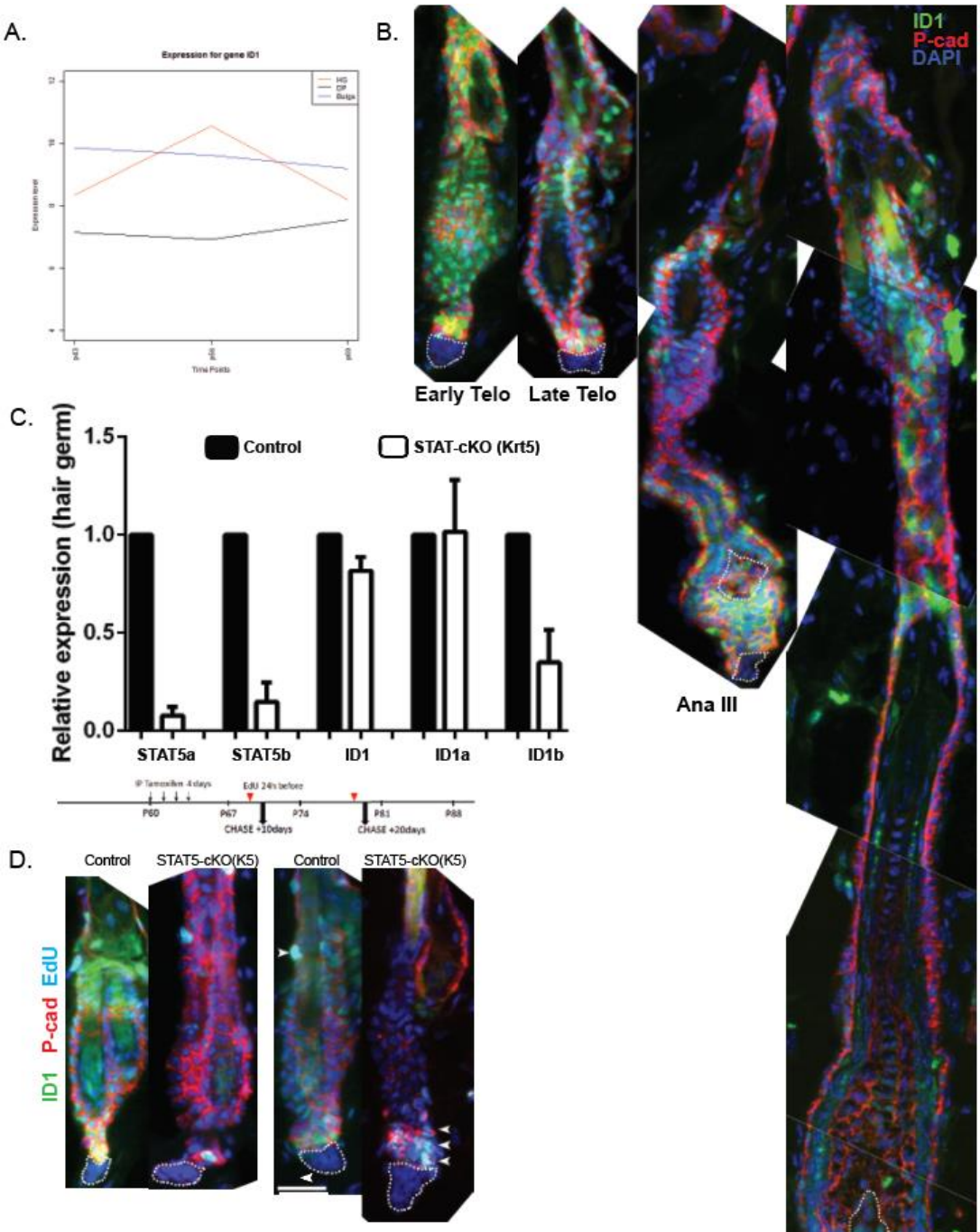

Figure 3.6. ID1 as a quiescence factor in HFSCs. A. ID1 expression peaks in mid-telogen (red line) according to datasets published by Greco et al. **B.** IF studies of a HF as it progresses from telogen to anagen. Nuclear ID1 (green) is prominent in the telogen HFSC, and is not expressed in the proliferative ORS or matrix during anagen. ID1 expression is maintained in the bulge throughout. Dotted line circles the DP. **C**. STAT5 ablation is associated with a selective downregulation of the ID1b isoform in HG. n = 3 mice per genotype. Data are mean ± SEM. **D.** STAT5 ablation is associated with loss of nuclear ID1 in both bulge and HG, and proliferation of the HG as seen by EdU incorporation (arrowheads). Scale bars = 25µm.

Initial Experiments: Attempted ablation of STAT3$^{FL/FL}$ mice did not induce anagen

Early in the project, we asked if STAT3 had a similar role in maintaining HFSC quiescence by genetically ablating STAT3 during mid-telogen. Using the same *K5-CreERT$_2$, K15-CrePR* and *K17-CreERT$_2$* drivers (last one data not shown), no early entry into anagen was observed, unlike the STAT5 ablation experiments described earlier (Figure 3.6).

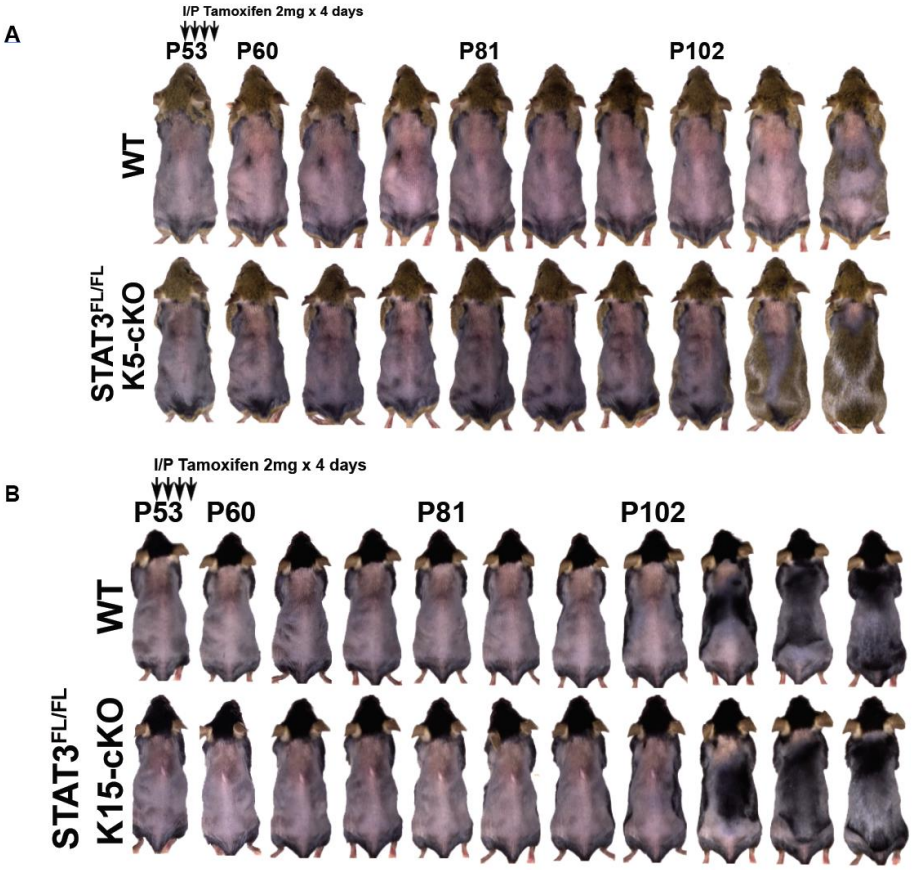

Figure 3.7. STAT3 ablation in the skin/HF with the **A.** K5-CreERT$_2$ driver, and in the HFSC with the **B.** K15-CrePR driver were not associated with significantly earlier telogen. K17-CreER data not shown.

STAT3 expression was unchanged despite tamoxifen administration

During analysis of these experiments, we were puzzled that we were not able to show ablation of STAT3 by immunofluorescence, or by Western blot in the isolated epidermis of homozygous mutant mice (Figure 3.7A-B). In order to address this, we first checked the validity of out *K17-CreERT$_2$* driver by breeding the *STAT3$^{FL/FL}$* locus into a *K17-CreERT$_2$::R26-mTmG* reporter strain. Tamoxifen induction of this mouse (*K17-CreERT$_2$::STAT3$^{FL/FL}$::R26-mTmG)* resulted in mGFP expression restricted to the HF (Figure 3.7C), reflecting the expected spatial and temporal expression of a functional Cre recombinase. To determine whether the genomic recombination had taken place, we used flow cytometry to isolate the GFP+ cells of the HF, and demonstrated, disappointingly, that STAT3 was not ablated using two different sets of primers (Figure 3.7D).

Upstream loxP site was disrupted in the STAT3$^{FL/FL}$ mouse

Because the Cre recombinase enzyme was functional and expressed in an expected manner as revealed by our reporter mouse, in order to determine the reason for the failed recombination event, we next asked if there was a mutation within with the floxed STAT3 allele itself. Sequencing primers were designed to flank Introns 17 and 20 of the STAT3 allele [256], where the *loxP* sites were inserted. While the 34bp *loxP* sequence was found intact in Intron 20, we failed to locate the other *loxP* site in Intron 17 (Figure 3.8). This unfortunate discovery came after nearly 1 year of work on the STAT3 allele, and taught us a lesson to always sequence the *loxP* sites in a new floxed mouse line!

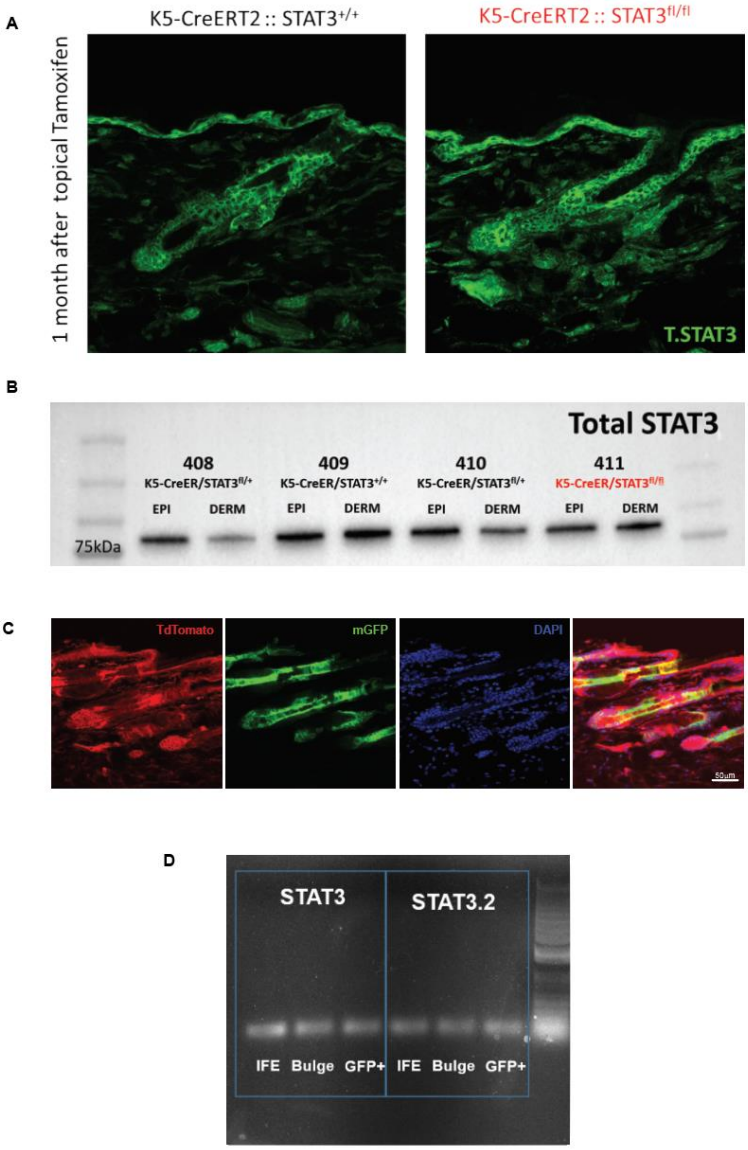

Figure 3.8. Assessment of STAT3$^{FL/FL}$ mice. A. IF studies for total STAT3 in skin and HF of *K5-CreERT$_2$::STAT3$^{FL/FL}$* mice and control littermates showed no difference expression. **B.** Western blot for total STAT3 in dissociated epidermal and dermal fractions of *K5-CreERT$_2$::STAT3$^{FL/FL}$* mice and control littermates shows no significant reduction in STAT3 expression in mutant skin. **C.** IF studies of *K17-CreERT$_2$::R26-mTmG* shows that the Cre-recombinase is functional, and expressed only in the HF, as expected. **D.** qRT-PCR of FAC-sorted GFP+ cells in *K17-CreERT$_2$::R26-mTmG::STAT3$^{FL/FL}$* mice shows these cells to be expressing STAT3. Two sets of primers were used: STAT3 and STAT3.2. Scale bars = 50μm.

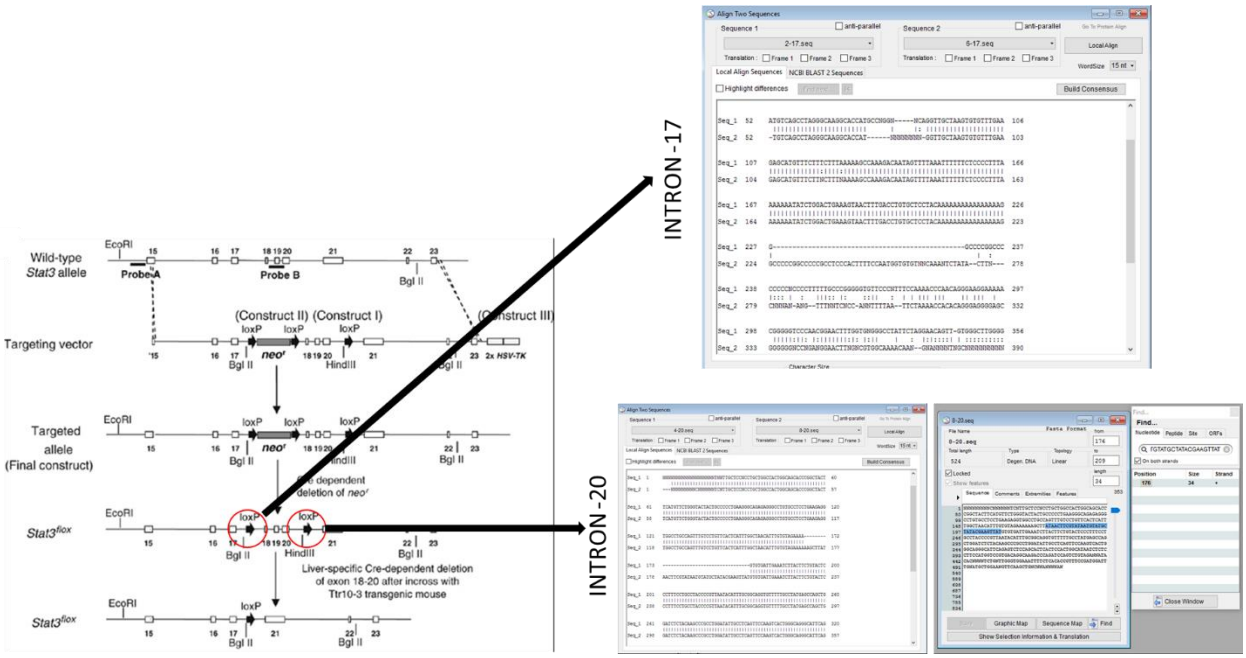

Figure 3.9. **Sequencing of *loxP* sites in introns 17 and 20 of STAT3 locus**. $STAT3^{FL/FL}$ mice developed by Moh et al, 2007 were obtained from the Jackson Laboratories. Genotyping primers targeted intron-20, which had the intact *loxP* site. Sequencing of intron-17 showed loss of the other *loxP* site.

Second set of Experiments: Epidermal STAT3 ablation – with intact loxP sites

After ordering a new $STAT3^{FL/WT}$ breeder pair from Jackson Laboratories, homozygous $STAT3^{FL/FL}$ were generated and genomic DNA was immediately sequenced to verify the presence and integrity of both loxP sites. This time, the *loxP* sites in both Introns 17 and 20 were present and intact (Figure 3.9A). These mice were further bred with *K5-CreERT*$_2$ mice, and Tamoxifen induction of STAT3 ablation in mid-telogen (P53-P60) was carried out in 2 separate litters to date. Preliminary results (work is ongoing) show that anagen initiation does not occur at the time typical for *K5-CreERT*$_2$*::STAT5a/b*$^{FL/FL}$ ablation (ie. around 3 weeks after tamoxifen administration) (Figure 3.9B). While these preliminary data support our hypothesis of

different roles of STAT3 and STAT5 in the hair cycle, these mice require extensive characterization and will be carried forward by others in the lab.

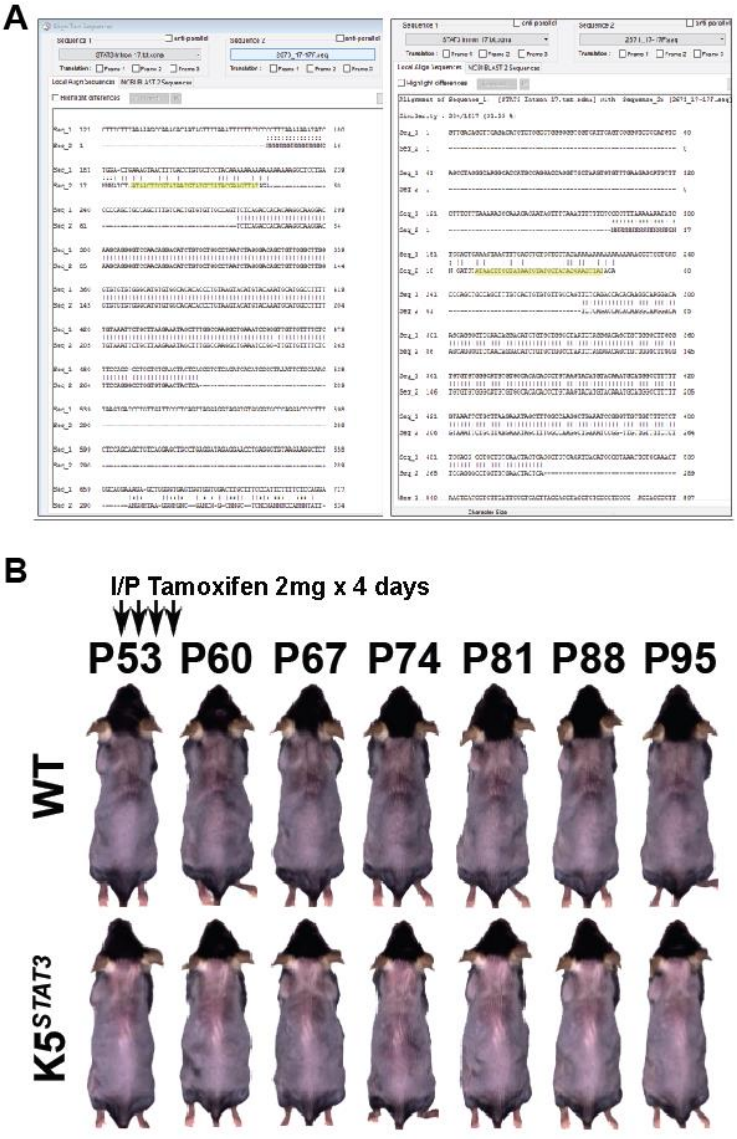

Figure 3.10. A. Sequencing of Intron 17 of new STAT3$^{FL/FL}$ mice re-ordered from Jackson Laboratories, with the 34-mer loxP site highlighted in yellow. **B.** Preliminary epidermal STAT3 ablation during mid-telogen showing no effect on the telogen-to-anagen transition, supporting our hypothesis of differential roles for STAT3 and STAT5 in the hair cycle. Results representative of 2 litters.

DISCUSSION

While both JAK-STAT3 and JAK-STAT5 signaling are dispensable for HF morphogenesis [19, 115, 118, 119], they appear to have distinct roles in the adult hair cycle. Most of the other signaling pathways of the hair cycle are believed to have been reprised from HF morphogenesis [9], whereas the role of JAK-STAT signaling in the control of the hair cycle appears to be most physiologically relevant during adulthood.

Genetic ablation of STAT5 in the various compartments of the skin and HF suggested that the HG is the most sensitive compartment that responds to JAK-STAT5 inhibition. This finding is in agreement with our previous observation that the HG is also the first to proliferate in response to pharmacological JAK-inhibition [104], and also in spontaneous anagen [52]. Greco et al also found the HG to be the most transcriptionally dynamic population during telogen [52], which may in part reflect active JAK-STAT5 signaling by OSM to promote quiescence.

Other signals that have been postulated to maintain HFSC quiescence include BMP2/4-SMAD1/5 signaling from the dermis and subcutaneous fat [39], FGF-18 and BMP-6 signaling from the K6+ inner bulge [40], and autocrine Wnt/Axin-2 signaling from the HFSC themselves [41]. These signals may contribute in part to defining the epigenetic state of HFSCs. BMP4 in particular leads to reduction of H3 K4/K9/K27me3 methylation in HFSCs, which allows stem cell plasticity and self-renewal [257]. Wnt signaling in the HFSC niche has also been associated with downstream Tcf3/Tcf4 occupancy in the HFSC-related genes, where they act to repress stem cell activation [258]. While the effect of JAK-STAT signaling on these complex interactions has not been studied in the HFSC, STAT5 has been shown to be involved in chromatin re-organization in cultured mammary epithelial cells [259].

Our data suggests that STAT5 ablation in the HFSC leads to distinct changes of Tcf3/Tcf4 in the bulge vs HG (ie. both are repressed in the bulge at D20, but Tcf3 is upregulated >> Tcf4 in the HG), which is likely to affect the transcriptional status of HFSCs in significant ways. Interestingly, JAK-STAT3 downstream of OSM signaling in human mammary epithelial cells has been reported to cooperate with TGF-β/SMAD3 signaling to regulate senescence in human mammary epithelial cells [208]. This pathway is highjacked by breast cancer to drive epithelial-mesenchymal transition to increase invasiveness [260]. STAT/SMAD interactions should be explored further in the HFSC, since we uncovered ID1 to be a possible STAT5-response gene in the HG, where it has previously been linked to pSMAD-1/5 signaling [13]. Thus, cross-talk and interactions between these various signaling pathways are likely to contribute to varying patterns of activation observed during the normal hair cycle [63].

JAK-STAT signaling during adulthood may allow the hair cycle to respond to environmental insults. The stereotypical phases of regression and regeneration during the hair cycle can be utilized for wound healing, hair regrowth and even *de novo* HF neogenesis. While JAK-STAT3 signaling appears to be required for entry into spontaneous anagen, this pathway can be circumvented in the case of plucking, whereby anagen initiation can proceed in the absence of STAT3 [19]. This redundancy in signaling pathways allows for the regrowth of hair that has been plucked or removed forcibly by initiating the hair cycle, independently of JAK-STAT3 signaling. JAK-STAT5 signaling in the HFSC is central for maintaining quiescence, which is not a feature that is prominent during morphogenesis. Thus, in adulthood, JAK-STAT5 signaling by OSM during normal telogen, as well as by PRL during pregnancy and lactation [120], act to prevent premature or unnecessary HFSC activation and proliferation, in order to maintain the stem cell niche of the HF.

Due to a defective *loxP* site, our *STAT3*$^{FL/FL}$ mice experiments were unfortunately not initially successful. The defective *loxP* was uncovered after about a year of failed experiments and troubleshooting, and advice from many colleagues and advisors. Fortunately, although STAT3 and STAT5 have similar dynamics across telogen, our experiments showed that ablation of STAT5 alone in the epidermis and HF is sufficient to induce anagen.

Whether STAT5-ablation-induced anagen is a STAT3-dependent process will be an interesting question for future research. Future experiments on STAT3/STAT5 double-cKO mice will highlight the differences between spontaneous anagen and experimentally-induced anagen in rodents, and may reveal similar processes in humans. If anagen resulting from STAT5-ablation was STAT3 dependent, it may truly reflect spontaneous anagen more so than other forms of experimentally-induced anagen, and could be a useful new model for studying the hair cycle in mammals. The ability to manipulate these processes pharmacologically with increasingly specific small molecule inhibitors of the JAK-STAT pathway could expand the current treatments for the various forms of human alopecia.

CHAPTER 4. DISCUSSION

SUMMARY

In this body of work, I defined the role of JAK-STAT signaling in the maintenance of HFSC quiescence during telogen. This question arose from previous observations in our lab that application of topical JAK inhibitors was a potent inducer of anagen in mouse telogen skin. Using a variety of methods, I identified the JAK-STAT5 signaling pathway in HFSCs to be the mechanism by which quiescence is achieved. I also identified OSM as a likely upstream ligand that inhibits HFSC proliferation, and a distinct subset of TREM2+ macrophages that is the source of OSM during early-to-mid telogen. Genetic analysis of this subset of macrophages suggest they are ontologically similar to microglia, and may represent a class of skin-resident macrophages that function to coordinate regeneration and remodeling required during the hair cycle.

FUTURE DIRECTIONS

The identification of the OSM-OSMR-JAK-STAT5 axis that maintains quiescence and prevents HFSC proliferation in telogen provides us with a candidate "*chalone*" that has negative, inhibitory properties in the hair cycle. This discovery, along with the identification of the TREM2+ trichophages as the source of OSM, raises more interesting questions.

Role of JAK-STAT3 and JAK-STAT5 signaling in experimentally induced vs spontaneous anagen

My work in this thesis shows that JAK-STAT5 signaling is necessary for maintaining HFSC quiescence during telogen. However, evidence from the *K5-Cre::STAT3*$^{FL/FL}$ mouse studies by Sano et al suggest that STAT3 may play a role in anagen initiation, rather than maintaining HFSC quiescence. Intriguingly, while epidermal STAT3 ablation blocked entry into spontaneous anagen, it did not interfere with or prevent plucking-induced anagen. This finding suggests distinct pathways may regulate entry into spontaneous (STAT3-dependent) vs experimentally-induced anagen (STAT3-independent) [19]. I have also recently ablated STAT3 in the epidermis using *K5-CreERT*$_2$ with fresh *STAT3*$^{FL/FL}$ mice, and observed no effect on HFSC quiescence during telogen.

How JAK-STAT3 and JAK-STAT5 signaling interact to control the hair cycle should be explored. Whether *K5-CreERT*$_2$*::STAT3*$^{FL/FL}$ mice are able to initiate anagen induced by topical JAK inhibitors is an intriguing question, in light of STAT3-dependent and independent pathways to hair growth. Negative results from this experiment will strengthen the case that JAK inhibitor induced anagen closely resembles spontaneous anagen, and can be used as a new research model, in addition to plucking- and depilation-induced anagen, which induce immunological insults that may confound some experiments. Further, by targeting genetic ablation of STAT3 and/or STAT5 to the skin and HF, it should be possible to assess if STAT3 loss will prevent anagen induced by STAT5 ablation during telogen.

Determining the origin, fate and lineage of TREM2+ macrophages in the skin

The identification of this rare, discrete subset of macrophages could only have been achieved with single-cell RNA sequencing. This small population would have been easily missed in bulk RNA-seq experiments, and flow sorting with traditional M1 and M2 markers would also have

overlooked this sub-population because of the known heterogeneity of TRMs [92]. However, their presence in the skin opens up many new avenues for research.

For example: Do TREM2+ trichophages have other functions in the skin? Macrophages have been described to function at several points in the hair cycle, and are undoubtedly essential in skin homeostasis. Microglia-like macrophages have been postulated to be involved in the remodeling of Merkel cell-neurite complexes (D. Owens, personal communication), and could have additional roles in cyclic HF regeneration. Using a *TREM2-CreER* transgenic mouse to ablate this subset of macrophages at various points of the hair cycle, and detailed morphometric analysis of the HF and appendages at various timepoints would reveal the extent of their contribution. Further, the role of trichophages in wound healing and wound-induced HF neogenesis should also be studied.

Interestingly, these TREM2+ trichophages share genetic ontology with microglia of the CNS, which are long-resident tissue resident macrophages derived from the embryonic yolk sac [98]. While most macrophages in the skin are believed to be derived from circulating monocytes, it will be intriguing to ask if there is a small, persistent yolk-sac derived population in the skin that give rise to trichophages, and whether the dermal tissue microenvironment plays a role in determining the function of this population. I generated preliminary data in which *Csf1r-CreER::R26-TdTomato* pregnant dams were induced with tamoxifen at E8.5 to label yolk-sac derived macrophages, and found that less than 1% of the adult dermal macrophages arise from this population, compared with 85.9% of labelled microglia in the brain (Figure 4.1A). Some TREM2+ trichophages that cluster distinctly at P45 are also positive for CCR2 (Figure 4.1B), suggesting that they are recruited to the skin from the circulation during adulthood, and are not of yolk sac origin. Whether this cluster is heterogenous is an open question. Depleting the yolk

sac-derived population with an E8.5-labelled *Csf1r-CreER::R26-iDTR* mouse during early telogen would determine if this subpopulation is the only OSM-producing subset in the skin.

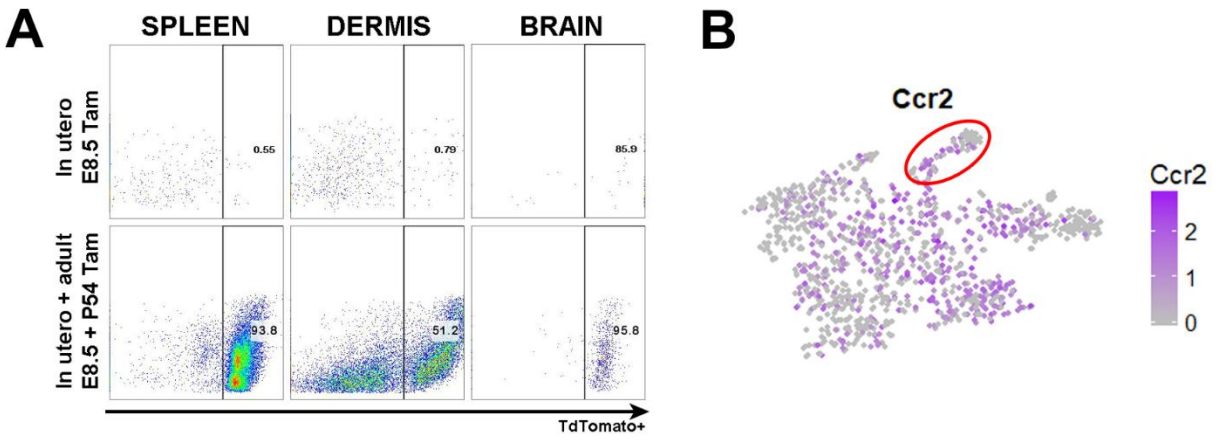

Figure 4.1. Preliminary lineage tracing of skin macrophages. A. Macrophages were labeled at E8.5 by administering a pregnant dam with tamoxifen, and half of the litter was given another single dose of tamoxifen at P54. Pups were analyzed at P56. TdTomato+ cells were gated on CD45+ F4/80+ CD11b+ macrophages. Yolk sac derived macrophages are only labeled at E8.5, and comprise 0.79% of the dermal macrophages but 85.9% of CNS microglia. One dose of tamoxifen in adulthood labels around half of dermal macrophages. B. Single-cell RNA-seq data of dermal CD45+ immune cells. TREM2+ OSM-producing trichophages (red circle) are also partially CCR2+, suggesting a portion of them is recruited to the skin from the circulation.

Our data show a reduction of the TREM2+ trichophages during telogen. Unfortunately, single-cell RNA sequencing and FACS are unable to determine the actual fate of these cells. To study the fate of these trichophages, a TREM2+ reporter mouse is required to perform lineage tracing of these cells. Do TREM2+ trichophages die, leave, or differentiate into other macrophage subsets over telogen? Do they become theTNF-producing macrophages that mediate plucking-induced anagen [82]? The current available macrophage and microglia reporter mice are not well-suited for this experiment because they are not specific for this distinct TREM2+ subpopulation. For example, while *CX3CR1*^{GFP} mice label microglia in the CNS, their expression

on dermal macrophages is weak and not specific enough to target the TREM2+ population (Figure 4.2).

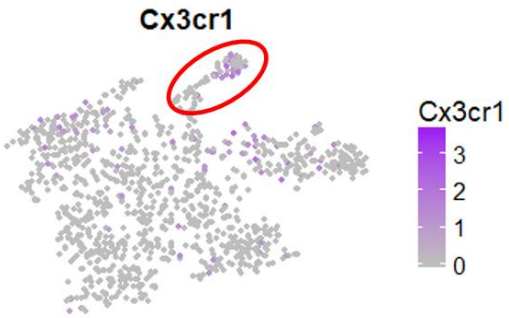

Figure 4.2. CX3CR1 expression in P45 dermal CD45+ immune cells. TREM2+ trichophages (red circle) will not be exclusively labelled with a CX3CR1^{GFP} reporter, which is used to perform lineage tracing of microglia in the CNS.

The role of macrophages and OSM in human androgenetic alopecia (AGA)

We obtained balding scalp from discarded surgical specimens of males with AGA, and using RNA-seq, compared their gene expression with non-balding occiput scalp using excess tissue hair transplantation procedures. Our preliminary human data using these unmatched balding/non-balding scalp samples from male donors suggest that balding scalp is enriched for macrophage markers and OSM (Figure 4.3A). Immunofluorescence studies of balding male AGA scalp also show increased FCGR1A+ macrophages that contain OSM (Figure 4.3B). Future endeavors to replicate this finding in matched samples should clarify OSM-producing macrophages are indeed associated with AGA. If confirmed, the concept of the miniaturized HF in AGA may be considered a form of arrested telogen and efforts to reawaken the HFSC in this condition with macrophage inhibition may be a feasible line of future investigation.

A

Gene	Fold change balding vs non-balding	p-value
FCGR1A	49.50	4.604E-02
CSF3	20.29	9.255E-03
OSM	18.94	1.456E-02
PROK2	15.43	4.343E-02
EMR1	13.40	4.998E-03
ADAMTS4	13.06	3.494E-02
PAX8	12.03	8.106E-05
PLAUR	9.10	3.903E-02
CD300C	8.63	4.534E-02
PI3	8.60	2.994E-02
CCR1	8.40	4.733E-03

B

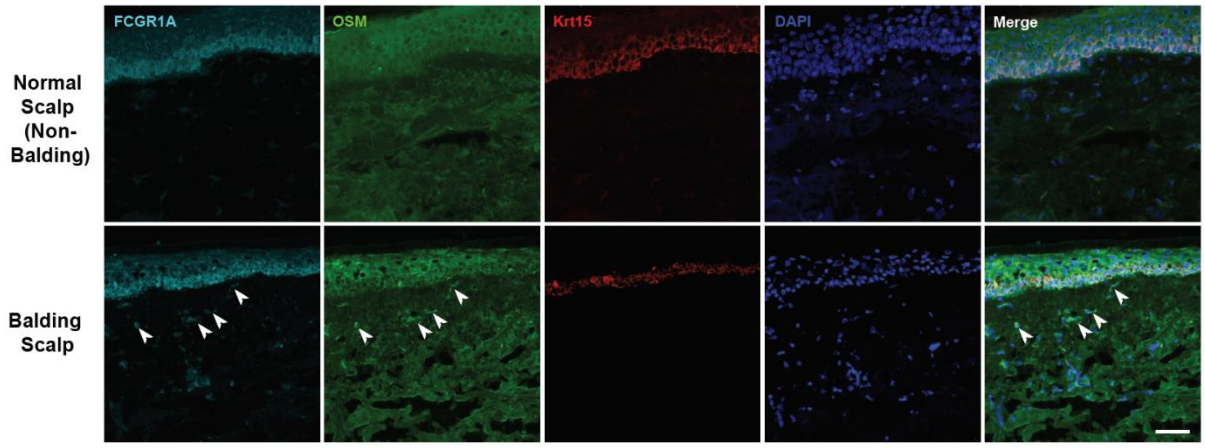

Figure 4.3. Macrophages and OSM in human AGA scalp. **A**. RNA-seq data from unmatched balding vs non-balding scalp showing enrichment of macrophage-related genes in green, and OSM in red, in the balding samples. **B**. Immunofluorescence studies of balding vs non-balding scalp showing more FCGR1A+ macrophages that co-localize with OSM in balding scalp. Scale bar = 50μm.

Assess the role of macrophages in the pathogenesis and maintenance of Alopecia Areata (AA)

This project was inspired by a serendipitous observation made in our lab while investigating the efficacy of JAK inhibitors in the treatment of AA, therefore we should define role of macrophages and OSM in AA pathogenesis and disease progression. Using the C3H/HeJ mouse model of AA, and the macrophage inhibition techniques described in this thesis, the role of macrophages in AA can be interrogated.

Due to their presence and ultrastructural features during murine catagen, Parakkal et al suggest that macrophages may be involved in actively resorbing remnants of the involuted HF during

catagen. While macrophages are not professional antigen presenting cells (APCs), they may be actively processing HF antigens and epitopes that might be key in inducing autoimmunity in C3H/HeJ mice. Macrophage depletion with neutralizing antibodies or pharmacological (Pexidartinib) methods in the C3H-H3J model, along with analysis of macrophage and dendritic cell (DC) populations during AA disease development will address this pressing question.

We have shown in this thesis that macrophages are required for maintaining HFSC quiescence in telogen. Since the NKG2D+ CD8+ effector cells in AA are believed to preferentially attack anagen HFs, it is compelling to ask if macrophage ablation during active AA will accelerate or attenuate the disease. It will be interesting to ask whether macrophages control the hair cycle during AA disease progression, or perhaps whether macrophages interact with the effector cells of AA to affect the presentation of disease. The presentation of AA in humans and mice (patches of alopecia that seem to spread centrifugally) suggest that a diffusible signal or a migratory cell may be involved in the progression of AA. This issue can be addressed by genetic and pharmacological macrophage inhibition, coupled with intravital imaging and lineage tracing of macrophages during the course of AA.

CONCLUSIONS

In this thesis, I have established a role for the JAK-STAT signaling pathway in the complex network of cells and signals that control the mammalian hair cycle. I have shown that JAK-STAT5 signaling in the HFSC during early- and mid-telogen is required for maintaining the quiescence of hair follicles, and disruption of this signaling by pharmacological or genetic means is sufficient for initiating hair growth. Further, I have identified potential downstream effectors of JAK-STAT5 signaling (ie. ID1) that may act in concert with other signaling pathways to maintain quiescence of the HFSC.

Using state-of-the-art techniques like single-cell RNA sequencing, I uncovered a distinct subset of OSM-producing macrophages in the telogen dermis that contribute to the JAK-STAT5 mediated quiescence in the HFSC.

JAK-STAT signaling, while ubiquitous in stem cells and immune cells, may have distinct and complementary functions, even within the same cell type, as exemplified by JAK-STAT3 vs JAK-STAT5 signaling in the HFSC. Future development of JAK inhibitors with increased selectivity for specific JAK isoforms, and even direct specific STAT inhibitors, will refine our ability to target different cellular processes. This work highlights the potential of these drugs in modulating immune function, stem cell quiescence, and hair follicle regeneration, with relevance to human hair disorders.

MATERIALS AND METHODS

EXPERIMENTAL MODELS AND SUBJECT DETAILS

Animals

Mice were bred and maintained in the Russ Berrie Medical Sciences Pavilion Animal Facility in accordance with guidelines of the Institute of Comparative Medicine (ICM) and Institutional Animal Care and Use Committee (IACUC) of Columbia University. The Facility is specific pathogen-free, and all mice were socially housed under a 12 hour light/dark cycle. All mice were bred in the facility so as to have documented birth dates for accurate ages. All experiments were performed during the early- to mid-telogen phase of the hair cycle, or at the end of the previous anagen phase (P35 – P60), unless otherwise specified. *K5-CreERT2::OSMRβ*$^{FL/FL}$ or *K5-CreERT2::STAT5a/b*$^{FL/FL}$ were compared with control littermates (No CreER or *OSMRβ*$^{wt/wt}$*/STAT5a/b*$^{wt/wt}$), as were experiments using *K14-CreER, K17-CreERT2* and *K15-CrePR* drivers. *Csf1r-CreER* mice (originally FVB) were backcrossed at least 6-9 generations into a C57BL/6 background. For genetic ablation of macrophages, *Csf1r-CreER::R26-iDTR* mice were compared with control WT littermates (no CreER or no *R26-iDTR*). *Csf1r-CreER* mice were generously provided by Dr. Tony Ferrante, and *R26-iDTR* mice were provided by Dr. David Owens.

Human Samples

De-identified human tissue was obtained under protocol number IRB-AAAE1921. Excess human scalp tissue from dermatological surgeries was collected in DMEM/10% FBS and transported to the lab on ice.

Tamoxifen Induction

Tamoxifen (Sigma-Aldrich) was dissolved in corn oil to a concentration of 10mg/ml, and mice were injected intraperitoneally (200µl) under light-protected conditions for 4 consecutive days.

EdU

5-ethnyl-2'-deoxyuridine (EdU, Life Technologies) was dissolved in sterile PBS to a concentration of 10mg/ml. For cellular dynamic studies, a single dose of 50µg/g was injected intraperitoneally 24 hours prior to sacrifice.

MATERIALS DETAILS

Hair Cycle Manipulation

Mice were carefully shaved with clippers during telogen to reveal the pink skin typical of the telogen phase 1 week prior to the experiment. Mice that were inadvertently wounded were not used. Anagen was induced by topical application of 2% Ruxolitinib in DMSO to the right side of the dorsal skin daily for 5 consecutive days. The hair cycle was observed and documented with standardized photographs taken prior to the first treatment, and then twice weekly thereafter. Murine IL-6, LIF or OSM (100ng/ml, 50ng/ml, 125ng/ml respectively) were dissolved in sterile PBS and 100µl was injected into the center of the field of application daily for 10 consecutive days, beginning with the first application of Ruxolitinib.

Neutralizing Antibodies

Neutralizing antibodies to OSMR (7.5µg) were injected intradermally into the dorsal telogen skin daily for 14 days from P60 (mid-telogen). Neutralizing antibodies to Csf1r (AFS98) and F4/80 (CI:A3-1) were diluted in sterile PBS, and 500µg was injected intradermally into the dorsal

telogen skin for 14 consecutive days. Neutralizing antibodies to CD25 (PC61.5) were injected intraperitoneally every other day (250µg/dose x 3) from P53, prior to anagen induction at P60.

Flow Cytometry

Dorsal skin was processed for either epidermal or dermal single-cell suspensions for stem cell or immune cell analysis by flow cytometry. Full thickness skin was harvested and defatted, and floated on 0.25% Trypsin for 30 min at 37°C. Epidermal cells were scraped off and titurated in DMEM/10%FBS before filtering through a 70µm mesh and centrifuged to obtain the epidermal cell pellet. The dermis was macerated finely with dissection scissors and re-suspended in 5ml DMEM with 0.2% Collagenase IV and 300U DNase 1, and incubated in a 37°C water bath for 40 minutes. The digested dermis was titurated in DMEM/10%FBS and filtered through a 70µm mesh and centrifuged. Mouse brain tissue was physically macerated with glass slides, and digested with 0.2% Collagenase IV and DNase, filtered, and microglia were isolated with a 30%-37%-70% Percoll gradient. Cells were labelled with conjugated surface antibodies listed in the Key Resources Table in DMEM/2%FBS for 1h on ice, and washed and labelled with live/dead Hoescht stain prior to FACS. Flow cytometry was performed on the Influx sorter in the Columbia University Flow Cytometry Core. Epidermal cell suspensions were used for HFSC stem cell analysis, and dermal suspensions were sorted for dermal papilla and immune cell experiments. Cells were collected in DMEM/10%FBS for cell culture, or in Trizol for RNA extraction. Flow cytometry data was analyzed using FlowJo software (FlowJo, LLC).

Cell Culture

HFSCs (ITGA6+ Sca-1-) cells were collected from flow cytometry and plated onto 6-well plates, and maintained with Cnt-07S keratinocyte media. In vitro stimulation experiments were carried out when keratinocytes were 80-90% confluent. Confluent HFSCs were pre-treated with JAK

inhibitors (tofacitinib, ruxolitinib or PF-06651600, all at 10μM) for 20 min, and murine OSM was added for a final concentration of 10ng/ml or 20ng/ml for 15 min. For clonogenic assays, HFSCs were plated at a density of 10,000 cells per well and maintained for 2 weeks. For analysis of clonogenicity, plates were washed with PBS, and keratinocytes were fixed in situ with 4% paraformaldehyde (PFA) for 1 hour, followed by staining with 1% (wt/vol) Rhodamine B (Sigma-Aldrich) for 1h. Clones were quantified using a backlight.

qRT-PCR

Sorted cell populations, epidermal sheets or dermal tissue was collected in Trizol and flash-frozen overnight at -80°C. RNA was extracted with the QIAgen RNeasy Micro Kit and cDNA was made using Superscript IV with a 2:1 mixture of random hexamers and oligo-dT primers. Semi-quantitative PCR for genes listed in the Key Resources Table was performed using SYBR Green PCR mix on an Applied Biosystems 7300 Real-Time PCR System. Primers for GAPDH were used in each reaction as a housekeeping control, and fold changes were calculated using the δ-δ Ct algorithm.

Genomic Sequencing

For sequencing of *loxP* sites, primers were designed manually around target introns. Genomic DNA was extracted from tails or ears snipped from weaned pups and PCR was performed with Platinum PCR Supermix (Thermo Fisher Scientific). PCR product was gel purified with QIAquick Gel Extraction Kit and sent for sequencing with forward primers at Genewiz (https://clims3.genewiz.com/). Reported .SEQ files were analyzed with Serial Cloner against genomic sequences of the target gene.

Western Blot

Cells were lyzed in RIPA buffer in the presence of protease and phosphatase inhibitors on ice, and protein lysates were resuspended in Laemmli sample buffer. Whole-cell lysates were fractionated on TGX Stain-free protein gels and transferred to a PVDF membrane, blocked with 5% non-fat milk in TBST, and incubated with antibodies listed in the Key Resources Table (all 1:1000, diluted in TBST/3%BSA) overnight. Membranes were washed the following day and incubated with HRP-conjugated secondary antibodies (1:5000), washed, and developed with Luminata Forte Western HRP Substrate and visualized on the BioRAD ChemiDOC MP Imaging system. GAPDH or β-actin were used as loading controls, depending on the mass of the proteins of interest.

Immunofluorescence and Histology

For immunofluorescence (IF) studies, dorsal skin or human scalp biopsies were submerged in 4% PFA for 1 hour, washed in PBS, and allowed to sink in 30% sucrose overnight before being embedded and frozen in OCT over liquid nitrogen. Samples were sectioned at 8µm thickness onto SuperFrost Plus glass slides (Fisher Scientific), blocked with 2% fish skin gelatin in PBS/0.3%Triton-X, and labelled with primary antibodies listed in Key Resources Table overnight at 4°C. Primary antibodies were washed off the following day, and labelled with fluorescence-conjugated secondary antibodies (1:1000), and images were acquired on a Zeiss LSM 5 Exciter Confocal microscope. EdU labelling was carried out with Click-iT Plus Alexa Fluor 647nm Imaging Kit according to manufacturer's protocol. For histology, formalin-fixed paraffin-embedded (FFPE) sections of mouse dorsal skin were rehydrated in increasingly dilute ethanol, and stained with hematoxylin and eosin.

shRNA

Hairpin sequences containing scramble or OSM 21mers obtained from the TRC RNAi consortium were cloned into the pLKO.1 library vector between the AgeI and EcoRI restriction sites. Modified pLKO.1 vector, along with helper packaging plasmids pMD2.G and pCMVδR8.2, were transfected into 293FT cells in the presence of Lipofectamine 3000 reagent, used according to manufacturer's protocol. Supernatant containing lentivirus was harvested 48 hours after transfection, filtered through a 0.45µm syringe filter, concentrated with PEG-it viral precipitant, resuspended in sterile PBS, and stored at -80°C until required.

Macrophage Inhibition

For in vivo macrophage inhibition, the small molecule Pexidartinib/PLX3397 was administered topically (2mM in DMSO) or subcutaneously (1mM in corn oil) for 5 consecutive days from P60. For OSM knock-down, peritoneal macrophages were harvested from adult C57BL/6 mice and cultured in DMEM/F12/15%FBS/0.3mMCa2+ the presence of 0.1mg/ml M-CSF to polarize them to an "M2-like" phenotype. Lentiviral precipitate containing scrambled or OSM shRNA added to the media in the presence of 8µg/ml protamine sulphate, and the cells were centrifuged at 3000rpm for 1h at 32°C to enhance transduction. Successful transductions were enriched with puromycin (1µg/ml) selection, counted and used for the patch assay.

Hair Reconstitution Assays

Neonatal (P0 or P1) mice were sacrificed and skins were harvested for the patch assay. Neonatal skins were enzymatically separated with 0.25% trypsin, and the dermis was further digested with 0.3% collagenase/DNase. Neonatal keratinocytes and dermal cells were counted recombined in a 1:1 ratio (106 cells each) and resuspended in 100µl of media (1:1 mix of DMEM/10%FBS and CnT-0.7S) and injected intradermally into the dorsal skin of a nude mouse.

For pharmacological/cytokine treatment, tofacitinib (400nM) and/or OSM (25ng/ml) was added. For macrophage inhibition assays, 20 x 103 macrophages (either freshly sorted by FACS, or cultured) were added to the cell slurry before injection into the Foxn1nu-2J nude mouse.

Single-cell RNA Sequencing

Live CD45+ immune cells from the dermis was isolated by FACS at early, mid and late telogen, captured on a microfluidic chip, and processed for single-cell RNA sequencing with the 10X Genomics Chromium 3' Solution platform. cDNA synthesized by this method was amplified and sequenced on an Illumina NextSeq. Cells with <500 or >2000 genes were excluded from analysis, as were cells with >105 UMIs (reflecting doublets) or mitochondrial genes >0.8% (reflecting dying cells). 1186 highly variable genes were identified based on their average expression and variance, and used for clustering analysis. Principle component analysis (PCA) on variable genes was performed by JackStraw analysis to identify significant PCs ($p<0.05$), and t-Distributed Stochastic Neighbor Embedding (t-SNE) plots were made based on the first 28 PCs for all immune cells at all timepoints, and 10 PCs for just the macrophages at P45. Further analysis and presentation of data was performed with the Seurat R package (http://satijalab.org/seurat/install.html).

REFERENCES

1. Iversen, O.H., *The Chalones*, in *Tissue Growth Factors*, R. Baserga, Editor. 1981, Springer.
2. Houck, J.C. and H. Hennings, *Chalones. Specific endogenous mitotic inhibitors.* FEBS Lett, 1973. **32**(1): p. 1-8.
3. Iversen, O.H., E. Aandahl, and K. Elgjo, *The effect of an epidermis-specific mitotic inhibitor (chalone) extracted from epidermal cells.* Acta Pathol Microbiol Scand, 1965. **64**(4): p. 506-10.
4. Benestad, H.B., T. Rytomaa, and K. Kiviniemi, *The cell specific effect of the granulocyte chalone demonstrated with the diffusion chamber technique.* Cell Tissue Kinet, 1973. **6**(2): p. 147-54.
5. Paus, R., K.S. Stenn, and R.E. Link, *Telogen skin contains an inhibitor of hair growth.* Br J Dermatol, 1990. **122**(6): p. 777-84.
6. Muller-Rover, S., et al., *A comprehensive guide for the accurate classification of murine hair follicles in distinct hair cycle stages.* J Invest Dermatol, 2001. **117**(1): p. 3-15.
7. Stenn, K.S. and R. Paus, *Controls of hair follicle cycling.* Physiol Rev, 2001. **81**(1): p. 449-494.
8. Rezza, A., et al., *Signaling Networks among Stem Cell Precursors, Transit-Amplifying Progenitors, and their Niche in Developing Hair Follicles.* Cell Rep, 2016. **14**(12): p. 3001-18.
9. Lee, J. and T. Tumbar, *Hairy tale of signaling in hair follicle development and cycling.* Semin Cell Dev Biol, 2012. **23**(8): p. 906-16.
10. Andl, T., et al., *WNT signals are required for the initiation of hair follicle development.* Dev Cell, 2002. **2**(5): p. 643-53.
11. St-Jacques, B., et al., *Sonic hedgehog signaling is essential for hair development.* Curr Biol, 1998. **8**(19): p. 1058-68.
12. Woo, W.M., H.H. Zhen, and A.E. Oro, *Shh maintains dermal papilla identity and hair morphogenesis via a Noggin-Shh regulatory loop.* Genes Dev, 2012. **26**(11): p. 1235-46.
13. Genander, M., et al., *BMP signaling and its pSMAD1/5 target genes differentially regulate hair follicle stem cell lineages.* Cell Stem Cell, 2014. **15**(5): p. 619-33.
14. Glover, J.D., et al., *Hierarchical patterning modes orchestrate hair follicle morphogenesis.* PLoS Biol, 2017. **15**(7): p. e2002117.
15. Sennett, R. and M. Rendl, *Mesenchymal-epithelial interactions during hair follicle morphogenesis and cycling.* Semin Cell Dev Biol, 2012. **23**(8): p. 917-27.
16. Chase, H.B., *Growth of the hair.* Physiol Rev, 1954. **34**(1): p. 113-26.
17. Chase, H.B. and G.J. Eaton, *The growth of hair follicles in waves.* Ann N Y Acad Sci, 1959. **83**: p. 365-8.
18. Collins, H.H., *Studies of normal moult and of artificially induced regeneration of pelage in Peromyscus.* J Exp Zool, 1918. **27**: p. 73-99.
19. Sano, S., et al., *Two distinct signaling pathways in hair cycle induction: Stat3-dependent and -independent pathways.* Proc Natl Acad Sci U S A, 2000. **97**(25): p. 13824-9.
20. Domagala, Z., et al., *The sequence of lanugo pattern development on the trunk wall in human fetuses.* Adv Clin Exp Med, 2017. **26**(6): p. 967-972.
21. Krause, K. and K. Foitzik, *Biology of the hair follicle: the basics.* Semin Cutan Med Surg, 2006. **25**(1): p. 2-10.
22. Halloy, J., et al., *Modeling the dynamics of human hair cycles by a follicular automaton.* Proc Natl Acad Sci U S A, 2000. **97**(15): p. 8328-33.

23. Oh, J.W., et al., *A Guide to Studying Human Hair Follicle Cycling In Vivo.* J Invest Dermatol, 2016. **136**(1): p. 34-44.
24. Malkud, S., *Telogen Effluvium: A Review.* J Clin Diagn Res, 2015. **9**(9): p. WE01-3.
25. Lolli, F., et al., *Androgenetic alopecia: a review.* Endocrine, 2017. **57**(1): p. 9-17.
26. Rebora, A., et al., *Distinguishing androgenetic alopecia from chronic telogen effluvium when associated in the same patient: a simple noninvasive method.* Arch Dermatol, 2005. **141**(10): p. 1243-5.
27. Suzuki, S., et al., *Localization of rat FGF-5 protein in skin macrophage-like cells and FGF-5S protein in hair follicle: possible involvement of two Fgf-5 gene products in hair growth cycle regulation.* J Invest Dermatol, 1998. **111**(6): p. 963-72.
28. Suzuki, S., et al., *Dual-mode regulation of hair growth cycle by two Fgf-5 gene products.* J Invest Dermatol, 2000. **114**(3): p. 456-63.
29. Cho, Y.M., et al., *Hair-cycle-dependent expression of parathyroid hormone-related protein and its type I receptor: evidence for regulation at the anagen to catagen transition.* J Invest Dermatol, 2003. **120**(5): p. 715-27.
30. Castela, M., et al., *Igf1r signalling acts on the anagen-to-catagen transition in the hair cycle.* Exp Dermatol, 2017. **26**(9): p. 785-791.
31. Hebert, J.M., et al., *FGF5 as a regulator of the hair growth cycle: evidence from targeted and spontaneous mutations.* Cell, 1994. **78**(6): p. 1017-25.
32. Sundberg, J.P., et al., *Angora mouse mutation: altered hair cycle, follicular dystrophy, phenotypic maintenance of skin grafts, and changes in keratin expression.* Vet Pathol, 1997. **34**(3): p. 171-9.
33. Higgins, C.A., et al., *FGF5 is a crucial regulator of hair length in humans.* Proc Natl Acad Sci U S A, 2014. **111**(29): p. 10648-53.
34. Parakkal, P.F., *Role of macrophages in collagen resorption during hair growth cycle.* J Ultrastruct Res, 1969. **29**(3): p. 210-7.
35. Mesa, K.R., et al., *Niche-induced cell death and epithelial phagocytosis regulate hair follicle stem cell pool.* Nature, 2015. **522**(7554): p. 94-7.
36. Eichmuller, S., et al., *Clusters of perifollicular macrophages in normal murine skin: physiological degeneration of selected hair follicles by programmed organ deletion.* J Histochem Cytochem, 1998. **46**(3): p. 361-70.
37. Geyfman, M., et al., *Resting no more: re-defining telogen, the maintenance stage of the hair growth cycle.* Biol Rev Camb Philos Soc, 2015. **90**(4): p. 1179-96.
38. Zhang, J., et al., *Bone morphogenetic protein signaling inhibits hair follicle anagen induction by restricting epithelial stem/progenitor cell activation and expansion.* Stem Cells, 2006. **24**(12): p. 2826-39.
39. Plikus, M.V., et al., *Cyclic dermal BMP signalling regulates stem cell activation during hair regeneration.* Nature, 2008. **451**(7176): p. 340-4.
40. Hsu, Y.C., H.A. Pasolli, and E. Fuchs, *Dynamics between stem cells, niche, and progeny in the hair follicle.* Cell, 2011. **144**(1): p. 92-105.
41. Lim, X., et al., *Axin2 marks quiescent hair follicle bulge stem cells that are maintained by autocrine Wnt/beta-catenin signaling.* Proc Natl Acad Sci U S A, 2016. **113**(11): p. E1498-505.
42. Trempus, C.S., et al., *Enrichment for living murine keratinocytes from the hair follicle bulge with the cell surface marker CD34.* J Invest Dermatol, 2003. **120**(4): p. 501-11.
43. Ohyama, M., *Hair follicle bulge: a fascinating reservoir of epithelial stem cells.* J Dermatol Sci, 2007. **46**(2): p. 81-9.
44. Mardaryev, A.N., et al., *Lhx2 differentially regulates Sox9, Tcf4 and Lgr5 in hair follicle stem cells to promote epidermal regeneration after injury.* Development, 2011. **138**(22): p. 4843-52.

45. Folgueras, A.R., et al., *Architectural niche organization by LHX2 is linked to hair follicle stem cell function.* Cell Stem Cell, 2013. **13**(3): p. 314-27.
46. Horsley, V., et al., *NFATc1 balances quiescence and proliferation of skin stem cells.* Cell, 2008. **132**(2): p. 299-310.
47. Wang, L., et al., *Foxc1 reinforces quiescence in self-renewing hair follicle stem cells.* Science, 2016. **351**(6273): p. 613-7.
48. Lay, K., T. Kume, and E. Fuchs, *FOXC1 maintains the hair follicle stem cell niche and governs stem cell quiescence to preserve long-term tissue-regenerating potential.* Proc Natl Acad Sci U S A, 2016. **113**(11): p. E1506-15.
49. Yuhki, M., et al., *BMPR1A signaling is necessary for hair follicle cycling and hair shaft differentiation in mice.* Development, 2004. **131**(8): p. 1825-33.
50. Rendl, M., L. Polak, and E. Fuchs, *BMP signaling in dermal papilla cells is required for their hair follicle-inductive properties.* Genes Dev, 2008. **22**(4): p. 543-57.
51. Zhou, L., et al., *CD133-positive dermal papilla-derived Wnt ligands regulate postnatal hair growth.* Biochem J, 2016. **473**(19): p. 3291-305.
52. Greco, V., et al., *A two-step mechanism for stem cell activation during hair regeneration.* Cell Stem Cell, 2009. **4**(2): p. 155-69.
53. Hsu, Y.C., L. Li, and E. Fuchs, *Emerging interactions between skin stem cells and their niches.* Nat Med, 2014. **20**(8): p. 847-56.
54. Morgan, B.A., *The dermal papilla: an instructive niche for epithelial stem and progenitor cells in development and regeneration of the hair follicle.* Cold Spring Harb Perspect Med, 2014. **4**(7): p. a015180.
55. Rompolas, P., et al., *Live imaging of stem cell and progeny behaviour in physiological hair-follicle regeneration.* Nature, 2012. **487**(7408): p. 496-9.
56. Rompolas, P., K.R. Mesa, and V. Greco, *Spatial organization within a niche as a determinant of stem-cell fate.* Nature, 2013. **502**(7472): p. 513-8.
57. Chi, W., E. Wu, and B.A. Morgan, *Dermal papilla cell number specifies hair size, shape and cycling and its reduction causes follicular decline.* Development, 2013. **140**(8): p. 1676-83.
58. Zhou, L., et al., *Dermal sheath cells contribute to postnatal hair follicle growth and cycling.* J Dermatol Sci, 2016. **82**(2): p. 129-31.
59. Rahmani, W., et al., *Hair follicle dermal stem cells regenerate the dermal sheath, repopulate the dermal papilla, and modulate hair type.* Dev Cell, 2014. **31**(5): p. 543-58.
60. Chase, H.B., W. Montagna, and J.D. Malone, *Changes in the skin in relation to the hair growth cycle.* Anat Rec, 1953. **116**(1): p. 75-81.
61. Hansen, L.S., et al., *The influence of the hair cycle on the thickness of mouse skin.* Anat Rec, 1984. **210**(4): p. 569-73.
62. Festa, E., et al., *Adipocyte lineage cells contribute to the skin stem cell niche to drive hair cycling.* Cell, 2011. **146**(5): p. 761-71.
63. Plikus, M.V., et al., *Analyses of regenerative wave patterns in adult hair follicle populations reveal macro-environmental regulation of stem cell activity.* Int J Dev Biol, 2009. **53**(5-6): p. 857-68.
64. Liao, C.P., et al., *Identification of hair shaft progenitors that create a niche for hair pigmentation.* Genes Dev, 2017. **31**(8): p. 744-756.
65. Botchkareva, N.V., et al., *SCF/c-kit signaling is required for cyclic regeneration of the hair pigmentation unit.* FASEB J, 2001. **15**(3): p. 645-58.
66. Haeberle, H. and E.A. Lumpkin, *Merkel Cells in Somatosensation.* Chemosens Percept, 2008. **1**(2): p. 110-118.
67. Moll, I., R. Paus, and R. Moll, *Merkel cells in mouse skin: intermediate filament pattern, localization, and hair cycle-dependent density.* J Invest Dermatol, 1996. **106**(2): p. 281-6.

68. Botchkarev, V.A., et al., *Hair cycle-dependent plasticity of skin and hair follicle innervation in normal murine skin.* J Comp Neurol, 1997. **386**(3): p. 379-95.
69. Peters, E.M., et al., *Hair-cycle-associated remodeling of the peptidergic innervation of murine skin, and hair growth modulation by neuropeptides.* J Invest Dermatol, 2001. **116**(2): p. 236-45.
70. Marshall, K.L., et al., *Touch Receptors Undergo Rapid Remodeling in Healthy Skin.* Cell Rep, 2016. **17**(7): p. 1719-1727.
71. Chow, A., et al., *CD169(+) macrophages provide a niche promoting erythropoiesis under homeostasis and stress.* Nat Med, 2013. **19**(4): p. 429-36.
72. Lilla, J.N. and Z. Werb, *Mast cells contribute to the stromal microenvironment in mammary gland branching morphogenesis.* Dev Biol, 2010. **337**(1): p. 124-33.
73. Gouon-Evans, V., M.E. Rothenberg, and J.W. Pollard, *Postnatal mammary gland development requires macrophages and eosinophils.* Development, 2000. **127**(11): p. 2269-82.
74. Aurora, A.B. and E.N. Olson, *Immune modulation of stem cells and regeneration.* Cell Stem Cell, 2014. **15**(1): p. 14-25.
75. Paus, R., et al., *Generation and cyclic remodeling of the hair follicle immune system in mice.* J Invest Dermatol, 1998. **111**(1): p. 7-18.
76. Maurer, M., R. Paus, and B.M. Czarnetzki, *Mast cells as modulators of hair follicle cycling.* Exp Dermatol, 1995. **4**(4 Pt 2): p. 266-71.
77. Maurer, M., et al., *Activated skin mast cells are involved in murine hair follicle regression (catagen).* Lab Invest, 1997. **77**(4): p. 319-32.
78. Arck, P.C., et al., *Stress inhibits hair growth in mice by induction of premature catagen development and deleterious perifollicular inflammatory events via neuropeptide substance P-dependent pathways.* Am J Pathol, 2003. **162**(3): p. 803-14.
79. Peters, E.M., et al., *Control of human hair growth by neurotrophins: brain-derived neurotrophic factor inhibits hair shaft elongation, induces catagen, and stimulates follicular transforming growth factor beta2 expression.* J Invest Dermatol, 2005. **124**(4): p. 675-85.
80. Johnson, E. and F.J. Ebling, *The Effect of Plucking Hairs during Different Phases of the Follicular Cycle.* J Embryol Exp Morphol, 1964. **12**: p. 465-74.
81. Tasseff, R., et al., *Mouse hair cycle expression dynamics modeled as coupled mesenchymal and epithelial oscillators.* PLoS Comput Biol, 2014. **10**(11): p. e1003914.
82. Chen, C.C., et al., *Organ-level quorum sensing directs regeneration in hair stem cell populations.* Cell, 2015. **161**(2): p. 277-90.
83. Ali, N., et al., *Regulatory T Cells in Skin Facilitate Epithelial Stem Cell Differentiation.* Cell, 2017. **169**(6): p. 1119-1129 e11.
84. Ito, M., et al., *Wnt-dependent de novo hair follicle regeneration in adult mouse skin after wounding.* Nature, 2007. **447**(7142): p. 316-20.
85. Gay, D., et al., *Fgf9 from dermal gammadelta T cells induces hair follicle neogenesis after wounding.* Nat Med, 2013. **19**(7): p. 916-23.
86. Jameson, J., et al., *A role for skin gammadelta T cells in wound repair.* Science, 2002. **296**(5568): p. 747-9.
87. Singh, T.P., et al., *Monocyte-derived inflammatory Langerhans cells and dermal dendritic cells mediate psoriasis-like inflammation.* Nat Commun, 2016. **7**: p. 13581.
88. Serezani, A.P., et al., *IL-4 impairs wound healing potential in the skin by repressing fibronectin expression.* J Allergy Clin Immunol, 2017. **139**(1): p. 142-151 e5.
89. Castellana, D., R. Paus, and M. Perez-Moreno, *Macrophages contribute to the cyclic activation of adult hair follicle stem cells.* PLoS Biol, 2014. **12**(12): p. e1002002.

90. Hulsmans, M., et al., *Macrophages Facilitate Electrical Conduction in the Heart.* Cell, 2017. **169**(3): p. 510-522 e20.
91. Lue, L.F., C. Schmitz, and D.G. Walker, *What happens to microglial TREM2 in Alzheimer's disease: Immunoregulatory turned into immunopathogenic?* Neuroscience, 2015. **302**: p. 138-50.
92. Gordon, S., A. Pluddemann, and F. Martinez Estrada, *Macrophage heterogeneity in tissues: phenotypic diversity and functions.* Immunol Rev, 2014. **262**(1): p. 36-55.
93. Martinez, F.O. and S. Gordon, *The M1 and M2 paradigm of macrophage activation: time for reassessment.* F1000Prime Rep, 2014. **6**: p. 13.
94. Mills, C.D., et al., *M-1/M-2 macrophages and the Th1/Th2 paradigm.* J Immunol, 2000. **164**(12): p. 6166-73.
95. Tamoutounour, S., et al., *Origins and functional specialization of macrophages and of conventional and monocyte-derived dendritic cells in mouse skin.* Immunity, 2013. **39**(5): p. 925-38.
96. Cecchini, M.G., et al., *Role of colony stimulating factor-1 in the establishment and regulation of tissue macrophages during postnatal development of the mouse.* Development, 1994. **120**(6): p. 1357-72.
97. Dai, X.M., et al., *Targeted disruption of the mouse colony-stimulating factor 1 receptor gene results in osteopetrosis, mononuclear phagocyte deficiency, increased primitive progenitor cell frequencies, and reproductive defects.* Blood, 2002. **99**(1): p. 111-20.
98. Ginhoux, F., et al., *Fate mapping analysis reveals that adult microglia derive from primitive macrophages.* Science, 2010. **330**(6005): p. 841-5.
99. McGovern, N., et al., *Human dermal CD14(+) cells are a transient population of monocyte-derived macrophages.* Immunity, 2014. **41**(3): p. 465-477.
100. Petukhova, L., et al., *Genome-wide association study in alopecia areata implicates both innate and adaptive immunity.* Nature, 2010. **466**(7302): p. 113-7.
101. Jabbari, A., et al., *Genetic basis of alopecia areata: a roadmap for translational research.* Dermatol Clin, 2013. **31**(1): p. 109-17.
102. Xing, L., et al., *Alopecia areata is driven by cytotoxic T lymphocytes and is reversed by JAK inhibition.* Nat Med, 2014. **20**(9): p. 1043-9.
103. Betz, R.C., et al., *Genome-wide meta-analysis in alopecia areata resolves HLA associations and reveals two new susceptibility loci.* Nat Commun, 2015. **6**: p. 5966.
104. Harel, S., et al., *Pharmacologic inhibition of JAK-STAT signaling promotes hair growth.* Sci Adv, 2015. **1**(9): p. e1500973.
105. Stark, G.R. and J.E. Darnell, Jr., *The JAK-STAT pathway at twenty.* Immunity, 2012. **36**(4): p. 503-14.
106. O'Shea, J.J., et al., *The JAK-STAT pathway: impact on human disease and therapeutic intervention.* Annu Rev Med, 2015. **66**: p. 311-28.
107. Rodig, S.J., et al., *Disruption of the Jak1 gene demonstrates obligatory and nonredundant roles of the Jaks in cytokine-induced biologic responses.* Cell, 1998. **93**(3): p. 373-83.
108. Neubauer, H., et al., *Jak2 deficiency defines an essential developmental checkpoint in definitive hematopoiesis.* Cell, 1998. **93**(3): p. 397-409.
109. Takeda, K., et al., *Targeted disruption of the mouse Stat3 gene leads to early embryonic lethality.* Proc Natl Acad Sci U S A, 1997. **94**(8): p. 3801-4.
110. Akira, S., *Functional roles of STAT family proteins: lessons from knockout mice.* Stem Cells, 1999. **17**(3): p. 138-46.
111. Babon, J.J., et al., *The molecular regulation of Janus kinase (JAK) activation.* Biochem J, 2014. **462**(1): p. 1-13.

112. Minegishi, Y., et al., *Human tyrosine kinase 2 deficiency reveals its requisite roles in multiple cytokine signals involved in innate and acquired immunity.* Immunity, 2006. **25**(5): p. 745-55.
113. Mogensen, T.H., M.A. Jakobsen, and C.S. Larsen, *Identification of a novel STAT3 mutation in a patient with hyper-IgE syndrome.* Scand J Infect Dis, 2013. **45**(3): p. 235-8.
114. Mogensen, T.H., *STAT3 and the Hyper-IgE syndrome: Clinical presentation, genetic origin, pathogenesis, novel findings and remaining uncertainties.* JAKSTAT, 2013. **2**(2): p. e23435.
115. Sano, S., et al., *Keratinocyte-specific ablation of Stat3 exhibits impaired skin remodeling, but does not affect skin morphogenesis.* EMBO J, 1999. **18**(17): p. 4657-68.
116. Chan, K.S., et al., *Disruption of Stat3 reveals a critical role in both the initiation and the promotion stages of epithelial carcinogenesis.* J Clin Invest, 2004. **114**(5): p. 720-8.
117. Chan, K.S., et al., *Forced expression of a constitutively active form of Stat3 in mouse epidermis enhances malignant progression of skin tumors induced by two-stage carcinogenesis.* Oncogene, 2008. **27**(8): p. 1087-94.
118. Teglund, S., et al., *Stat5a and Stat5b proteins have essential and nonessential, or redundant, roles in cytokine responses.* Cell, 1998. **93**(5): p. 841-50.
119. Yao, Z., et al., *Stat5a/b are essential for normal lymphoid development and differentiation.* Proc Natl Acad Sci U S A, 2006. **103**(4): p. 1000-5.
120. Goldstein, J., et al., *Calcineurin/Nfatc1 signaling links skin stem cell quiescence to hormonal signaling during pregnancy and lactation.* Genes Dev, 2014. **28**(9): p. 983-94.
121. Wang, Z., et al., *Conditional deletion of STAT5 in adult mouse hematopoietic stem cells causes loss of quiescence and permits efficient nonablative stem cell replacement.* Blood, 2009. **113**(20): p. 4856-65.
122. Yoneda, A., et al., *Vitamin A and insulin are required for the maintenance of hepatic stellate cell quiescence.* Exp Cell Res, 2016. **341**(1): p. 8-17.
123. Legrand, J.M., et al., *STAT5 Activation in the Dermal Papilla Is Important for Hair Follicle Growth Phase Induction.* J Invest Dermatol, 2016. **136**(9): p. 1781-91.
124. Flores, A., et al., *Lactate dehydrogenase activity drives hair follicle stem cell activation.* Nat Cell Biol, 2017.
125. Waickman, A.T., J.Y. Park, and J.H. Park, *The common gamma-chain cytokine receptor: tricks-and-treats for T cells.* Cell Mol Life Sci, 2016. **73**(2): p. 253-69.
126. Gee, K., et al., *The IL-12 family of cytokines in infection, inflammation and autoimmune disorders.* Inflamm Allergy Drug Targets, 2009. **8**(1): p. 40-52.
127. Kulig, P., et al., *IL-12 protects from psoriasiform skin inflammation.* Nat Commun, 2016. **7**: p. 13466.
128. Chan, J.R., et al., *IL-23 stimulates epidermal hyperplasia via TNF and IL-20R2-dependent mechanisms with implications for psoriasis pathogenesis.* J Exp Med, 2006. **203**(12): p. 2577-87.
129. Yang, B., et al., *IL-27 Facilitates Skin Wound Healing through Induction of Epidermal Proliferation and Host Defense.* J Invest Dermatol, 2017. **137**(5): p. 1166-1175.
130. Taga, T. and T. Kishimoto, *Gp130 and the interleukin-6 family of cytokines.* Annu Rev Immunol, 1997. **15**: p. 797-819.
131. Kwack, M.H., et al., *Dihydrotestosterone-inducible IL-6 inhibits elongation of human hair shafts by suppressing matrix cell proliferation and promotes regression of hair follicles in mice.* J Invest Dermatol, 2012. **132**(1): p. 43-9.
132. Turksen, K., et al., *Interleukin 6: insights to its function in skin by overexpression in transgenic mice.* Proc Natl Acad Sci U S A, 1992. **89**(11): p. 5068-72.
133. Krueger, J., et al., *Expression and function of interleukin-6 in epithelial cells.* J Cell Biochem, 1991. **45**(4): p. 327-34.

134. Grossman, R.M., et al., *Interleukin 6 is expressed in high levels in psoriatic skin and stimulates proliferation of cultured human keratinocytes.* Proc Natl Acad Sci U S A, 1989. **86**(16): p. 6367-71.
135. Zhao, L., J.J. Melenhorst, and L. Hennighausen, *Loss of interleukin 6 results in delayed mammary gland involution: a possible role for mitogen-activated protein kinase and not signal transducer and activator of transcription 3.* Mol Endocrinol, 2002. **16**(12): p. 2902-12.
136. Zarling, J.M., et al., *Oncostatin M: a growth regulator produced by differentiated histiocytic lymphoma cells.* Proc Natl Acad Sci U S A, 1986. **83**(24): p. 9739-43.
137. Yu, M., et al., *Interleukin-6 cytokine family member oncostatin M is a hair-follicle-expressed factor with hair growth inhibitory properties.* Exp Dermatol, 2008. **17**(1): p. 12-9.
138. Rabeony, H., et al., *Inhibition of keratinocyte differentiation by the synergistic effect of IL-17A, IL-22, IL-1alpha, TNFalpha and oncostatin M.* PLoS One, 2014. **9**(7): p. e101937.
139. Hu, J., et al., *Leukemia inhibitory factor induces epidermal hyperplasia in patients with amyotrophic lateral sclerosis.* J Invest Dermatol, 2000. **115**(3): p. 486-92.
140. Szepietowski, J.C., A. Reich, and R.C. McKenzie, *The multifunctional role of leukaemia inhibitory factor in cutaneous biology.* Acta Dermatovenerol Alp Pannonica Adriat, 2004. **13**(4): p. 125-9.
141. Dunglison, G.F., D.H. Barlow, and I.L. Sargent, *Leukaemia inhibitory factor significantly enhances the blastocyst formation rates of human embryos cultured in serum-free medium.* Hum Reprod, 1996. **11**(1): p. 191-6.
142. Li, W.H., et al., *IL-11, IL-1alpha, IL-6, and TNF-alpha are induced by solar radiation in vitro and may be involved in facial subcutaneous fat loss in vivo.* J Dermatol Sci, 2013. **71**(1): p. 58-66.
143. De Miguel, M.P., et al., *Leukemia inhibitory factor and ciliary neurotropic factor promote the survival of Sertoli cells and gonocytes in coculture system.* Endocrinology, 1996. **137**(5): p. 1885-93.
144. Lee, S.W., et al., *The effect of growth hormone on fibroblast proliferation and keratinocyte migration.* J Plast Reconstr Aesthet Surg, 2010. **63**(4): p. e364-9.
145. Safari, M., L. Ghahari, and M.D. Zoroufchi, *Effects of epidermal growth factor, platelet derived growth factor and growth hormone on cultured rat keratinocytes cells in vitro.* Pak J Biol Sci, 2014. **17**(7): p. 931-6.
146. Craven, A.J., et al., *Prolactin delays hair regrowth in mice.* J Endocrinol, 2006. **191**(2): p. 415-25.
147. Foitzik, K., et al., *Prolactin and its receptor are expressed in murine hair follicle epithelium, show hair cycle-dependent expression, and induce catagen.* Am J Pathol, 2003. **162**(5): p. 1611-21.
148. Girolomoni, G., J.T. Phillips, and P.R. Bergstresser, *Prolactin stimulates proliferation of cultured human keratinocytes.* J Invest Dermatol, 1993. **101**(3): p. 275-9.
149. Jin, E., J.M. Kim, and S.W. Kim, *Priming of mononuclear cells with a combination of growth factors enhances wound healing via high angiogenic and engraftment capabilities.* J Cell Mol Med, 2013. **17**(12): p. 1644-51.
150. de Graaf, C.A. and D. Metcalf, *Thrombopoietin and hematopoietic stem cells.* Cell Cycle, 2011. **10**(10): p. 1582-9.
151. Sorg, H., et al., *The nonhematopoietic effects of erythropoietin in skin regeneration and repair: from basic research to clinical use.* Med Res Rev, 2013. **33**(3): p. 637-64.
152. Kang, B.M., et al., *Erythropoietin promotes hair shaft growth in cultured human hair follicles and modulates hair growth in mice.* J Dermatol Sci, 2010. **59**(2): p. 86-90.

153. Sorg, H., et al., *Effects of erythropoietin in skin wound healing are dose related.* FASEB J, 2009. **23**(9): p. 3049-58.
154. Yasumura, S., et al., *Expression of interleukin 2 receptors on human carcinoma cell lines and tumor growth inhibition by interleukin 2.* Int J Cancer, 1994. **59**(2): p. 225-34.
155. Morhenn, V.B., et al., *Effects of recombinant interleukin 1 and interleukin 2 on human keratinocytes.* J Invest Dermatol, 1989. **93**(1): p. 121-6.
156. Matsue, H., P.R. Bergstresser, and A. Takashima, *Keratinocyte-derived IL-7 serves as a growth factor for dendritic epidermal T cells in mice.* J Immunol, 1993. **151**(11): p. 6012-9.
157. Clark, R.A. and C. Schlapbach, *TH9 cells in skin disorders.* Semin Immunopathol, 2017. **39**(1): p. 47-54.
158. Weber, B., et al., *Distinct interferon-gamma and interleukin-9 expression in cutaneous and oral lichen planus.* J Eur Acad Dermatol Venereol, 2017. **31**(5): p. 880-886.
159. Niehues, H., et al., *Keratinocyte Proliferation and Differentiation on IL-9 Stimulation: An Explorative In vitro Study.* Acta Derm Venereol, 2017. **97**(6): p. 741-742.
160. Fehniger, T.A. and M.A. Caligiuri, *Interleukin 15: biology and relevance to human disease.* Blood, 2001. **97**(1): p. 14-32.
161. Jones, A.M., et al., *The clinical significance and impact of interleukin 15 on keratinocyte cell growth and migration.* Int J Mol Med, 2016. **38**(3): p. 679-86.
162. Dooms, H., et al., *Quiescence-inducing and antiapoptotic activities of IL-15 enhance secondary CD4+ T cell responsiveness to antigen.* J Immunol, 1998. **161**(5): p. 2141-50.
163. Hermes, B., et al., *Upregulation of TNF-alpha and IL-3 expression in lesional and uninvolved skin in different types of urticaria.* J Allergy Clin Immunol, 1999. **103**(2 Pt 1): p. 307-14.
164. Tazawa, T., et al., *Relative importance of IL-4 and IL-13 in lesional skin of atopic dermatitis.* Arch Dermatol Res, 2004. **295**(11): p. 459-64.
165. Junghans, V., T. Jung, and C. Neumann, *Human keratinocytes constitutively express IL-4 receptor molecules and respond to IL-4 with an increase in B7/BB1 expression.* Exp Dermatol, 1996. **5**(6): p. 316-24.
166. Phipps, S., et al., *Intravenous anti-IL-5 monoclonal antibody reduces eosinophils and tenascin deposition in allergen-challenged human atopic skin.* J Invest Dermatol, 2004. **122**(6): p. 1406-12.
167. Wakugawa, M., et al., *Elevated levels of eotaxin and interleukin-5 in blister fluid of bullous pemphigoid: correlation with tissue eosinophilia.* Br J Dermatol, 2000. **143**(1): p. 112-6.
168. Braunstein, S., et al., *GM-CSF activates regenerative epidermal growth and stimulates keratinocyte proliferation in human skin in vivo.* J Invest Dermatol, 1994. **103**(4): p. 601-4.
169. Wesoly, J., Z. Szweykowska-Kulinska, and H.A. Bluyssen, *STAT activation and differential complex formation dictate selectivity of interferon responses.* Acta Biochim Pol, 2007. **54**(1): p. 27-38.
170. van der Fits, L., et al., *In psoriasis lesional skin the type I interferon signaling pathway is activated, whereas interferon-alpha sensitivity is unaltered.* J Invest Dermatol, 2004. **122**(1): p. 51-60.
171. Ghoreishi, M., M. Martinka, and J.P. Dutz, *Type 1 interferon signature in the scalp lesions of alopecia areata.* Br J Dermatol, 2010. **163**(1): p. 57-62.
172. Yaar, M., et al., *Effects of alpha and beta interferons on cultured human keratinocytes.* J Invest Dermatol, 1985. **85**(1): p. 70-4.
173. Ito, T., et al., *Interferon-gamma is a potent inducer of catagen-like changes in cultured human anagen hair follicles.* Br J Dermatol, 2005. **152**(4): p. 623-31.

174. Nickoloff, B.J., G. Mahrle, and V. Morhenn, *Ultrastructural effects of recombinant gamma-interferon on cultured human keratinocytes.* Ultrastruct Pathol, 1986. **10**(1): p. 17-21.
175. King, A., et al., *Regenerative Wound Healing: The Role of Interleukin-10.* Adv Wound Care (New Rochelle), 2014. **3**(4): p. 315-323.
176. Seifert, M., et al., *Keratinocyte unresponsiveness towards interleukin-10: lack of specific binding due to deficient IL-10 receptor 1 expression.* Exp Dermatol, 2003. **12**(2): p. 137-44.
177. Sumikawa, Y., et al., *Hair cycle control by leptin as a new anagen inducer.* Exp Dermatol, 2014. **23**(1): p. 27-32.
178. Tadokoro, S., et al., *Leptin promotes wound healing in the skin.* PLoS One, 2015. **10**(3): p. e0121242.
179. Sakai, H., et al., *Signaling mechanism underlying the promotion of keratinocyte migration by angiotensin II.* Mol Pharmacol, 2015. **87**(2): p. 277-85.
180. Lee, H.J., et al., *Serotonin induces melanogenesis via serotonin receptor 2A.* Br J Dermatol, 2011. **165**(6): p. 1344-8.
181. El-Nour, H., et al., *Study of innervation, sensory neuropeptides, and serotonin in murine contact allergic skin.* Immunopharmacol Immunotoxicol, 2005. **27**(1): p. 67-76.
182. Maurer, M., et al., *The mast cell products histamine and serotonin stimulate and TNF-alpha inhibits the proliferation of murine epidermal keratinocytes in situ.* J Dermatol Sci, 1997. **16**(1): p. 79-84.
183. Sugawara, K., et al., *Cutaneous consequences of inhibiting EGF receptor signaling in vivo: normal hair follicle development, but retarded hair cycle induction and inhibition of adipocyte growth in Egfr(Wa5) mice.* J Dermatol Sci, 2010. **57**(3): p. 155-61.
184. Blumenberg, M., *Profiling and metaanalysis of epidermal keratinocytes responses to epidermal growth factor.* BMC Genomics, 2013. **14**: p. 85.
185. Rheinwald, J.G. and H. Green, *Epidermal growth factor and the multiplication of cultured human epidermal keratinocytes.* Nature, 1977. **265**(5593): p. 421-4.
186. Watowich, S.S., et al., *Cytokine receptor signal transduction and the control of hematopoietic cell development.* Annu Rev Cell Dev Biol, 1996. **12**: p. 91-128.
187. Vainchenker, W., A. Dusa, and S.N. Constantinescu, *JAKs in pathology: role of Janus kinases in hematopoietic malignancies and immunodeficiencies.* Semin Cell Dev Biol, 2008. **19**(4): p. 385-93.
188. Quintas-Cardama, A., et al., *Janus kinase inhibitors for the treatment of myeloproliferative neoplasias and beyond.* Nat Rev Drug Discov, 2011. **10**(2): p. 127-40.
189. Boulay, J.L., J.J. O'Shea, and W.E. Paul, *Molecular phylogeny within type I cytokines and their cognate receptors.* Immunity, 2003. **19**(2): p. 159-63.
190. Heinrich, P.C., et al., *Interleukin-6-type cytokine signalling through the gp130/Jak/STAT pathway.* Biochem J, 1998. **334 (Pt 2)**: p. 297-314.
191. Murakami, M., et al., *IL-6-induced homodimerization of gp130 and associated activation of a tyrosine kinase.* Science, 1993. **260**(5115): p. 1808-10.
192. Minshall, E., et al., *IL-11 expression is increased in severe asthma: association with epithelial cells and eosinophils.* J Allergy Clin Immunol, 2000. **105**(2 Pt 1): p. 232-8.
193. Pennica, D., et al., *Expression cloning of cardiotrophin 1, a cytokine that induces cardiac myocyte hypertrophy.* Proc Natl Acad Sci U S A, 1995. **92**(4): p. 1142-6.
194. Thier, M., et al., *Trophic effects of cardiotrophin-1 and interleukin-11 on rat dorsal root ganglion neurons in vitro.* Brain Res Mol Brain Res, 1999. **64**(1): p. 80-4.
195. Mitchell, M.H., et al., *Enhancement of in vitro murine embryo development by recombinant leukemia inhibitory factor.* J Soc Gynecol Investig, 1994. **1**(3): p. 215-9.

196. Ali, S.A., et al., *Examination of pathways involved in leukemia inhibitory factor (LIF)-induced cell growth arrest using label-free proteomics approach.* J Proteomics, 2017. **168**: p. 37-52.
197. Liu, X., A.J. Teichtahl, and I.P. Wicks, *Interleukin-6 in rheumatoid arthritis - from the laboratory to the bedside.* Curr Pharm Des, 2015. **21**(17): p. 2187-97.
198. Tanabe, A., et al., *Interleukin 6 induces the hair follicle growth phase (anagen).* J Dermatol Sci, 2006. **43**(3): p. 210-3.
199. Malik, N., et al., *Molecular cloning, sequence analysis, and functional expression of a novel growth regulator, oncostatin M.* Mol Cell Biol, 1989. **9**(7): p. 2847-53.
200. Horn, D., et al., *Regulation of cell growth by recombinant oncostatin M.* Growth Factors, 1990. **2**(2-3): p. 157-65.
201. Dey, G., et al., *Signaling network of Oncostatin M pathway.* J Cell Commun Signal, 2013. **7**(2): p. 103-8.
202. Sporeno, E., et al., *Oncostatin M binds directly to gp130 and behaves as interleukin-6 antagonist on a cell line expressing gp130 but lacking functional oncostatin M receptors.* J Biol Chem, 1994. **269**(15): p. 10991-5.
203. !!! INVALID CITATION !!! {}.
204. Sennett, R., et al., *An Integrated Transcriptome Atlas of Embryonic Hair Follicle Progenitors, Their Niche, and the Developing Skin.* Dev Cell, 2015. **34**(5): p. 577-91.
205. Rose, T.M., et al., *Oncostatin M (OSM) inhibits the differentiation of pluripotent embryonic stem cells in vitro.* Cytokine, 1994. **6**(1): p. 48-54.
206. Xiao, F., et al., *Oncostatin M inhibits myoblast differentiation and regulates muscle regeneration.* Cell Res, 2011. **21**(2): p. 350-64.
207. Tiffen, P.G., et al., *A dual role for oncostatin M signaling in the differentiation and death of mammary epithelial cells in vivo.* Mol Endocrinol, 2008. **22**(12): p. 2677-88.
208. Bryson, B.L., et al., *STAT3-mediated SMAD3 activation underlies Oncostatin M-induced Senescence.* Cell Cycle, 2017. **16**(4): p. 319-334.
209. Doles, J., et al., *Age-associated inflammation inhibits epidermal stem cell function.* Genes Dev, 2012. **26**(19): p. 2144-53.
210. Miyaoka, Y., et al., *Oncostatin M inhibits adipogenesis through the RAS/ERK and STAT5 signaling pathways.* J Biol Chem, 2006. **281**(49): p. 37913-20.
211. Klausen, P., et al., *Oncostatin M and interleukin 6 inhibit cell cycle progression by prevention of p27kip1 degradation in HepG2 cells.* Oncogene, 2000. **19**(32): p. 3675-83.
212. Hintzen, C., et al., *Oncostatin M-induced and constitutive activation of the JAK2/STAT5/CIS pathway suppresses CCL1, but not CCL7 and CCL8, chemokine expression.* J Immunol, 2008. **181**(10): p. 7341-9.
213. Minehata, K., et al., *Oncostatin m maintains the hematopoietic microenvironment and retains hematopoietic progenitors in the bone marrow.* Int J Hematol, 2006. **84**(4): p. 319-27.
214. Rose-John, S., *Interleukin-6 Family Cytokines.* Cold Spring Harb Perspect Biol, 2017.
215. Muller-Newen, G., *The cytokine receptor gp130: faithfully promiscuous.* Sci STKE, 2003. **2003**(201): p. PE40.
216. Doucet, Y.S. and D.M. Owens, *Isolation and functional assessment of cutaneous stem cells.* Methods Mol Biol, 2015. **1235**: p. 147-64.
217. MacDonald, K.P., et al., *An antibody against the colony-stimulating factor 1 receptor depletes the resident subset of monocytes and tissue- and tumor-associated macrophages but does not inhibit inflammation.* Blood, 2010. **116**(19): p. 3955-63.
218. Segawa, M., et al., *Suppression of macrophage functions impairs skeletal muscle regeneration with severe fibrosis.* Exp Cell Res, 2008. **314**(17): p. 3232-44.

219. Weisser, S.B., et al., *Generation and characterization of murine alternatively activated macrophages.* Methods Mol Biol, 2013. **946**: p. 225-39.
220. Nimmerjahn, A., F. Kirchhoff, and F. Helmchen, *Resting microglial cells are highly dynamic surveillants of brain parenchyma in vivo.* Science, 2005. **308**(5726): p. 1314-8.
221. Hanisch, U.K. and H. Kettenmann, *Microglia: active sensor and versatile effector cells in the normal and pathologic brain.* Nat Neurosci, 2007. **10**(11): p. 1387-94.
222. Poliani, P.L., et al., *TREM2 sustains microglial expansion during aging and response to demyelination.* J Clin Invest, 2015. **125**(5): p. 2161-70.
223. Takahashi, K., et al., *TREM2-transduced myeloid precursors mediate nervous tissue debris clearance and facilitate recovery in an animal model of multiple sclerosis.* PLoS Med, 2007. **4**(4): p. e124.
224. Painter, M.M., et al., *TREM2 in CNS homeostasis and neurodegenerative disease.* Mol Neurodegener, 2015. **10**: p. 43.
225. Dardiotis, E., et al., *A novel mutation in TREM2 gene causing Nasu-Hakola disease and review of the literature.* Neurobiol Aging, 2017. **53**: p. 194 e13-194 e22.
226. Guerreiro, R.J., et al., *Using exome sequencing to reveal mutations in TREM2 presenting as a frontotemporal dementia-like syndrome without bone involvement.* JAMA Neurol, 2013. **70**(1): p. 78-84.
227. Botchkarev, V.A., et al., *Hair cycle-dependent changes in mast cell histochemistry in murine skin.* Arch Dermatol Res, 1995. **287**(7): p. 683-6.
228. Hoffman, U., et al., *Hair cycle-dependent changes in skin immune functions: anagen-associated depression of sensitization for contact hypersensitivity in mice.* J Invest Dermatol, 1996. **106**(4): p. 598-604.
229. Paus, R., et al., *Distribution and changing density of gamma-delta T cells in murine skin during the induced hair cycle.* Br J Dermatol, 1994. **130**(3): p. 281-9.
230. Gomez-Lechon, M.J., *Oncostatin M: signal transduction and biological activity.* Life Sci, 1999. **65**(20): p. 2019-30.
231. Hermanns, H.M., *Oncostatin M and interleukin-31: Cytokines, receptors, signal transduction and physiology.* Cytokine Growth Factor Rev, 2015. **26**(5): p. 545-58.
232. Boniface, K., et al., *Oncostatin M secreted by skin infiltrating T lymphocytes is a potent keratinocyte activator involved in skin inflammation.* J Immunol, 2007. **178**(7): p. 4615-22.
233. Pohin, M., et al., *Oncostatin M overexpression induces skin inflammation but is not required in the mouse model of imiquimod-induced psoriasis-like inflammation.* Eur J Immunol, 2016. **46**(7): p. 1737-51.
234. Matsuda, M., et al., *Oncostatin M causes liver fibrosis by regulating cooperation between hepatic stellate cells and macrophages in mice.* Hepatology, 2017.
235. Guihard, P., et al., *Induction of osteogenesis in mesenchymal stem cells by activated monocytes/macrophages depends on oncostatin M signaling.* Stem Cells, 2012. **30**(4): p. 762-72.
236. David, E., et al., *Oncostatin M is a growth factor for Ewing sarcoma.* Am J Pathol, 2012. **181**(5): p. 1782-95.
237. Hasegawa, M., et al., *Enhanced production of interleukin-6 (IL-6), oncostatin M and soluble IL-6 receptor by cultured peripheral blood mononuclear cells from patients with systemic sclerosis.* Rheumatology (Oxford), 1999. **38**(7): p. 612-7.
238. Ho, Y.Y., et al., *Cells from the skin of patients with systemic sclerosis secrete chitinase 3-like protein 1.* BBA Clin, 2014. **1**: p. 2-11.
239. Atamas, S.P. and B. White, *Cytokine regulation of pulmonary fibrosis in scleroderma.* Cytokine Growth Factor Rev, 2003. **14**(6): p. 537-50.

240. Hintzen, C., et al., *Box 2 region of the oncostatin M receptor determines specificity for recruitment of Janus kinases and STAT5 activation.* J Biol Chem, 2008. **283**(28): p. 19465-77.
241. Bausek, N., *JAK-STAT signaling in stem cells and their niches in Drosophila.* JAKSTAT, 2013. **2**(3): p. e25686.
242. Humphreys, R.C., et al., *Deletion of Stat3 blocks mammary gland involution and extends functional competence of the secretory epithelium in the absence of lactogenic stimuli.* Endocrinology, 2002. **143**(9): p. 3641-50.
243. Hughes, K. and C.J. Watson, *The spectrum of STAT functions in mammary gland development.* JAKSTAT, 2012. **1**(3): p. 151-8.
244. Mackay-Wiggan, J., et al., *Oral ruxolitinib induces hair regrowth in patients with moderate-to-severe alopecia areata.* JCI Insight, 2016. **1**(15): p. e89790.
245. Kennedy Crispin, M., et al., *Safety and efficacy of the JAK inhibitor tofacitinib citrate in patients with alopecia areata.* JCI Insight, 2016. **1**(15): p. e89776.
246. Hauser, P.J., et al., *STAT3 activation accompanies keratinocyte differentiation.* Cell Growth Differ, 1998. **9**(10): p. 847-55.
247. Kira, M., et al., *STAT3 deficiency in keratinocytes leads to compromised cell migration through hyperphosphorylation of p130(cas).* J Biol Chem, 2002. **277**(15): p. 12931-6.
248. Macias, E., D. Rao, and J. Digiovanni, *Role of stat3 in skin carcinogenesis: insights gained from relevant mouse models.* J Skin Cancer, 2013. **2013**: p. 684050.
249. Kanai, T., et al., *Identification of STAT5A and STAT5B target genes in human T cells.* PLoS One, 2014. **9**(1): p. e86790.
250. Basham, B., et al., *In vivo identification of novel STAT5 target genes.* Nucleic Acids Res, 2008. **36**(11): p. 3802-18.
251. Kretzschmar, K. and F.M. Watt, *Markers of epidermal stem cell subpopulations in adult mammalian skin.* Cold Spring Harb Perspect Med, 2014. **4**(10).
252. Alvarez, J.V. and D.A. Frank, *Genome-wide analysis of STAT target genes: elucidating the mechanism of STAT-mediated oncogenesis.* Cancer Biol Ther, 2004. **3**(11): p. 1045-50.
253. Nelson, E.A., et al., *Isolation of unique STAT5 targets by chromatin immunoprecipitation-based gene identification.* J Biol Chem, 2004. **279**(52): p. 54724-30.
254. Yamaji, D., et al., *Sequential activation of genetic programs in mouse mammary epithelium during pregnancy depends on STAT5A/B concentration.* Nucleic Acids Res, 2013. **41**(3): p. 1622-36.
255. Manrique, I., et al., *The inhibitor of differentiation isoform Id1b, generated by alternative splicing, maintains cell quiescence and confers self-renewal and cancer stem cell-like properties.* Cancer Lett, 2015. **356**(2 Pt B): p. 899-909.
256. Moh, A., et al., *Role of STAT3 in liver regeneration: survival, DNA synthesis, inflammatory reaction and liver mass recovery.* Lab Invest, 2007. **87**(10): p. 1018-28.
257. Lee, J., et al., *Signalling couples hair follicle stem cell quiescence with reduced histone H3 K4/K9/K27me3 for proper tissue homeostasis.* Nat Commun, 2016. **7**: p. 11278.
258. Lien, W.H., et al., *In vivo transcriptional governance of hair follicle stem cells by canonical Wnt regulators.* Nat Cell Biol, 2014. **16**(2): p. 179-90.
259. Xu, R., et al., *Sustained activation of STAT5 is essential for chromatin remodeling and maintenance of mammary-specific function.* J Cell Biol, 2009. **184**(1): p. 57-66.
260. Junk, D.J., et al., *Oncostatin M promotes cancer cell plasticity through cooperative STAT3-SMAD3 signaling.* Oncogene, 2017. **36**(28): p. 4001-4013.

APPENDIX A. KEY RESOURCES TABLE

REAGENT or RESOURCE	SOURCE	IDENTIFIER
Antibodies		
Anti-Mouse OSMRβ	R&D Systems	Cat# MAB662
Anti-Mouse pSTAT1 (Y701) (58D6)	Cell Signaling	Cat# 9167
Anti-Mouse pSTAT3 (Y705) (D3A7)	Cell Signaling	Cat# 9145
Anti-Mouse pSTAT3 (S727)	Abcam	Cat# ab86430
Anti-Mouse pSTAT5 (Y694) (C11C5)	Cell Signaling	Cat# 9359
Anti-Mouse pMEK-1/2 (Ser217/221) (41G9)	Cell Signaling	Cat# 9154
Anti-Mouse pERK-1/2 (Thr202/Tyr204) (197G2)	Cell Signaling	Cat# 4377
Anti-Mouse pAkt (Thr308) (C31E5E)	Cell Signaling	Cat# 2965
Anti-Mouse mTOR (7C10)	Cell Signaling	Cat# 2983
Anti-Mouse β-actin-HRP	Santa Cruz	Cat# sc-47778
Anti-Mouse GAPDH (6C5)	Santa Cruz	Cat# sc-32233
Anti-Mouse ITGA6 FITC	Serotec	Cat# MCA699F
Anti-Mouse CD34 A700	eBioscience	Cat# 56-0341-82
Anti-Mouse Sca-1 APC	eBioscience	Cat# 17-5981-81
Anti-Mouse P-cadherin PE	R&D Systems	Cat# FAB761P
Anti-Mouse P-cadherin	R&D Systems	Cat# AF761
Anti-Mouse gp130	Neuromics	Cat# MO15024
Anti-Mouse/Human Keratin 15	Covance	Cat# PCK-153P-100
Anti-Mouse CD34	eBioscience	Cat# 14-0341-82
Anti-Mouse CD45 FITC	Biolegend	Cat# 103108
Anti-Mouse Integrin-α9 PE	R&D Systems	Cat# FAB3827P
Anti-Mouse F4/80 PE-Cy7	BioLegend	Cat# 123114
Anti-Mouse CD11b APC	BD Pharmingen	Cat# 557686
Anti-Mouse CD11b PE	eBioscience	Cat# 12-0112-81
Anti-Mouse CD163 FITC	BioRAD	Cat# MCA342F
Anti-Mouse CD206 APC	eBioscience	Cat# 17-2061-82
Anti-Mouse I-A/I-E APC	Biolegend	Cat# 107617
Anti-Mouse OSM	Abcam	Cat# ab133748
Anti-Mouse CD11b	Abcam	Cat# ab8878
Anti-Mouse Aif-1/Iba-1	R&D Systems	Cat# AF761
Anti-Mouse F4/80	Life Technologies	Cat# 14-4801-82
Anti-Mouse Trem2	Abcam	Cat# ab95470
Anti-Mouse Trem2-APC	R&D Systems	Cat# FAB17291A
InVivoMAb Anti-Mouse Csf1R (CD115)	BioXCell	Cat# AFS98
InVivoMAb Anti-mouse F4/80 (CI:A3-1)	BioXCell	Cat# BE0206
InVivoPlus Anti-mouse CD25 (IL-2Rα) (PC-61.5.3)	BioXCell	Cat# BP0012

InVivoPlus Mouse IgG2 isotype control	BioXCell	Cat# BP0086
Anti-Human FCGR1A	Abcam	Cat# ab104273
Anti-Human Oncostatin M (G-1)	Santa Cruz	Cat# sc-390253
Anti-Mouse/Human Keratin 14	BioLegend	Cat# PRB-155P
Bacterial and Virus Strains		
pLKO.1 - TRC cloning vector	Addgene	Cat# 10878
pMD2.G – packaging plasmid	Addgene	Cat# 12259
pCMV delta R8.2 – packaging plasmid	Addgene	Cat# 12263
Chemicals, Peptides, and Recombinant Proteins		
DMSO	Sigma-Aldrich	Cat# D2650-100ML
Ruxolitinib	APExBIO	Cat# INCB018424
Tofacinitb	Abmole Bioscience	Cat# CP-690550
Recombinant Murine Oncostatin M (OSM)	R&D Systems	Cat# 495-MO-025
Trypsin 2.5%	Fisher Scientific	Cat# 15090046
Collagenase IV from Clostridium histolyticum	Sigma-Aldrich	Cat# C5138
DNase I	Sigma-Aldrich	Cat# D5025
CnT-07S Keratinocyte media	CELLnTEC	Cat# CnT-07
Diphtheria Toxin from Corynebacterium diphtheriae	Sigma-Aldrich	Cat# D0564
Tamoxifen	Sigma-Aldrich	Cat# T5648-1G
EdU (5-ethynyl-2'-deoxyuridine)	Life Technologies	Cat# A10044
Hoescht 33342 trihydrochloride, trihydrate	Invitrogen	Cat# H3570
Pexidartinib	Selleckchem	Cat# S7818
Recombinant Murine M-CSF	Peprotech	Cat# 315-02
Lipofectamine 3000 Transfection Reagent	Thermo Fisher	Cat# L3000008
PEG-it viral precipitant	System Biosciences	Cat# LV810A-1
Critical Commercial Assays		
Click-iT™ Plus EdU Alexa Fluor™ 647 Imaging Kit	ThermoFisher	Cat# C10640
RNeasy Micro Kit	QIAgen	Cat# 74004
RNAscope®	Advanced Cell Diagnostics	Cat# 320850
Deposited Data		
GSE15185	Greco et al, Cell Stem Cell 2009 Feb 6;4(2):155-69	
Experimental Models: Organisms/Strains		
Mouse: C57BL/6J	The Jackson Laboratory	JAX: 000664
Mouse: B6N.129S6(Cg)-Krt5$^{tm1.1(cre/ERT2)Blh}$/J	The Jackson Laboratory	JAX: 029155
Mouse: B6;129-Osmr$^{tm1.1Nat}$/J	The Jackson Laboratory	JAX: 011081
Mouse: B6.129S6-Stat5b^{tm1Mam} Stat5a^{tm2Mam}/Mmjax	The Jackson Laboratory	JAX: 32053-JAX

Mouse: FVB-Tg(Csf1r-cre/Esr1*)1Jwp/J	The Jackson Laboratory	JAX: 019098
Mouse: C57BL/6-Gt(ROSA)26Sor$^{tm1(HBEGF)Awai}$/J	The Jackson Laboratory	JAX: 007900
Mouse: C57BL/6-Tg(Foxp3-DTR/EGFP)23.2Spar/Mmjax	The Jackson Laboratory	JAX: 32050-JAX
Mouse: B6(SJL)-Foxn1nu-2J/GrsrJ	The Jackson Laboratory	JAX: 016195
Oligonucleotides		
Osmr F	TCT GGG TGG AGA ATT ATA GC	N/A
Osmr R	CCA GGA ACT CCA GTT GCC CC	N/A
Osm F	ATG CAG ACA CGG CTT CTA AGA	N/A
Osm R	TTG GAG CAG CCA CGA TTG G	N/A
STAT5a F	CGC CAG ATG CAA GTG TTG TAT	N/A
STAT5a R	TCC TGG GGA TTA TCC AAG TCA AT	N/A
STAT5b F	CAC AGT GGA TCG AAA GCC AAG	N/A
STAT5b R	AGC TGG GTG GCC TTA ATG TTC	N/A
Keratin 17 F	ACC ATC CGC CAG TTT ACC TC	N/A
Keratin 17 R	CTA CCC AGG CCA CTA GCT GA	N/A
Il6st (gp130) F	GGT CAA CTT TTG GAA CCG TG	N/A
Il6st (gp130) R	GCA GCA TGG TTG GTC TTC C	N/A
Osm shRNA F	CGGCACAATATCCTCGGCATA	N/A
Osm shRNA R	TATGCCGAGGATATTGTGCCG	N/A
GAPDH F	TGG CCT TCC GTG TTC CTA C	N/A
GAPDH R	GAG TTG CTG TTG AAG TCG CA	N/A
STAT3 F	GCC AAG GAG ACA TGC AGG	N/A
STAT3 R	CGC CAG CTC ACT CAC AAT GC	N/A
STAT3.2 F	GCT GGC TGA GAA GCT CCT AGG	N/A
STAT3.2 R	CAG ACC CAG AAG GAG AAG C	N/A
STAT3 – Intron 17 sequencing F	GCT GGC TGA GAA GCT CCT AGG	N/A
STAT3 – Intron 17 sequencing R	TGA GTA GTT CAC ACC AGG CC	N/A
STAT3 – Intron 20 sequencing F	GGT GGA AAA GGA CAT CAG TGG	N/A
STAT3 – Intron 20 sequencing R	GGT GTA TGG CTC TAC AGA CTG G	N/A
Software and Algorithms		
Graphpad Prism	Graphpad Software, Inc	http://www.graphpad.com/
FlowJo	FlowJo, LLC	https://www.flowjo.com/solutions/flowjo
ImageJ	MIH Version	https://imagej.nih.gov/ij/download.html
Loupe Cell Browser	10X Genomics	https://support.10xgenomics.com/single-cell-gene-expression/software/downloads/latest
Seurat	R Package	http://satijalab.org/seurat/

APPENDIX B. List of Abbreviations

AA	Alopecia Areata
ACTH	Adrenocorticotrophic Hormone
AGA	Androgenetic Alopecia
Aif-1	Allograft Inflammatory Factor 1
APC	Antigen Presenting Cell
BDNF	Brain-Derived Neurotrophic Factor
BMP	Bone Morphogenetic Protein
CCDN1	Cyclin-D1
CCL2	C-C Chemokine Ligand 2
CCR2	C-C Chemokine Receptor Type 2
CDKN1a	Cyclin Dependent Kinase Inhibitor 1A
CX3CR1	CX_3C Chemokine Receptor Type 3
CD-	Cluster of Differentiation-
CFA	Colony Forming Assay
ChIP	Chromatin Immunoprecipitation
Cish	Cytokine Inducible SH2 Containing Protein
cKO	Conditional Knock-Out
CNS	Central Nervous System
Cre	Causes REcombination
CreER	Cre-recombinase Estrogen Receptor
CrePR	Cre-recombinase Progesterone Receptor
CNTF	Ciliary Neurotrophic Factor
CSF1	Colony Stimulating Factor-1 (aka M-CSF)

Csf1r	Colony Stimulating Facotr-1 receptor
CT-1	Cardiotrophin-1
DC	Dendritic Cell
DF	Dermal Fibroblasts
DP	Dermal Papilla
DTA	Diphtheria Toxin A
EdU	5-ethynyl-2'-deoxyuridine
ESC	Embryonic Stem Cells
GFP	Green Fluorescent Protein
GH	Growth Hormone
GM-CSF	Granulocyte-macrophage colony-stimulating factor
FACS	Fluorescence-activated cell sorting
FGF	Fibroblast Growth Factor
FoxC1	Forkhead Box C1
HF	Hair Follicle
HFSC	Hair Follicle Stem Cell
HG	Hair Germ
ID1	Inhibitor of DNA binding-1, or Inhibitor of Differentiation
iDTR	Inducible Diphtheria Toxin Receptor
IGF-1	Insulin-like Growth Factor-1
IFE	Interfollicular Epidermis
IFN	Interferon
IL-	Interleukin-
Il6st	Interleukin-6 signal transducer (gene name for gp130)
IRF-1	Interferon regulatory factor 1

IRS	Inner Root Sheath
JAK	Janus Kinase
K-	Keratin-
Lgr5	Leucine-rich repeat-containing G-protein coupled receptor 5
Lhx2	Lim-homeobox 2
LIF	Leukemia Inhibitory Factor
LIFRβ	Leukemia Inhibitory Factor Receptor
loxP	Locus of X-over P1
Mc	Melanocyte
M-CSF	Macrophage Colony Stimulating Factor (aka CSF1)
MEF	Mouse Embryonic Fibroblasts
MHC	Major Histocompatibility Complex
MRC1	Mannose Receptor C-Type 1 (CD206)
mTmG	Membrane-Tomato/membrane-GFP
Mx	Matrix
NFATc1	Nuclear Factor Of Activated T-Cells 1
NKG2D	Natural-killer group 2, Member D
ORS	Outer Root Sheath
OSM	Oncostatin M
OSMRβ	Oncostatin M receptor
P-cad	P-cadherin
PDGF-α	Platelet-derived growth factor-α
PIM1	Proviral Integration Site 1
PRL	Prolactin
PTHrp	Parathyroid hormone-related protein

qRT-PCR	Quantitative Reverse Transcription Polymerase Chain Reaction
R26-	Rosa 26
RNA	Ribonucleic Acid
SCC	Squamous Cell Carcinoma
scRNA-seq	Single-cell RNA sequencing
Shh	Sonic Hedgehog
SMAD	Small body size + Mothers Against Decapentaplegic (portmanteau)
SP	Substance P
SOX9	Sex determining region-box 9
STAT	Signal Transducers and Activators of Transcription
TAC	Transit Amplifying Cells
Tcf3	Transcription Factor 3
Tcf4	Transcription Factor 4
TdT	Tandem dimeric-Tomato
TE	Telogen Efluvium
TGFβ	Transforming Growth Factor-β
TNF	Tumor Necrosis Factor
T reg	Regulatory T Cell
TREM2	Triggering Receptor Expressed on Myeloid Cells 2
TRM	Tissue Resident Macrophage
WB	Western Blot
WIHN	Wound-induced HF neogenesis
Wnt	Wingless-related integration

APPENDIX C. LIST OF GENES ENRICHED IN CLUSTER 6

Most Upregulated Genes Cluster 6							
	Gene	p_val	avg_logFC		Gene	p_val	avg_logFC
1	Apoe	1.126E-50	3.59	51	Itgb5	8.5E-32	0.78
2	Ctsd	1.884E-67	2.46	52	Osm	1.6E-07	0.78
3	C1qb	1.347E-14	2.36	53	Blvrb	6.8E-19	0.77
4	C1qa	1.013E-12	2.31	54	Irf8	2E-10	0.76
5	C1qc	2.693E-11	2.17	55	Anxa3	1.7E-22	0.76
6	Lgmn	1.539E-27	1.81	56	Mgst1	2.6E-09	0.76
7	Spp1	2.634E-10	1.78	57	Plin2	3.9E-09	0.75
8	Ctsb	5.389E-26	1.68	58	Cebpb	4.4E-05	0.75
9	Trem2	1.156E-44	1.64	59	Bcas3	7.6E-30	0.73
10	Ms4a7	1.038E-15	1.62	60	Lair1	3E-17	0.72
11	Ftl1	3.036E-87	1.60	61	Sdcbp	2.5E-12	0.72
12	Cd63	3.711E-12	1.50	62	Ntpcr	1.4E-24	0.72
13	Rgs1	1.459E-11	1.38	63	Ctsl	5.8E-11	0.72
14	Fth1	1.682E-70	1.34	64	Akr1a1	5.5E-16	0.71
15	Hexb	2.274E-35	1.33	65	Cx3cr1	7.6E-08	0.71
16	Bcl2a1b	3.007E-10	1.21	66	Apobec1	1.1E-11	0.70
17	Cxcl16	8.769E-23	1.19	67	Tmem37	2.8E-16	0.70
18	Ctss	3.099E-47	1.13	68	Aprt	3.2E-12	0.69
19	Ninj1	2.146E-15	1.12	69	Cd5l	3.9E-06	0.69
20	Cd68	1.163E-32	1.10	70	Fyb	2.3E-10	0.69
21	Sepp1	1.77E-07	1.08	71	Lipa	1.3E-11	0.68
22	Lamp1	5.658E-22	1.07	72	Id2	5E-05	0.68
23	Msrb1	5.469E-15	1.07	73	Grn	5.1E-05	0.66
24	Prdx5	1.984E-18	1.06	74	Tyrobp	7.3E-19	0.65
25	Ikbkb	3.983E-27	1.04	75	Iscu	1.1E-10	0.64
26	Fcgr3	5.162E-18	1.04	76	Sdhb	1.3E-10	0.64
27	AF251705	4.904E-22	1.03	77	Rnase4	2.9E-08	0.64
28	Cotl1	1.93E-24	1.03	78	Cd14	0.00543	0.62
29	Ctsh	3.962E-34	1.02	79	Rgs2	3.9E-06	0.62
30	Ctsz	4.323E-25	1.01	80	Clec12a	1.3E-06	0.62
31	Cyp4f18	1.734E-19	1.01	81	U2af1	8.9E-13	0.62
32	Gngt2	2.666E-18	0.99	82	1110008F13Rik	1.8E-13	0.61
33	Aif1	7.169E-16	0.99	83	Ms4a6b	7.4E-09	0.60
34	Prdx1	1.684E-20	0.95	84	Ms4a6d	4.6E-08	0.60
35	Itm2b	5.891E-21	0.92	85	Ostf1	1.1E-10	0.60
36	Smpdl3a	2.166E-15	0.91	86	Fcgr4	4.8E-17	0.60
37	Cstb	1.067E-14	0.89	87	Atp6v1g1	6.1E-11	0.60
38	Acp5	8.186E-34	0.89	88	Pld3	5.7E-09	0.59
39	Hexa	2.475E-15	0.87	89	Taldo1	4E-08	0.59
40	Bst2	4.474E-14	0.87	90	Cmtm7	3.7E-07	0.59
41	Rgs10	3.269E-21	0.86	91	Apoc1	3.5E-09	0.59
42	Sat1	6.517E-14	0.86	92	Sgk1	5.1E-10	0.58
43	H3f3b	1.145E-19	0.85	93	Cyba	5.1E-09	0.58
44	Cd81	2.117E-09	0.85	94	Atp6v1f	2.2E-10	0.58
45	Id3	8.45E-08	0.82	95	Eif6	1.3E-08	0.57
46	Clta	1.228E-20	0.81	96	Gapdh	7.9E-10	0.57
47	Creg1	3.273E-17	0.80	97	Hilpda	1.4E-07	0.57
48	Thbs1	0.0018021	0.79	98	Il18bp	1.1E-12	0.57
49	AW112010	8.088E-07	0.79	99	Cd38	1.8E-17	0.57
50	Ccrl2	8.205E-08	0.79	100	Ier3	3.6E-05	0.57

APPENDIX D: ENRICHR RESULTS FOR CLUSTER 6 GENE EXPRESSION PROFILE

Term	Overlap	P-value	Adjusted P-value	Z-score	Combined Score	Genes
Microglia	6/90	3.60E-06	1.20E-04	-1.11	13.9134	C1QB;C1QA;PRDX1; HEXB;MS4A7;C1QC
Macrophage_bone_marrow_24h_LPS	9/551	3.00E-03	4.70E-02	-2.07	12.0769	BST2;FCGR3;PRDX5; GNGT2;PRDX1;NINJ1; MS4A7;SAT1;CXCL16
Macrophage_peri_LPS_thio_0hrs	9/353	1.30E-02	1.40E-01	-1.72	7.4463	CREG1;HEXA;AF251705; NINJ1;TREM2;CD68; CTSD;CTSB;LGMN
Osteoclasts	2/110	3.30E-02	2.70E-01	-1.05	3.584	HEXB;ACP5
Macrophage_peri_LPS_thio_1hrs	7/598	2.00E-01	9.30E-01	-2.13	3.3908	CSTB;RGS1;CREG1; CCRL2;AF251705;CTSS; CTSB
Osteoblast_day5	2/175	7.60E-02	4.90E-01	-1.24	3.1839	ID3;THBS1
Osteoblast_day14	2/301	1.80E-01	9.30E-01	-1.38	2.342	ID3;THBS1
Macrophage_peri_LPS_thio_7hrs	6/707	2.80E-01	1.00E+00	-1.68	2.1453	AW112010;CCRL2;CTSZ; MS4A7;CXCL16;CTSB
Mast_cells	2/515	3.90E-01	1.00E+00	-1.27	1.1964	H3F3B;OSM
Follicular_B-cells	2/603	4.70E-01	1.00E+00	-1.51	1.1508	IKBKB;CYP4F18
Mmacrophage_bone_marrow_0hr	3/180	3.80E-01	1.00E+00	-1.14	1.1212	C1QB;COTL1;C1QC
Dendritic_plasmacytoid_B220+	1/214	4.30E-01	1.00E+00	-1.26	1.0635	CTSH
Macrophage_bone_marrow_2hr_LPS	3/365	6.20E-01	1.00E+00	-1.38	0.6658	C1QB;NINJ1;C1QC
Osteoblast_day21	3/264	5.00E-01	1.00E+00	-0.95	0.6592	ITGB5;ID3;THBS1
mIMCD-3	1/300	5.40E-01	1.00E+00	-1.06	0.6451	CYP4F18
MEF	2/300	5.40E-01	1.00E+00	-1.06	0.6438	ITGB5;THBS1
Cornea	1/427	6.70E-01	1.00E+00	-1.05	0.413	TREM2
Granulocytes_mac1+gr1+	1/557	7.70E-01	1.00E+00	-1.46	0.3818	NINJ1
Placenta	1/411	6.60E-01	1.00E+00	-0.84	0.3499	CREG1
NK_cells	1/669	8.30E-01	1.00E+00	-1.31	0.2446	AW112010
Eyecup	2/828	8.90E-01	1.00E+00	-1.8	0.2107	IKBKB;ITGB5
Macrophage_bone_marrow_6hr_LPS	1/730	8.60E-01	1.00E+00	-1.23	0.1912	FCGR3
Kidney	2/554	7.70E-01	1.00E+00	-0.7	0.1839	PRDX5;SMPDL3A
Lacrimal_gland	1/749	8.60E-01	1.00E+00	-1.14	0.1674	HEXB
Lens	1/947	9.20E-01	1.00E+00	-1.14	0.0948	ITGB5
Lliver	2/928	9.20E-01	1.00E+00	-0.5	0.0442	APOE;SEPP1
Testis	1/59	1.0E+00	1.00E+00	-0.71	0.0001	AIF1